ABSTRACT

PAI, GANAPATI. Design of Dc-Assisted Mutually Coupled Switched Reluctance Machine (Under the direction of Dr. Iqbal Husain).

The thesis presents the design of a DC-Assisted Mutually Coupled Switched Reluctance Machine (DC-MCSRM) drive with low torque ripple over a wide speed range. The proposed design has been verified with system level simulations using finite element analysis (FEA).

A hybrid excitation topology for a Mutually Coupled Switched Reluctance Machine is proposed and the operating principle of the machine is defined. The performance of the machine is compared to the conventional switched reluctance machine. Coupled simulation of the FEA software has been used to verify the motor drive and the control algorithm was also tuned using the same approach.

A current profiling method has been developed to reduce the torque ripple of the machine. The method smoother operation and high operation over the entire speed range of operation. The torque ripple was minimized to 25% in the given operating range.

A hysteresis type current control is implemented for the phase current to accurately follow the reference current. The controller is initially verified by simulation and then an attempt to implement it in hardware is made.

Design of Dc-Assisted Mutually Coupled Switched Reluctance Machine

by
Ganapati Pai

A thesis submitted to the Graduate Faculty of
North Carolina State University
in partial fulfillment of the
requirements for the degree of
Master of Science

Electrical Engineering

Raleigh, North Carolina

2017

APPROVED BY:

Dr. Iqbal Husain
Committee Chair

Dr.Srdjan Lukic

Dr. Wensong Yu

DEDICATION

To my family and teachers

BIOGRAPHY

Ganapati Pai received his Bachelor of Technology degree from Veermata Jijabai Technological Institute, Mumbai, India in Electrical Engineering in 2014. He is currently pursuing his Master of Science from North Carolina State University in Electrical Engineering.

In 2013, he worked as a research intern at Indian Institute of Technology, Bombay on implementing a Maximum Power Point Tracking algorithm for single-phase solar stand-alone systems. In 2016, he was an Applications Engineering Intern at ON Semiconductor, Rhode Island. He is currently working as a Graduate Research Assistant at the FREEDM Systems Center. His primary research interests are in electric motor drives and renewable energy systems.

ACKNOWLEDGMENTS

I wish to express my deep sense of gratitude and indebtedness to my academic advisor, Dr. Iqbal Husain for his great support in the course of this research and opportunity to broaden my horizons.

I also thank Dr. Srdjan Lukic and Dr. Wensong Yu for their comments and suggestions. I am much obliged to Md. Ashfanoor Kabir for the assistance provided by him during this research project and his valuable suggestions. I would also like to thank the member of the Machine Design Group at NC State, the staff members of FREEDM Systems Center, for the facilities and support.

I thank my friends and family for their continuous support in my life and without whom this would not have been possible.

TABLE OF CONTENTS

LIST OF TABLES

LIST OF FIGURES

CHAPTER 1

INTRODUCTION

1.1 History of Switched Reluctance Machine

The Switched Reluctance Machine (SRM) was invented by Davidson in Scotland in 1838, where it was used to propel a locomotive on the Glasgow-Edinburgh Railway line [10]. Although the concept of a reluctance based machine was around since the 1800's, the mechanical switches of that time did not make Switched Reluctance Machine a feasible option for electric drive applications. It was in the 1970's, with the advent of fast-switching power semiconductor devices that the interest in SRM was revived. In 1971, Bedford filed an US Patent on the modern Switched Reluctance Motor and established the fundamental design and operating principles of the machine. With a high instantaneous torque, wide-speed range capability and a low cost rugged structure, the SRM is becoming a strong candidate as the preferred electric drive in multiple applications.

1.2 SRM Configuration

The switched reluctance machine uses the reluctance torque production technique to convert electrical energy into mechanical energy. The SRM has one of the simplest constructions of any electric machine. It has a doubly salient structure which contributes to reluctance torque production. It is also a singly excited machine, with independent phase windings on the stator. The rotor is a stack of magnetic steel laminations without any magnet or windings. A 3-phase 12/8 SRM is shown in Fig (1), which is a two-repetition of the basic 6/4 structure [1]. This machine is alternatively labeled as a 4 poles/phase machine where the stator windings on the diametrically opposite poles can be connected in series or in parallel to form one phase of the motor. When a stator phase is energized, the most adjacent rotor pole-pair is attracted towards the energized stator to minimize the reluctance of the magnetic path. Therefore, by energizing consecutive phases in succession, a unidirectional torque can be developed using an SRM.

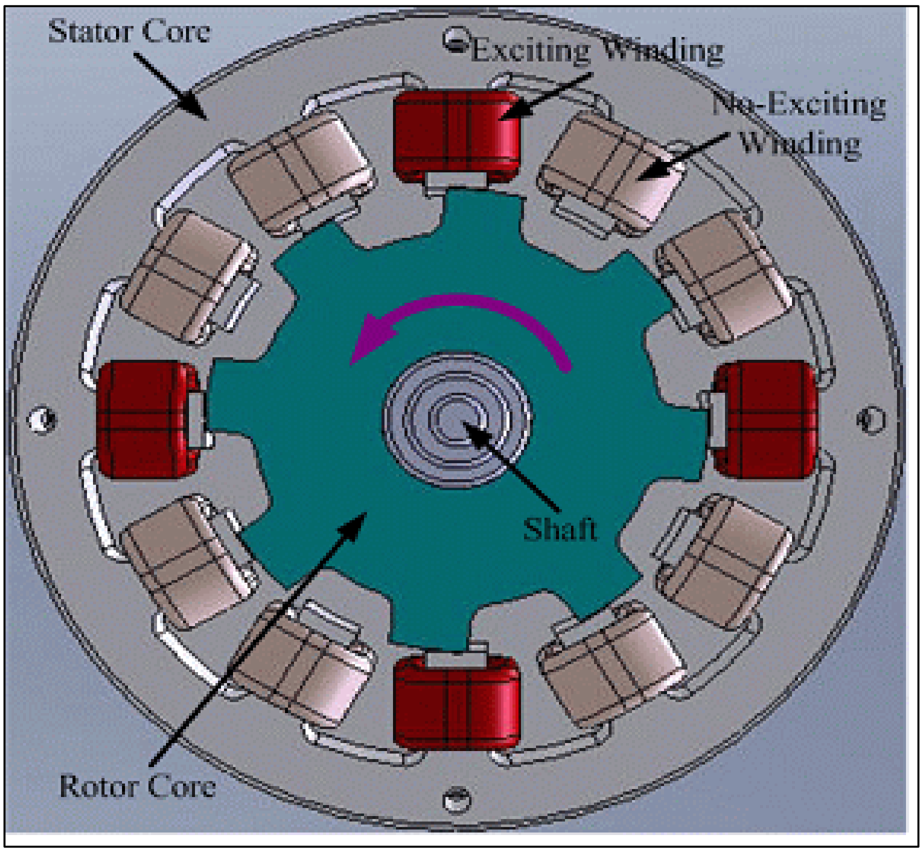

Figure 1: Cross sectional diagram of a 3 phase 12/8 switched reluctance machine

The aligned position of a phase is the position where the rotor and stator poles are aligned such as to provide the magnetic flux with a path of least reluctance. The unsaturated phase inductance (L_a) in this position. As the rotor poles move from aligned position to an unaligned position, the phase inductance gradually decreases and at the unaligned position, the phase inductance is the minimum(L_u). The stator and rotor pole arcs determine the extent of variation in phase inductance and thereby, a varying reluctance profile is obtained for each phase.

1.3 Research Motivation and Objectives

Any electric drive system consists of 3 major components, namely:

1. Controller Module
2. Power Inverter
3. 3-phase machine itself

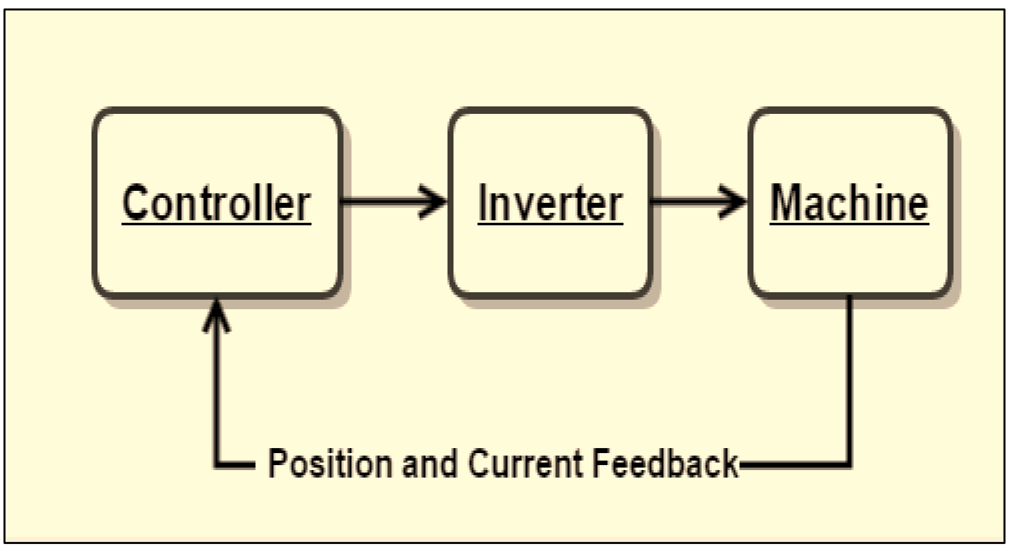

Figure 2: Electric Motor Drive System

1. The Controller Module: Based on the feedback from the motor parameters, such as the phase currents, phase voltages, encoder position etc., the controller module determines the gate pulses to the power inverter. The controller module implements the algorithm to ensure

either speed control of torque control of the machine. The controller module is implemented using high precision Digital Signal Processor Control Card or FPGA's. In this research, the Texas Instrument's DSP TMS320F38377D and TMS320F28012 32-bit MCUs are used to implement a hysteresis current control.

2. Power Inverter: Most 3-phase motor drive systems use the standard six-switch voltage source inverter to drive the motor. The operating nature of most 3-phase motors, where the 3-phase currents are mutually dependent on each other has resulted in the Standard VSI has preferred converter drive. The ease of implementing PWM control strategies and the wide range of availability of the standard VSI makes it a favorable choice for most industrial applications. However, for motors that require independent control of the phase currents, such as the switched reluctance motor, the asymmetric half-bridge converter is a suitable power inverter. The research focus has been to develop a switched reluctance drive system which can be excited using a standard voltage source inverter.

3. 3-Phase Motor: The choice of the motor is strongly motivated by the application it will be used in. If a Hybrid-Electric Vehicle application is to be considered, the Permanent Magnet Synchronous Motor is the preferred choice. The wide-operating speed range, the higher torque and power density, the ease of implement the Field Oriented Control using Space Vector PWM are the features that make the PMSM the preferred choice. However, the rotor structure has rare-earth Neodymium Permanent Magnets which substantially increase the cost of system. In recent years, there has been a focus to come up with an alternative for the PMSM and the Switched Reluctance Machine is a strong contender for the same. The robust

and low cost structure, high power and torque density, the lack of rare-earth magnets makes the switched reluctance motor a prime candidate.

The research motivation was to develop a switched reluctance drive system which can be driven using the standard six-switch inverter. This would allow us to overcome the major drawback of a SRM drive – the asymmetric bridge inverter.

1.4 Thesis Organization

The thesis starts with an introduction to the history and basic knowledge of the switched reluctance motor. It then covers the research motivation and current research work on the SRM

Chapter Two briefly describes the conventional switched reluctance machine and the mutually coupled switched reluctance machine (MCSRM). It also introduces the proposed hybrid excitation topologies; the Fully-Pitched DC-Assisted MCSRM and the Concentrated-Winding DC-Assisted MCSRM.

Chapter Three discussed the operating principle of the proposed hybrid excitation topologies and presents a comparison with the benchmark SRM. It also covers the electromagnetic design steps and analysis of the results.

Chapter Four presents a current profiling method to minimize the torque ripple. The developed method minimizes the torque ripple through a coupled design approach. The maximum operating speed of the machine and the torque profiles of the machine are used to develop the current profiles. A machine is simulated using MATLAB/Simulink and the simulation results are presented.

Chapter Five presents the hardware implementation and the experimental results. The approach was to initial implement a hysteresis current control on a 400W PMSM and then uses a similar approach to control the Concentrated-Winding DC-Assisted MSRM.

Chapter Six is the final chapter that presents the summary and the conclusion of the earlier chapter of the thesis. Suggestions for future research work are presented.

CHAPTER 2

DC-ASSISTED MUTUALLY COUPLED SWITCHED RELUCTANCE MACHINE

2.1 Introduction

The SRM is a single-excited machine with phase coils wound around diametrically opposite stator poles. Therefore, the phase excitation makes the rotor poles align with the excited stator pole to minimize the reluctance of magnetic path and generate the reluctance torque. There is complete magnetic decoupling between phases, and torque is produced due to rate of change of winding self-inductance. Therefore, the conventional SRM requires an asymmetrical half bridge inverter to provide the independent unipolar phase currents to excite the stator coils. An asymmetrical bridge inverter is an unconventional configuration which has resulted in conventional SRMs receiving less attention by the industries. In addition, freewheeling due to the pulsed nature of phase currents and the large size of filter capacitors [2][4] increases the converter size for conventional SRMs. Besides, unipolar operation increases the peak phase currents, thereby increasing the current stress on the power devices. To overcome these drawbacks of conventional SRM, there has been a focus in developing switched reluctance machines that can be excited using a standard six-switch voltage source inverter. This chapter introduces a DC-Assisted mutually coupled switched reluctance machine (DC-MCSRM) which overcomes the major drawbacks of a conventional SRM. A comparison of the operating principle of these machines is also provided in this chapter.

2.2 Switched Reluctance Machine

A conventional SRM typically operates under highly saturated magnetic conditions to maximize the utilization of the magnetic circuit. Hence, the flux linkage is a nonlinear function of stator current and rotor position given by

$$\lambda_{ph} = \lambda_{ph}(i_{ph}, \theta_{ph})$$

A high saliency ratio i.e. the ratio between the maximum and minimum unsaturated inductance levels is desired to achieve the highest possible torque per ampere. The cross-sectional view of a conventional 12/8 SRM is shown in the Fig (3).

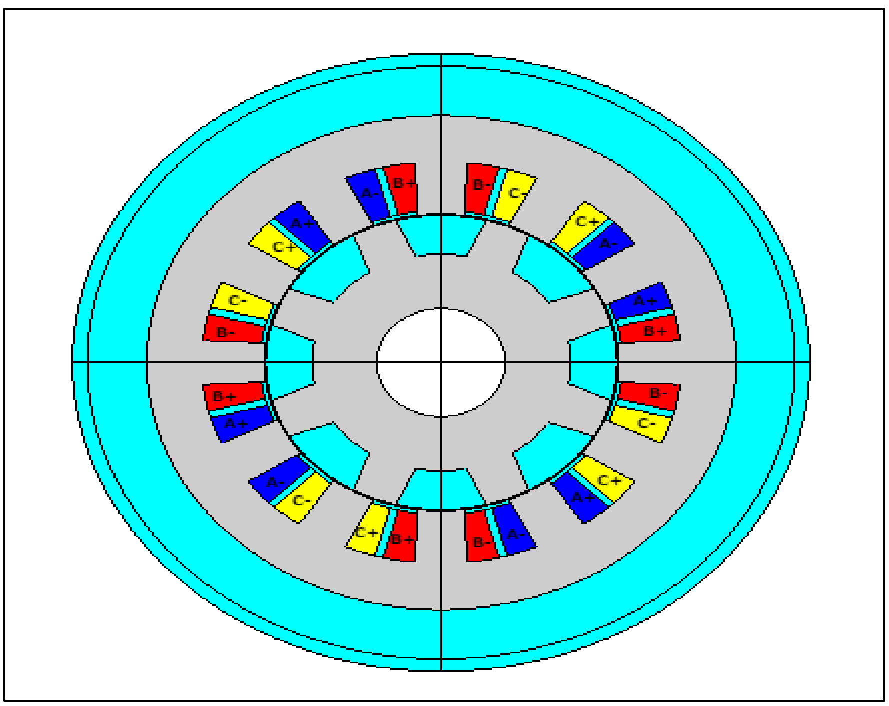

Figure 3: Cross sectional view of a conventional SRM

As we can see from the cross-sectional view, the 3 phase 12/8 SRM has a 4 coils/phase configuration, with each phase coil made up of N-turns of concentrated winding around each stator pole.

The general expression for the phase voltage of the SRM is [10[[11]:

$$V_{ph} = i_{ph}.R_{ph} + \frac{d\lambda}{dt}$$

Where, $'V_{ph}'$ is the DC-bus voltage, $'i_{ph}'$ is the instantaneous phase current, $'R_{ph}'$ is the winding resistance, and 'λ' is the phase flux-linkage. Assuming magnetic linearity, the voltage equation can be simplified as,

$$V_{ph} = i_{ph}.R_{ph} + L(\theta).\frac{di}{dt} + i_{ph}.\frac{dL(\theta)}{dt}.\omega$$

The last term in the above equation is the 'Back-EMF' developed in the SRM, which is similar to the back-EMF in a DC motor. However, unlike the DC motor, this back-EMF is not generated by a rotating magnetic field, instead, it is generated by the instantaneous rate of change of flux-linkage.

The SRM power inverter is unique from other multi-phase technologies. Each phase is independently controller by its own converter phase leg. The classical half-bridge converter is shown in Fig (4) is most commonly used for SRM operation.

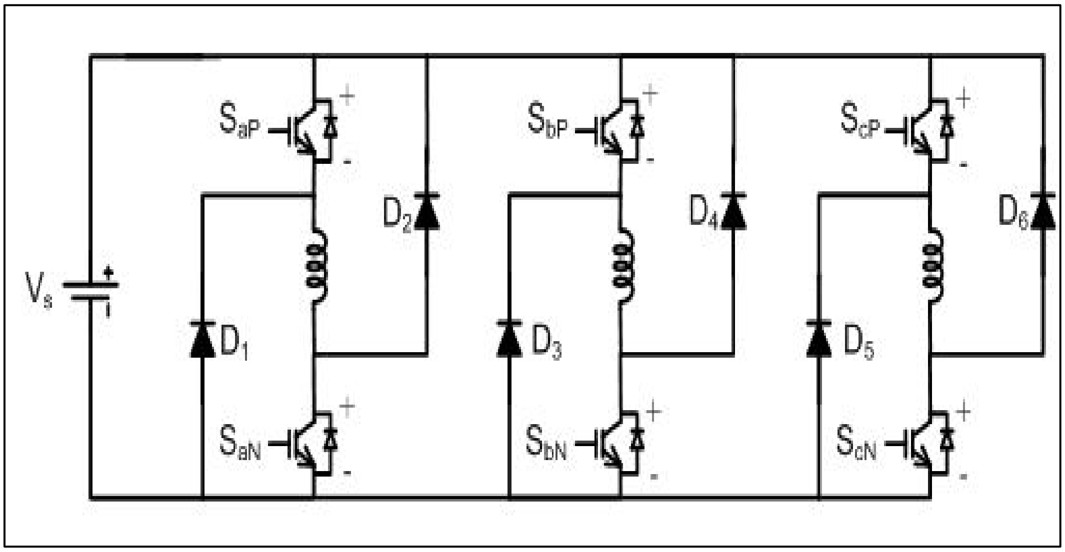

Figure 4: Asymmetric Half- Bridge Inverter

The top and bottom switches along with the freewheeling diodes are used for controlling the machine. To increase current in the phase both the top and bottom switches are turned ON. Zero voltage can be applied across a phase by turning off either the top or the bottom switch and negative voltage is applied by turning both the switches off, which is known as forced commutation. During this period, current flows through the freewheeling diodes until it drops down to zero. Each phase is independently controller by the controller and inverter. Due to absence of rotor windings, the SRM construction is very simple and robust, has a very low inertia and allows high-speed operation. Unlike induction motors, due to absence of rotor copper losses, SRM does not required thermal cooling and due to absence of permanent magnets, demagnetization at high operating temperature is not a concern. Due to unipolar nature of operation, the SRM is immune to shoot through faults and in comparison, to distributed winding machines; the concentrated winding topology helps reduce the overall cost of the system.

The primary disadvantage of SRM is the high torque ripple and the acoustic noise caused by the doubly salient structure of the machine. In recent years, researchers have been trying to minimize the torque ripple through either alternative machine designs or control techniques. Besides, rotor position information is required to developing a controller for a conventional SRM. Although, sensor less control techniques have also been developed. The major hurdle in the use of conventional SRMs for most high-power applications is the need for an asymmetric half-bridge power inverter to excite the machine. In recent years, there has been a focus on developing a new winding configuration for a reluctance machine what would enable the use of a standard six-switch voltage source inverter. Developing such characteristics in SRMs require torque production with mutual coupling of the phases. Barrie Mecrow first proposed a fully-pitched winding configuration for a SRM, which produced torque due to the rate of change of mutual inductance [5]. These machines are names as Mutually Coupled Switched Reluctance Machine (MCSRM). Various excitation patterns and winding configurations are possible with the MCSRM using the conventional six-switch voltage source inverter.

2.3 Mutually Coupled Switched Reluctance Machine (MCSRM)

Compared to conventional SRM that produces reluctance torque solely because of rate of change in self-inductance per phase, the MCSRM produces electromagnetic torque by utilizing the mutual inductance between the two phases. Because of the fundamental change in in operating mode, each phase of the machine contributes to positive torque production for considerably greater than one-half of the cycle of rotation, leading to more efficient utilization of the winding, and thereby the magnetic circuit. A number of different excitation patterns and winding configurations can be explored with a MCSRM. For the MCSRM, the per phase flux linkages are a non-linear function of not only position and current in that phase, but also a function of current in all other active phases. This makes the analysis of a MCSRM more complex is comparison to that of a SRM.

$$\lambda_{ph} = \lambda_{ph}(i_{pha}, i_{phb}, i_{phc}, \theta_{ph})$$

The cross-sectional view of a conventional 12/8 MCSRM is shown in the Fig (5).

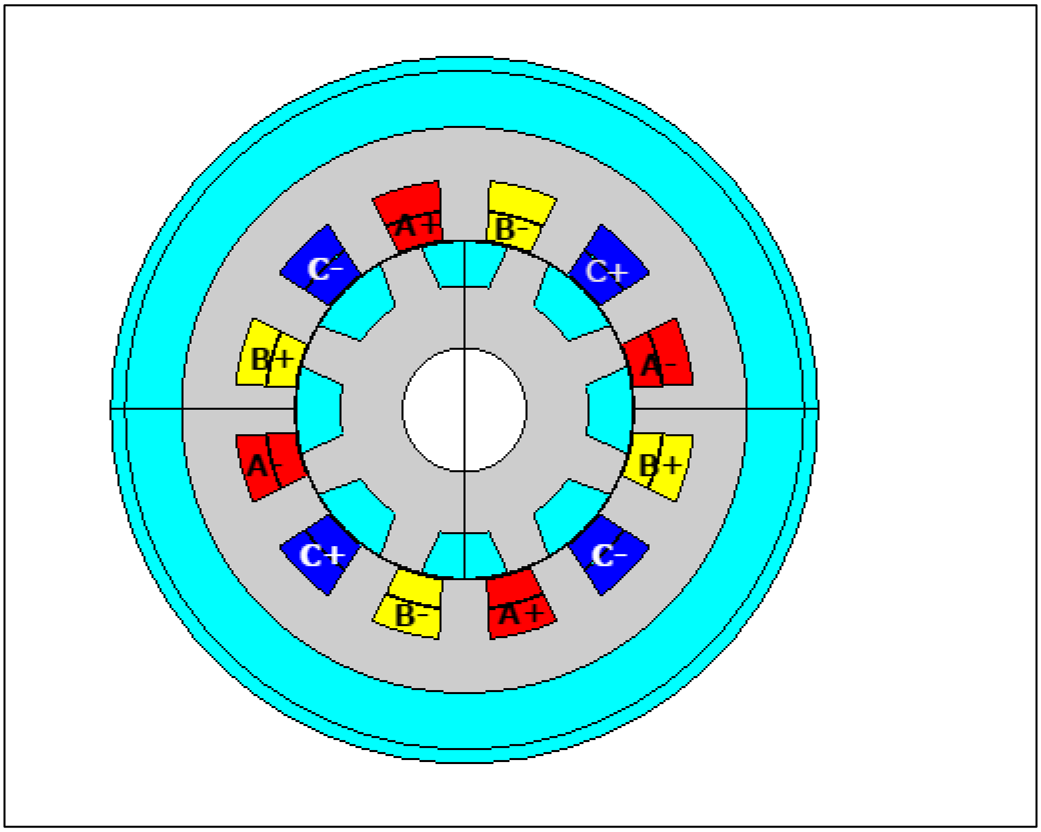

Figure 5: Cross sectional view of a MCSRM

It can be shown that the new fully-pitched winding configuration has a per phase self-inductance which is effectively independent of rotor position, while the mutual inductance between phase varies very rapidly with rotor position [2][4]. Thus, the rate of change of self-inductance is negligible and the electromagnetic torque is almost completely generated from the rate of change of mutual inductance between phases.

The general expression for the phase voltage of the MCSRM is like that of a SRM:

$$V_{ph} = i_{ph1}.R_{ph1} + \; i_{ph2}.R_{ph2} + \frac{d\lambda}{dt}$$

Where, $'V_{ph}'$ is the DC-bus voltage, $'i_{ph1} \; and \; i_{ph2}'$ are the instantaneous phase currents, $'R_{ph1} \; and \; R_{ph2}'$ are the winding resistance, and 'λ' is the phase flux-linkage. Assuming magnetic linearity, the voltage equation can be simplified as [5][9],

$$V_{ph} = \; i_{ph}.R_{ph} + \; M(\theta).\frac{di}{dt} + \; i_{ph}.\frac{dM(\theta)}{dt}.\omega$$

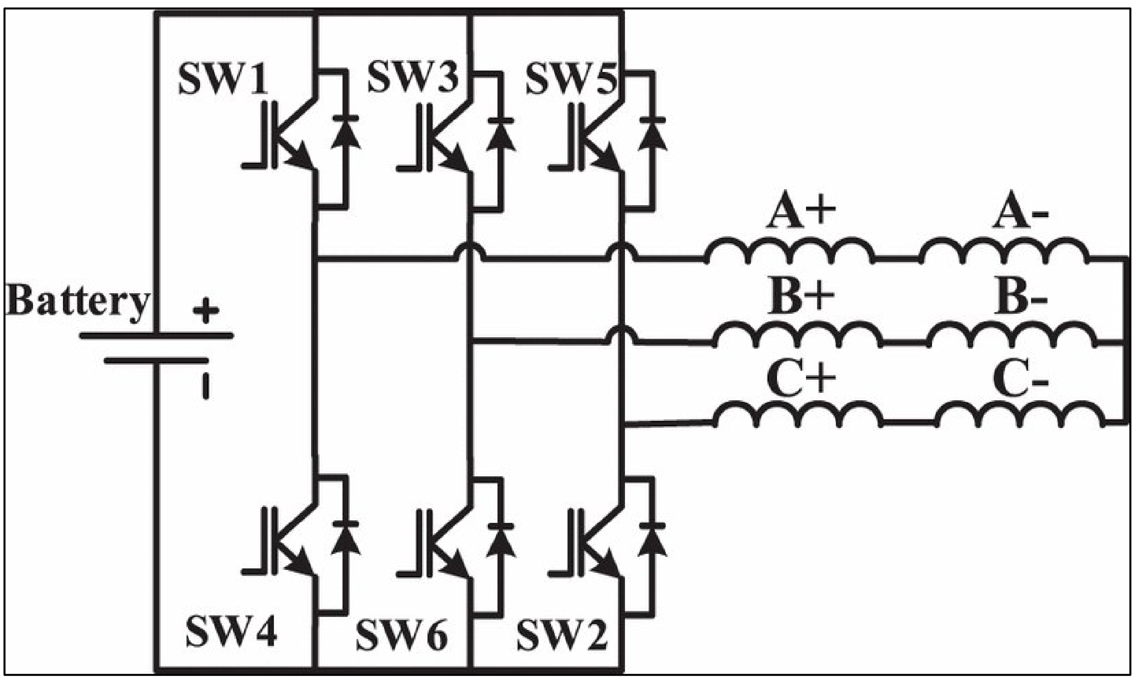

Figure 6: Standard Six-Switch Voltage Source Inverter (VSI)

A fully-pitched winding configuration will inevitably have a considerably increased end-winding length, but a multipole/per phase configuration, such as 12/8 configuration, can considerably reduce the end-winding lengths [12].

Both unipolar and bipolar excitation can produce positive torque in a MCSRM [15] [16]. The electromagnetic torque generated in a MCSRM is given by the following equation;

$$T_{em} = i_a . i_b . \frac{dM_{ab}}{d\theta}$$

If both the phase currents have unipolar excitation, positive torque is generated during the period of rotation when the mutual inductance between the two conducting phases is rising. However, if bipolar excitation schemes are used, then it is possible to generate positive torque when the mutual inductance between the phases is falling as well, provided the two-phase currents have opposite polarity. In addition, both bipolar sinusoidal and trapezoidal excitation schemes are possible [15]. For either of the bipolar excitation schemes, the summation of the 3-phase armature currents will be zero for a Y-connected MCSRM. Hence, a 3-phase standard six-switch voltage source inverter can be utilized for its armature excitations.

The advantages of a conventional SRM owing due to a simple rotor construction are present in a MCSRM as well. A MCSRM has the positive features of both the conventional SRM and a PM machine. Compared to a conventional SRM, the phase MMF contribution is twice for a MCSRM which improves the power factor of the machine. In addition, because of more efficient use of machine, larger MMF's per unit loss is generated and thereby the average torque is significantly higher than a conventional SRM. Although the machine volume tends to be a bit higher because of the end-turn length, the RMS current density is lower than a conventional SRM.

A major design constraint with the MCSRM is that the maximum constant power-speed range is limited by half the supply voltage. Since the machine is excited using a standard six-switch VSI, the 3-phase windings can be connected in either delta connection or star connection. With delta connected phase windings, circulating harmonic currents contribute to negative torque production and thereby resulting in increased torque ripple. A better current regulation can be achieved by using a Y-connected armature winding. But since, two phases are conducting simultaneously, only half of the bus-voltage will be available across each phase. In most applications, the machine is supposed to meet rated power requirements at base speed as well as maximum speed. In addition, the Back-EMF term is directly proportional to the operating speed and the electromagnetic torque is a function of phase currents. Therefore, operating the MCSRM at high speeds is particularly challenging considering the limitations at the supply voltage and maximum RMS current level constraint for the power devices of the inverter. To attain the wide constant power speed range, a higher rating converter or optimization with geometry parameters is necessary.

2.4 DC-assisted Mutually Coupled Switched Reluctance Machine

Two new hybrid winding topologies of mutually coupled switched reluctance machine are proposed using 3-phase standard six-switch inverter. The proposed topologies utilize the mutual coupling between phases to produce electromagnetic torque. A more through explanation of the operating principle and comparison with a conventional SRM for the same iron core geometry is presented in the next chapter. The proposed topologies show a higher torque and power density compared to a conventional SRM under the same excitation level and the torque ripple performance is also significantly improved [3]. The hybrid excitation topologies proposed include both fully-pitched (FP) and concentrated armature winding (CW) configurations. The power inverter for the proposed topologies is shown in the Fig (7):

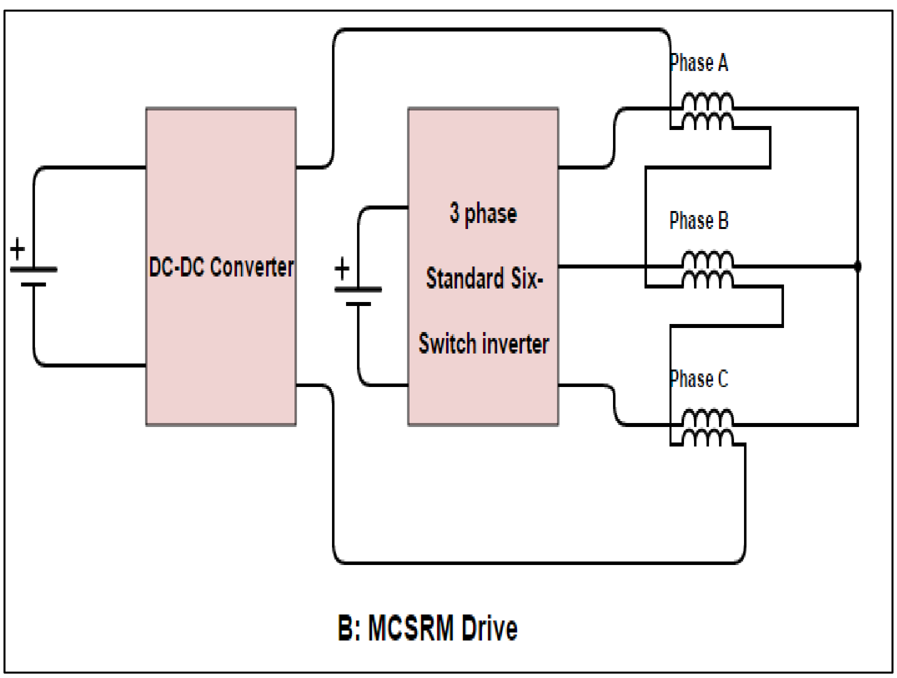

Figure 7: Inverter Drive for the DC-MCSRM

A standard 3-phase six switch voltage source inverter is used for bipolar excitation of the armature windings. Similar to a MCSRM, both sinusoidal and square-wave excitation sequence is possible. However, the focus of this research was square wave excitation of a concentrated winding DC-assisted MCSRM [14]. A separate Dc-dc converter is required to excite the field windings. A typical half-bridge inverter leg is used to regulate the field windings current to a fixed dc value.

a. Fully Pitched DC-assisted Mutually Coupled Switched Reluctance Machine

Fig (8) shows the cross-sectional view of the proposed fully-pitched dc-assisted mutually coupled SRM. The proposed topology has concentrated windings around

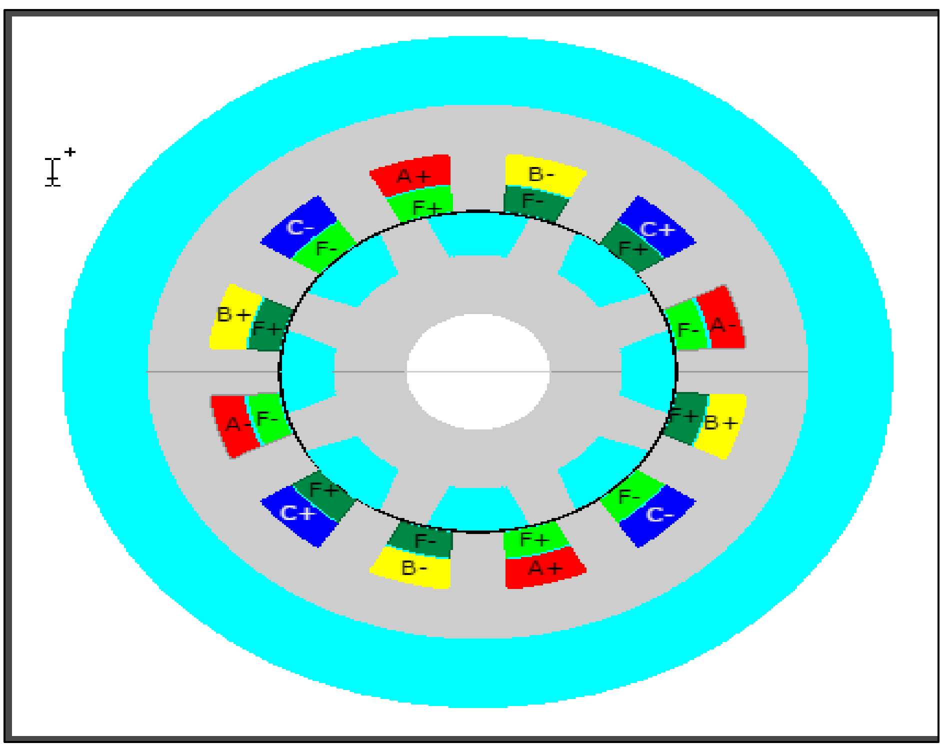

Figure 8: Fully-Pitched DC-Assisted MCSRM

each stator pole to carry a constant DC excitation [3]. The DC excitation results in alternating magnetic flux path being produced in consecutive stator poles. The phase windings have a fully-pitched configuration similar to that of a MCSRM. The fully-pitched armature topology has the advantage of better magnetic circuit utilization and better torque contribution from each phase compared to a conventional SRM. This topology also exhibits a higher rate of change in inductance from the unaligned position to the aligned position, which contributes to a higher average electro-magnetic torque production. A more detail analysis of the operating principle is done in the next chapter.

b. Concentrated Winding DC-assisted Mutually Coupled Switched Reluctance Machine

Fig (9) shows the cross-sectional view of the proposed concentrated winding dc-assisted mutually coupled SRM. This topology also has concentrated windings

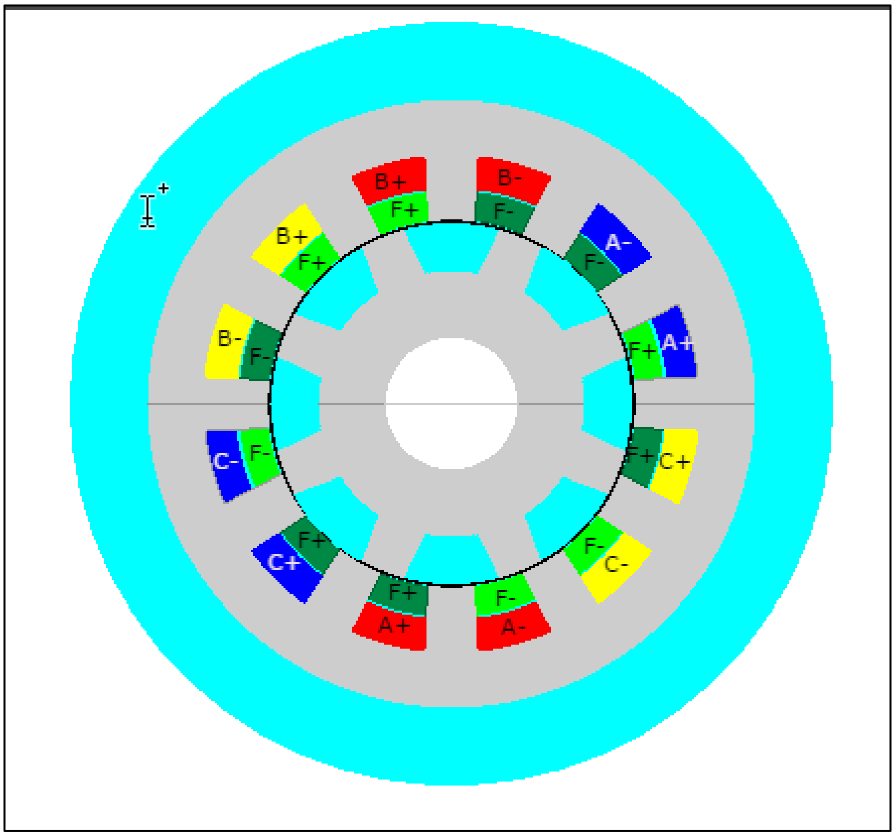

Figure 9: Concentrated Winding DC-MCSRM

around each stator pole to carry DC-excitation [3]. However, the winding sequence is different from that of a fully-pitched DC-assisted MCSRM. The DC-excitation results in alternating magnetic flux paths in consecutive stator poles for this configuration. The phase windings are also concentrated windings around each stator poles, similar to that of a conventional SRM. The field and armature windings are wound in such that each stator pole slot has the same polarity. Similar to the fully-pitched winding configuration, the concentrated winding configuration also has a better magnetic utilization and effective torque contribution from each phase in comparison to a conventional SRM. The concentrated winding configuration also has the added advantage of better torque ripple performance in comparison to a conventional SRM. Besides, the concentrated winding topology comes with the benefit of lower end-winding turn length requiring less copper and thereby, lower copper losses. A more detail analysis of the operating principle is done in the next chapter.

CHAPTER 3

FINITE ELEMENT ANALYSIS OF DC-ASSISTED MUTUALLY COUPLED SWITCHED RELUCTANCE MACHINE

3.1 Introduction

The advent of faster switching electronics has led to faster automation systems and have simplified the design optimization techniques for the SRM. The electromagnetic field analysis for the machine design has emerged more recently as a tool for optimizing designs. The most popular methods are based on finite element analysis (FEA), which is a design and analysis tool. An FEA package requires detailed input data for design and the results need skilled interpretation.

While designing a conventional SRM or a DC-assisted MCSRM, the initial sizing of the geometry, the static and magneto-dynamic FEA and system level simulations: all should be considered simultaneously. The other design objectives would be to optimize the torque density, power density, efficiency, and to minimize torque ripples.

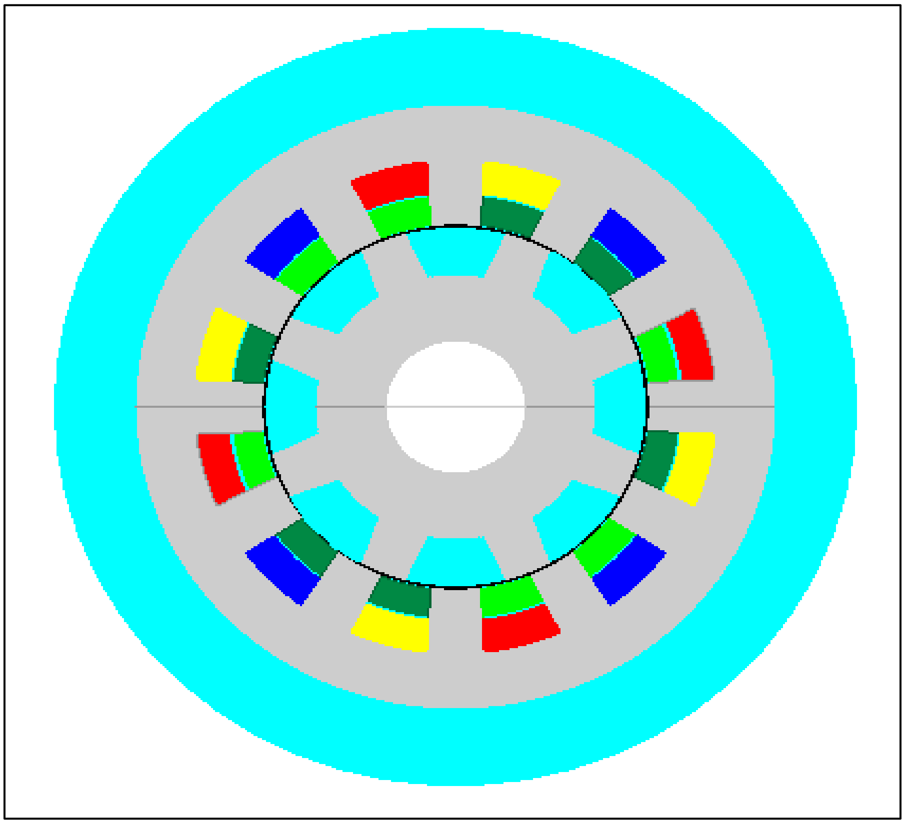

Figure 10: Cross sectional view of the FEA model of DC-MCSRM

3.2 Modelling of 12/8 DC-Assisted MCSRM in Flux2D

Flux2D is a commercially available finite element analysis tool used for the design and study of dynamics of electric systems. The DC-Assisted MCSRM is characterized by various mechanical parameters (number of stator and rotor poles, radius, dimensions, angles etc.,) and circuit parameters (number of coil turns, phase resistance, excitation current, phase inductance etc.) as given in Table 2 at the end of this chapter. The parameters given in Table 2 are those of a 660W, 3-phase 12/8 Maytag Neptune Washer SRM [17]. This is the benchmark SRM against which the performance of the DC-assisted MCSRM are compared.

The machine under test in this thesis is a Concentrated Winding DC-assisted MCSRM which was assembled by rewinding and reconnecting the bench-mark SRM.

The general steps followed to develop a finite element method based DC-MCSRM model as shown in Fig (10) using Flux2D are briefly discussed in the following section. The steps include:

a) Geometry Construction

b) Surface Meshing: The mesh analysis that involves creating mesh on the faces of the machine is crucial for accurate finite element calculations. The more fine the meshing is the more iterations the software takes to solve the equations and more precise the analysis is. The general approach is to use a dense meshing at crucial faces such as stator and rotor pole tip; and use a more relaxed meshing for regions such as stator back iron to save system memory and computational time [17].

c) Stator and Rotor Material: A non-linear steel material is chosen for stator and rotor of the DC-assisted MCSRM. B-H characteristics of the material can be modelled with knowledge of parameters such as the saturation magnetization $'J_s'$ and the initial relative slope of relative permeability. The B-H characteristics of the M-19 steel used to build the DC-assisted MCSRM is shown in Fig (11)

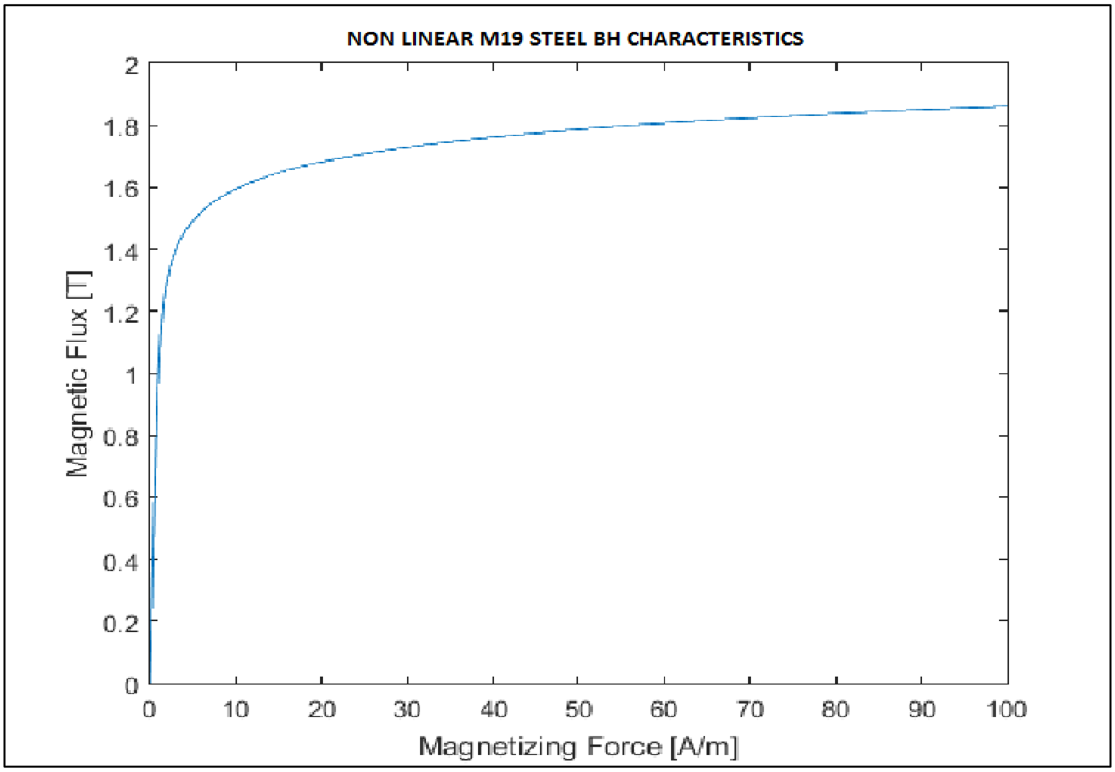

Figure 11: B-H characteristics of M19 Steel

d) Stator Coil Excitation Circuit: To obtain the flux-linkage and static torque characteristics through finite element analysis, it is necessary to excite the stator phase windings and the field windings with constant current values. For the 12/8 DC-assisted MCSRM, each phase has 2 stator poles and each pole consists of two coils (positive and negative). The current source value is changed to obtain the flux and torque characteristics at various current levels.

Since the basic approach for finite element analysis of a machine is defined, a more comprehensive comparison of the benchmark conventional SRM and the proposed hybrid excitation MCRM topologies can be conducted. Using FEA models, a comparison between the three topologies based on the magnetic circuit utilization is performed in the next section.

A detailed explanation of the operating principle of the machine follows and performance of the conventional SRM and Concentrated Winding DC-assisted MCSRM (The machine under test) is performed at the end of this chapter.

3.3 Magnetic Circuit Utilization of the DC-Assisted MCSRM

To ensure a fair comparison between the conventional SRM and the proposed hybrid excitation MCSRM, all the three machines are maintained at same phase excitation level. For the conventional SRM, the phase A winding is excited with constant current of 5.0A and for both the proposed hybrid excitation topologies, the DC-field winding is carrying a constant 5.0A current, while, Phase A winding carries a +5.0 A current and Phase B winding carries a -5.0A current.

In machines that produce reluctance torque, the magnetic flux distribution and magnetic flux path are a good measure of the torque generating capability of the machine. The magnetic circuit utilization is directly related to the phase contribution in the generation of electro-magnetic torque. In addition, the magnetic flux path are also an indication of the core losses in the given machine geometry. With the help of finite element analysis software, the magnetic field distribution under different phase excitation levels in the machine geometry can be obtained and this gives us an insight on the torque producing capability and the power density of the proposed machine geometries.

Fig (12) shows the magnetic field distribution in a conventional SRM with phase A carrying 5.0A current. The waveforms depict the magnetic field distribution when the rotor pole is perfectly aligned with the excited stator pole and when the rotor pole is unaligned with the excited stator pole.

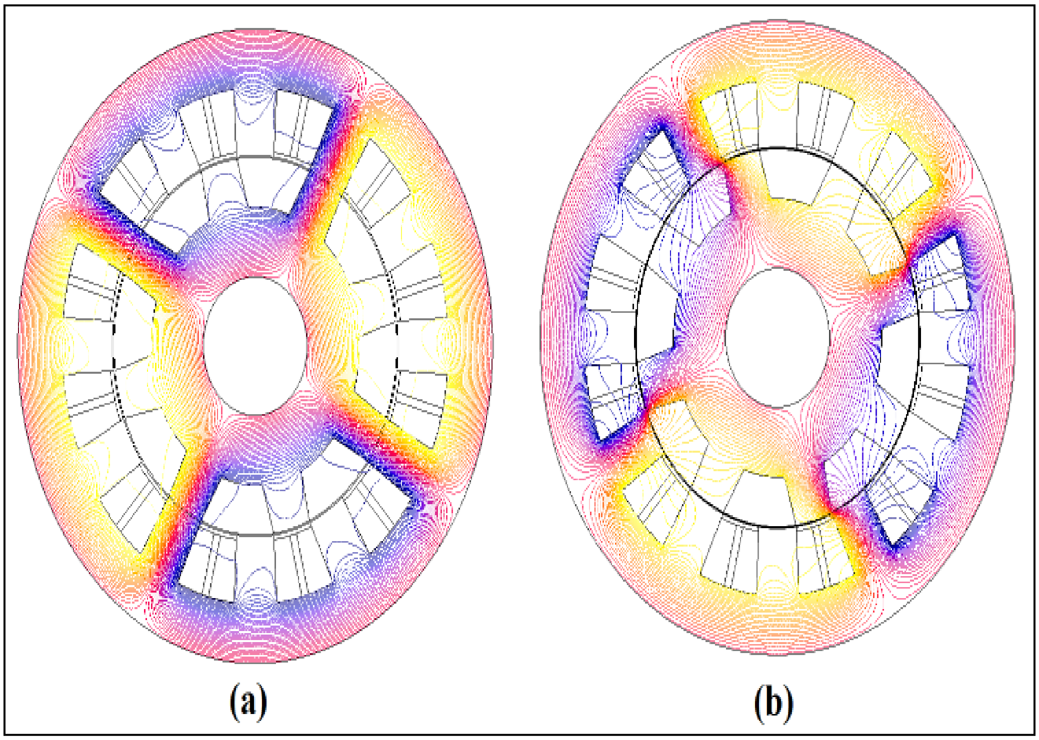

Figure 12: Magnetic field distribution of a conventional SRM (a) aligned position (b) unaligned position

At any given angular position, only 4 stator poles are involved in carrying the bulk of the magnetic flux through the magnetic circuit. In addition, the magnetic flux paths are longer resulting in higher core losses in the stator back iron.

Fig (13) shows the magnetic field distribution in a concentrated winding dc-assisted MCSRM.

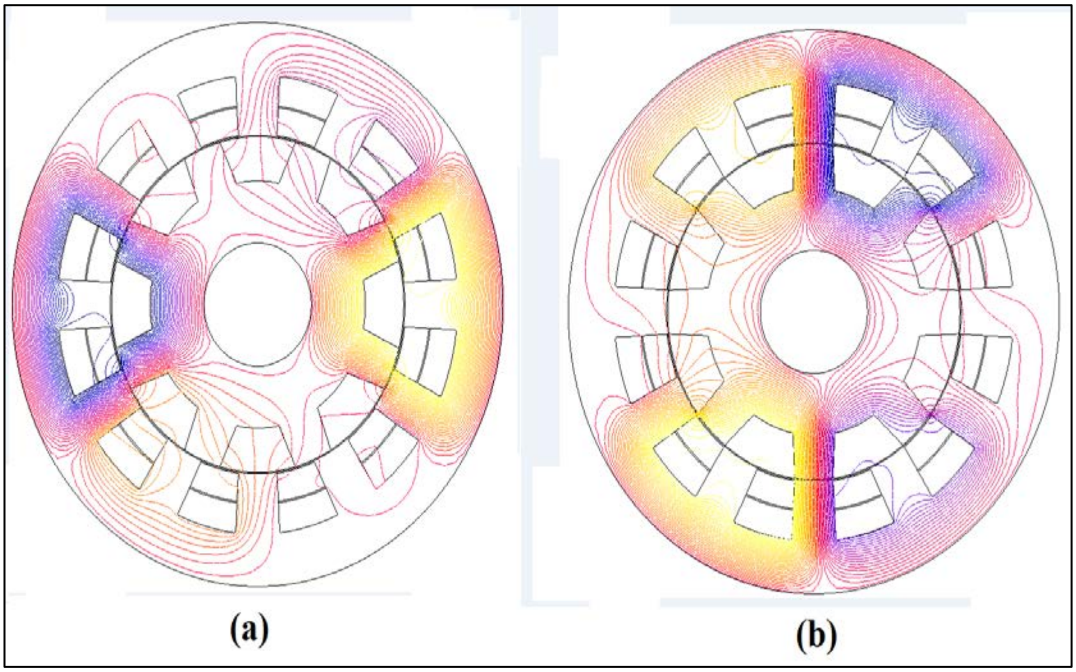

Figure 13: Magnetic field distribution of a concentrated winding DC-MCSRM (a) Unaligned position (b) Aligned position

As the phase and field winding is concentrated around a single stator tooth, this topology has the advantage of lower end-turn lengths, thereby requiring less copper than the fully-pitched topology. In addition, since bipolar excitation of 2 phases will produce positive motoring torque, in comparison to the conventional SRM, each phase of the concentrated winding DC-assisted MCSRM effectively contributes twice the amount of torque. Although, only 4 stator poles are involved in carrying the magnetic flux, the flux path lengths are 3/4th the flux path of the conventional SRM [3]. Thus, the increased torque contribution and the reduced core losses should result in the proposed topology to have a higher power and torque density in comparison to a conventional SRM.

Fig (14) shows the magnetic field distribution in a fully-pitched dc-assisted MCSRM.

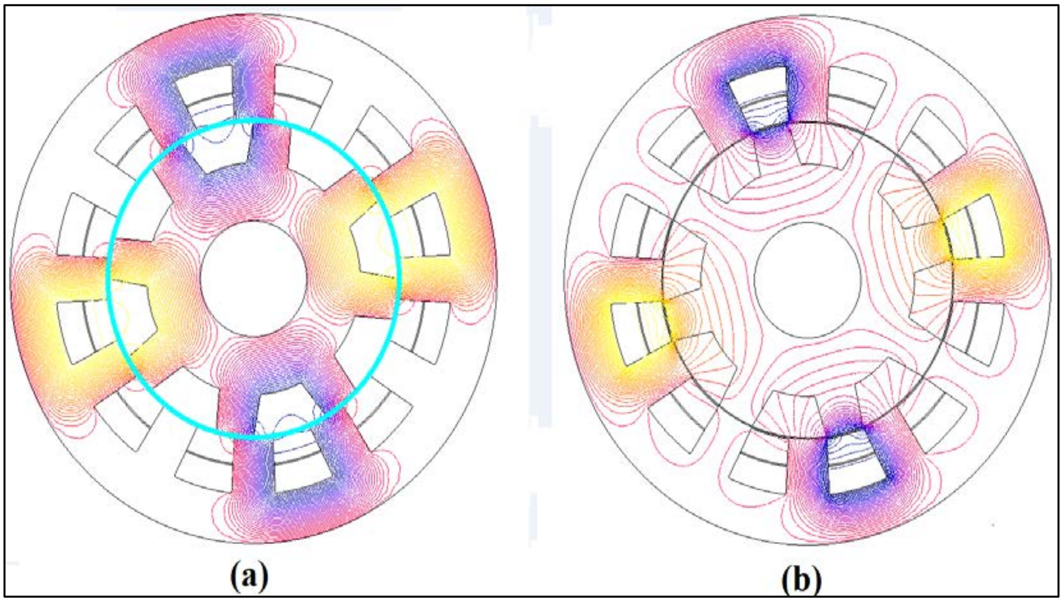

Figure 14: Magnetic field distribution of a Fully-Pitched DC-MCSRM (a) Aligned position (b) Unaligned position

Between the benchmark conventional SRM and the two proposed topologies, the fully-pitched DC-assisted MCSRM has the best magnetic circuit utilization. The fully-pitched configuration has the advantage of involving twice the number of stator poles with the similar phase excitation compared to that of a conventional SRM. This result in an increase in the effective torque contribution from each phase under the same excitation level and therefore, the fully-pitched configuration should deliver a higher average electromagnetic torque. In addition, the flux path for the fully-pitched configuration is almost half in comparison to that of the conventional SRM, since the magnetic flux flows through the two consecutive stator poles only. Thus, it can be concluded due to the reduced core losses and the improved effective torque contribution, the fully pitched configuration will have the highest power density and torque density of all the three machine topologies under consideration.

3.4 Advantage of the DC-assisted Winding

This section explains the energy conversion in a conventional Switched Reluctance Machine using the concept of co-energy and presents the advantage of adding a DC assisted excitation. Fig (15) presents a graphical interpretation of the energy conversion for a switched reluctance machine and Fig (16) represents the energy conversion plot for a DC-assisted SRM [13].

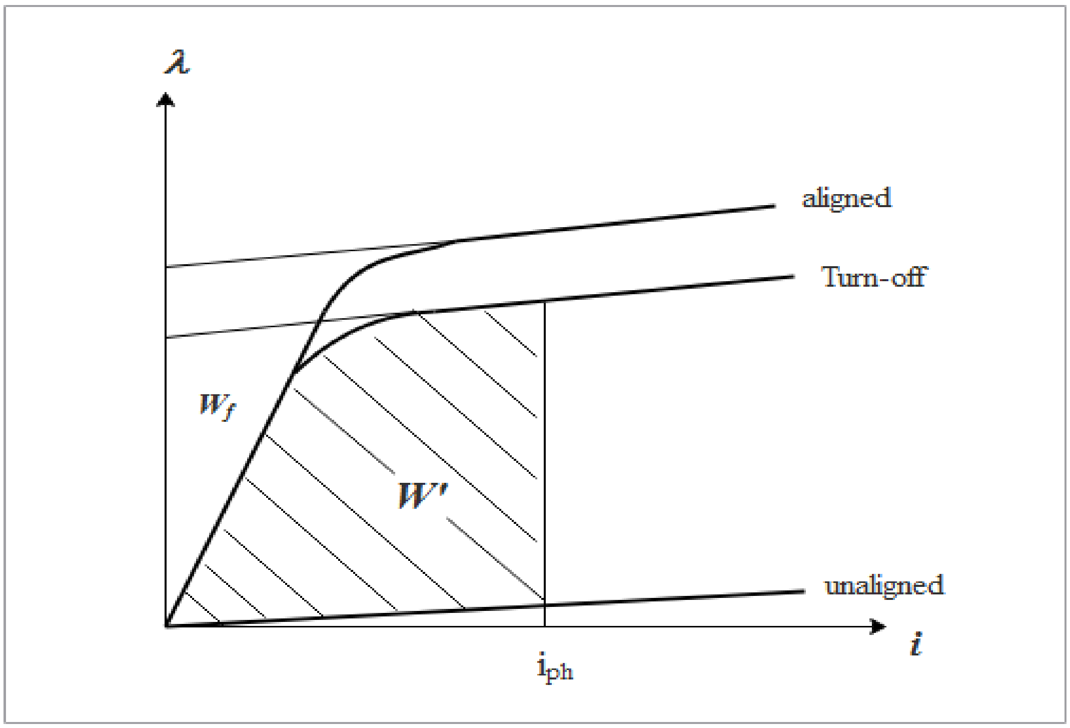

Figure 15: Energy conversion in a conventional SRM

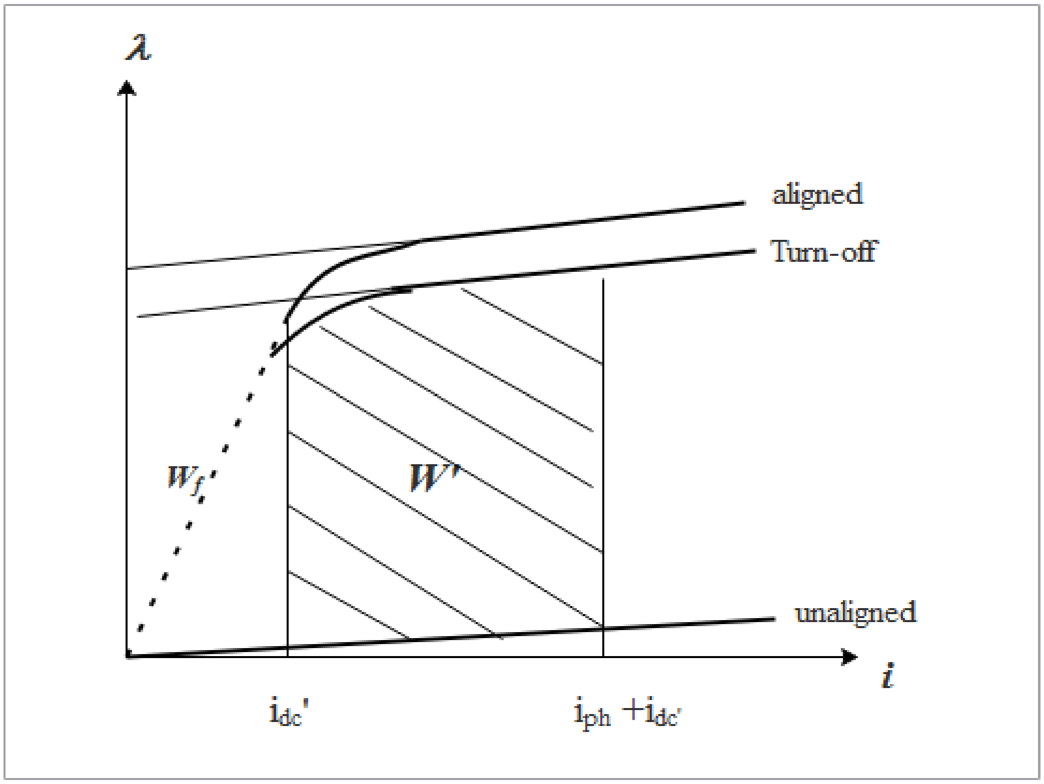

Figure 16: Energy conversion in a DC-assisted SRM

The mechanism of torque production in a conventional Switched Reluctance Machine is based on the inductance variations, which presents a conflict between high torque production demand and the low-cost demand for the drive. High commutation inductance results in high DC bus voltage of the drive, whereas for the same RMS current value, unipolar current operation raises the peak phase current to about 40% greater than that of machine using bipolar excitation. Fundamentally, the current in a conventional SRM is responsible for both field build-up and torque production. Therefore, torque production is heavily dependent upon current waveforms, and current turn on/off angles needs to be advanced to allow current build-up. The motivation behind using a DC-assisted excitation is to split each phase winding into two parts, one to be treated as normal phase windings and other to be fed by DC current to provide field excitation. This auxiliary winding helps achieve the built-in field excitation and better copper utilization such that the DC ampere-turns can be fully shared by the phase windings.

In a conventional SRM, at the turn on position, one part of the input energy is stored in magnetic field. With increasing inductance, the magnetic field energy will increase until the turn-off angle. The other part of the input energy will be converter to mechanical work and loss. The general expression of torque production is [13]

$$T = \frac{dW'}{d\theta}\bigg| i = const = \frac{\Delta W'}{\Delta\theta}\bigg| i = const$$

When the rotor position matches the turn-off position, phase switches are turned off. So the power source will stop to input energy and the stored magnetic field energy that needs to be released is feedback to the power source by the phase currents. The co-energy in a conventional SRM is given by [13]:

$$W' = \int_{o}^{iph} \lambda_{turn-off} di - W_o$$

Where W' is the co-energy and W_0 is the stored energy due to flux linkage.

Because of the DC-excitation, the co-energy is given as [13]:

$$W' = \int_{idc}^{iph+idc} \lambda_{turn-off} di - W_o$$

Thus, the DC-excitation has the potential to produce more torque than the conventional SRM since the energy conversion does not use the less effective triangular region due to the linear region of the B-H curve [13].

The other added advantage of the DC-excitation is that the turn-off angle of the phase currents can be much closer to the aligned position because the phase currents encounter only the saturated inductance and the change in inductance is minimal, allowing faster turn-off of phase currents at higher speed. In contrast, the conventional SRM encounters a significant variation in inductance near the aligned position and require advancing of the turn-off angle to prevent negative torque penalty.

As mentioned, the total DC ampere turns can be fully used throughout a period which makes maximum use of the DC winding copper and leads to a more efficient system. In addition, since the energy conversion area is a measure of the torque produced by the machine in every electrical stroke, for the same torque production the dc-assisted topology requires lower current values in comparison to a conventional SRM. This enables the use of smaller switches in the drive system and reduces the overall VA rating of the converter drive.

The primary disadvantage of the MCSRM was that the constant power torque-speed range was limited, because the effective voltage across each phase windings was only half the bus voltage at maximum. By using a DC-assisted field windings, the DC-link voltage per effective number of series turns in the machine will remain the same since each slot area of the hybrid topologies are radially fractional. Thus, the effective of back-EMF on phase current build up at high speed will be less in the proposed topologies, and this will allow high speed operation of the machine.

One can notice that the operation of the conventional SRM is limited to the first quadrant of the Flux-MMF graph. Thus, for a same co-energy area, the SRM converter will have to support higher phase currents and this will increase the converter cost. In the following section, the flux-linkage plots of the proposed hybrid topologies are presented to explain its benefits over the conventional SRMs.

3.5 Operating principle of the proposed hybrid excitation topologies

It was explained in the previous section, how the energy conversion area is a direct measure of the torque producing capability of the machine. It was also observed that the conventional SRM operates only in the first quadrant of the Flux-MMF graph, putting a stress on the converter VA ratings. The DC-assisted excitation helped reduce current carrying stress on the phase windings, since the Dc-current was now responsible for setting up the field excitation. Since the DC-field windings must carry constant current in saturated conditions, the overall stress on the inverter drive is reduced, thus reducing system cost. From the above trend, one can make a deduction that the converter VA ratings can be further reduced for the same torque producing capability, if the machine can operate in more than one quadrant of the Flux-MMF graph.

3.5.1 Fully-Pitched DC-assisted MCSRM

Fig (17) shows the magnetic flux linkage of the Fully-Pitched DC-assisted MCSRM, which was plotted to investigate the magnetic characteristics of the machine. The phase and field excitation of the concentrated winding-DC assisted MCSRM was also kept the same.

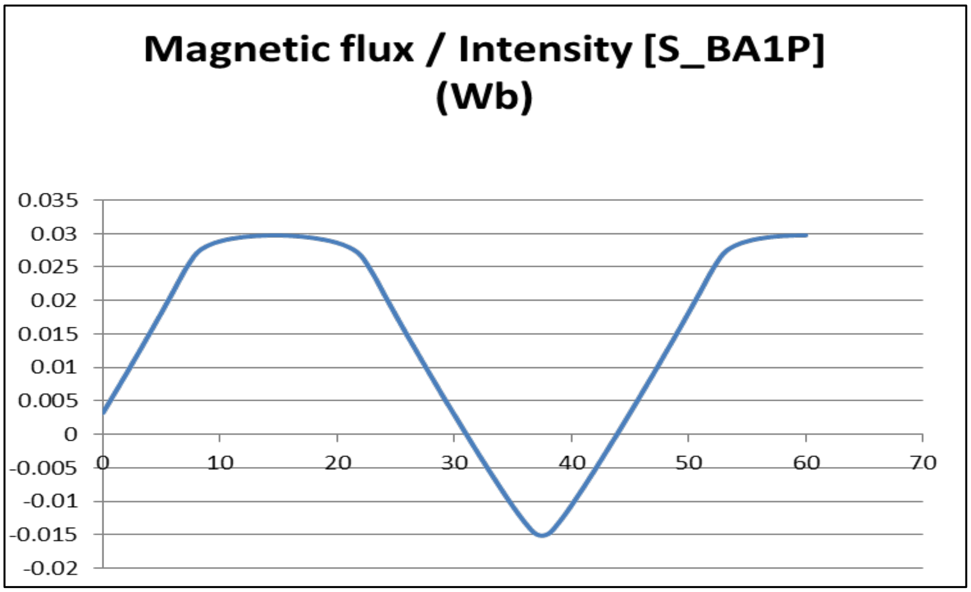

Figure 17: Magnetic Flux Linkage of Fully-pitched DC-MCSRM

The variation in the flux linkage from the aligned to the unaligned position is more for a fully-pitched configuration, which results in better torque capability. Since the flux links both positively and negatively, the Fully-pitched configuration exhibits a bipolar variation in flux linkage. In addition, since bipolar phase excitation is possible for the hybrid topology, the fully-pitched configuration has both bipolar flux and bipolar MMF variation, which implies that with this configuration the machine, operates in all the four quadrants of the flux-MMF graph. Thereby, to produce the same amount of torque, the fully-pitched configuration will require minimum phase current and the stress on the inverter will be minimum. Also, bipolar flux variation implies, the core will be less saturated in comparison to the concentrated winding topology, for the same phase excitation levels. Fig (18) and Fig (19) shows that as the rotor moves from the unaligned position to the aligned position, the flux links a phase both positively and negatively.

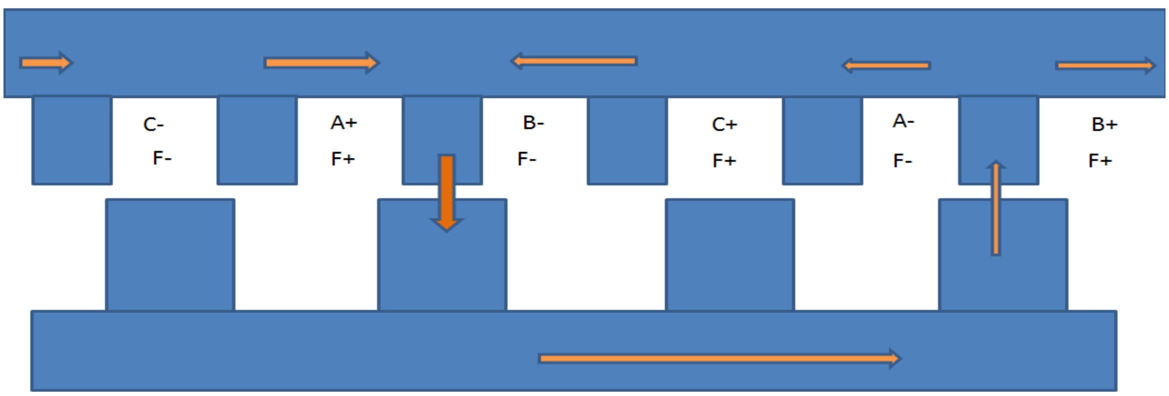

Figure 18: Fully-Pitched DC config - Aligned position. Flux links Phase A and Phase B winding positively, but links Phase C winding negatively

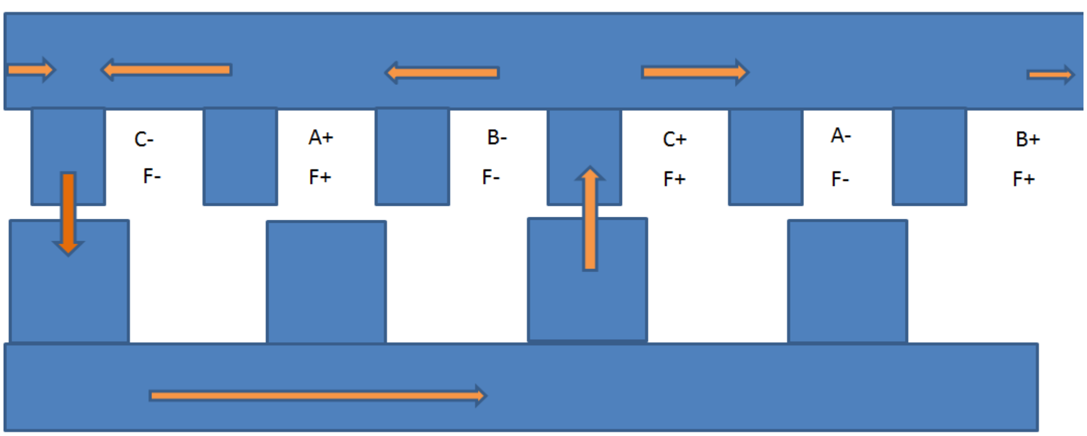

Figure 19: Fully-Pitched DC config - Unaligned position. Flux links Phase B and Phase C winding positively, but links Phase A winding negatively

3.5.2 Concentrated Winding DC-assisted MCSRM

Fig (20) shows the magnetic flux linkage of the Concentrated Winding DC-assisted MCSRM, which was plotted to investigate the magnetic characteristics of the machine.

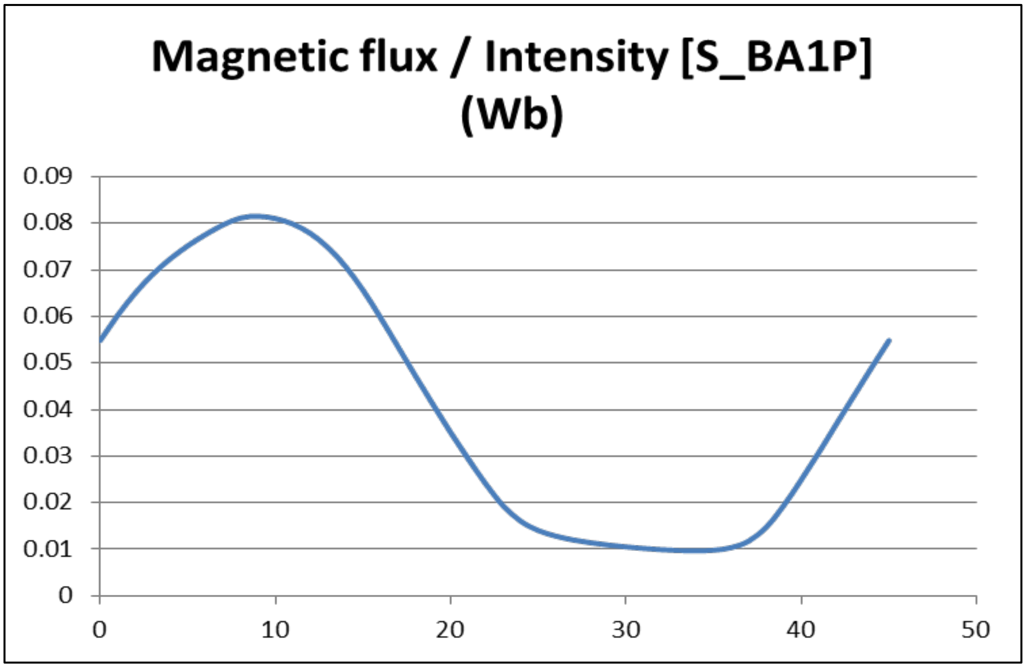

Figure 20: Magnetic Flux Linkage of Concentrated Winding DC-MCSRM

Unlike the fully-pitched configuration, the concentrated winding configuration does not exhibit bipolar variation in the flux linkage. This implies, as the rotor moves from the unaligned to the aligned position, the flux always links the phase windings positively. This is presented in Fig (21) & Fig (22). Because of unipolar flux variation and bipolar phase excitation, the concentrated winding configuration operates in the first 2 quadrants of the Flux-MMF graph. Thereby, the converter VA rating to produce a same amount of torque will be lower than that of a conventional SRM. In addition, the unipolar flux variation implies that the concentrated-winding topology will be more saturated for the same excitation level compared to the fully-pitched configuration. This would result in a lower back-EMF being generated under the same speed and phase excitation level and therefore, higher operating speeds can be achieved with the concentrated winding topology.

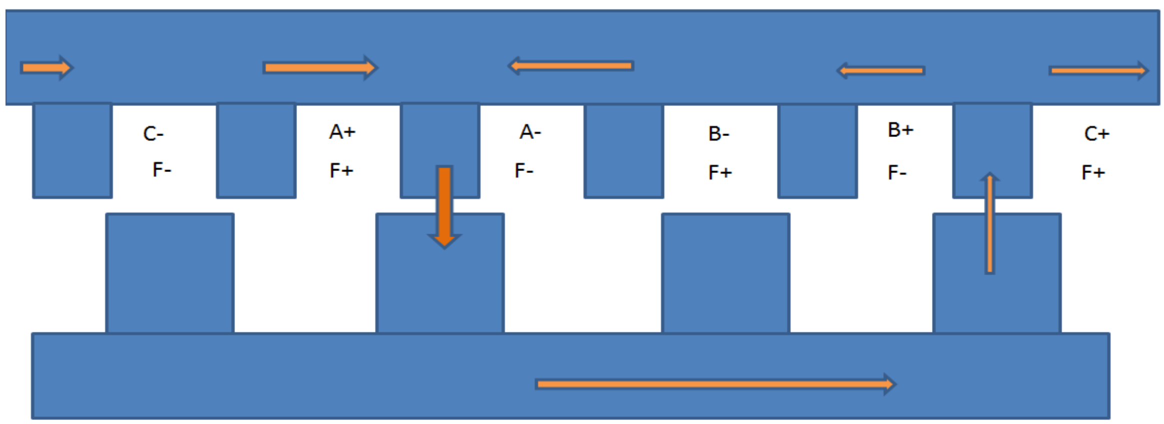

Figure 21: Concentrated Winding DC config - Aligned position. Flux links Phase A winding positively, but does not link Phase B and Phase C winding

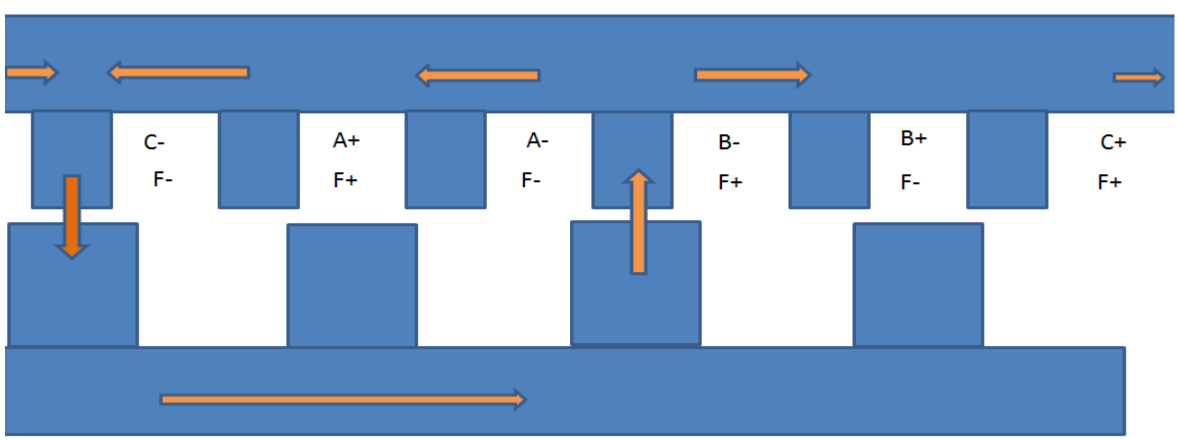

Figure 22: Concentrated Winding DC config - Unaligned position. Flux links Phase B winding positively, but does not link Phase A and Phase B winding

3.6 Comparison of benchmark SRM and concentrated-winding DC assisted MCSRM

A 660W, 3-phase 12/8 Maytag Neptune Washer SRM was selected as the benchmark conventional SRM. Fig (23) and Fig (24) shows the benchmark SRM against which, the proposed hybrid excitation topology was compared. Fig (25) presents the stator of the benchmark SRM. The stator windings were rewound and reconnected as a concentrated winding DC-assisted MCSRM. The number of turns per stator slots was held constant for both the machines, so that the performance can be completely verified based on their winding configurations.

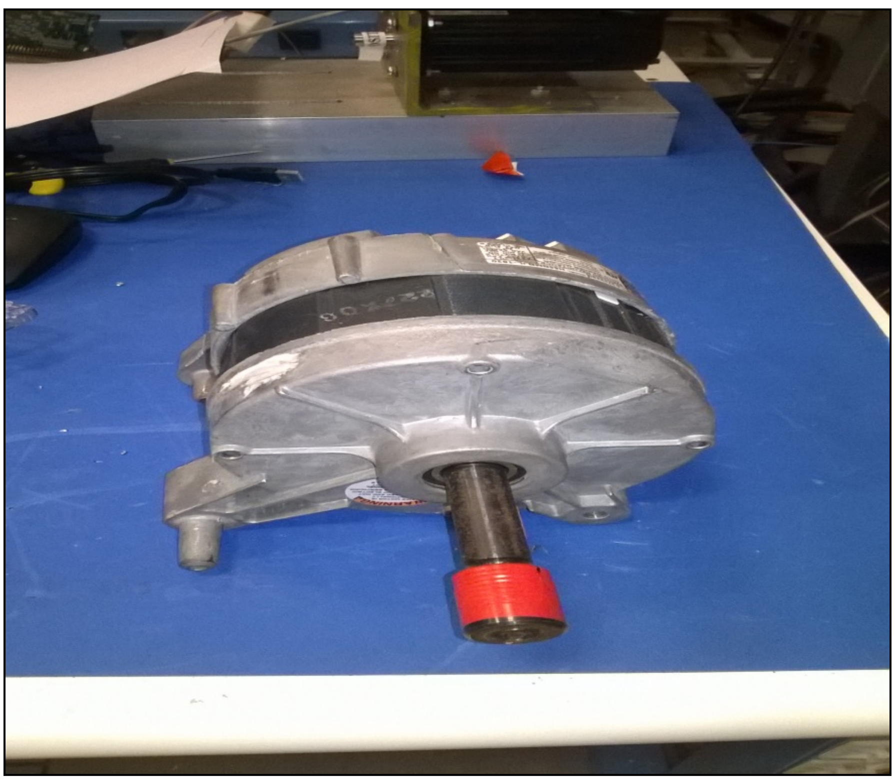

Figure 23: The 3 phase, 660 W, 12/8 Neptune Maytag Benchmark SRM

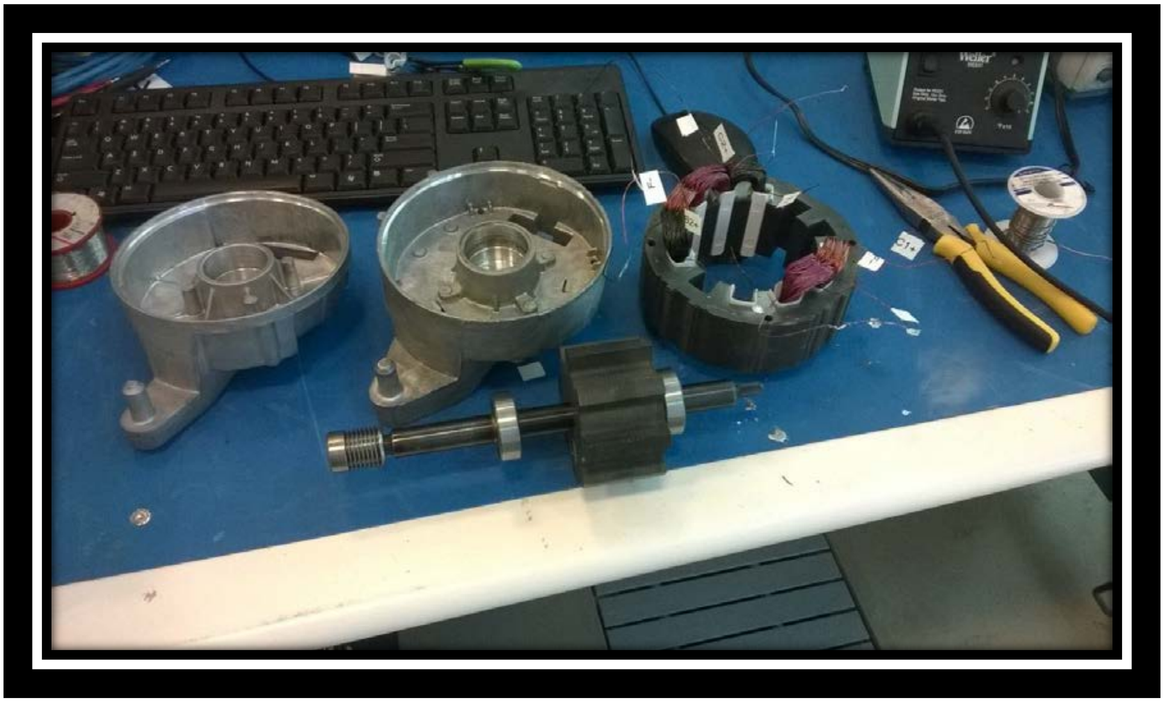

Figure 24: The 3 phase, 660 W, 12/8 Neptune Maytag Benchmark SRM

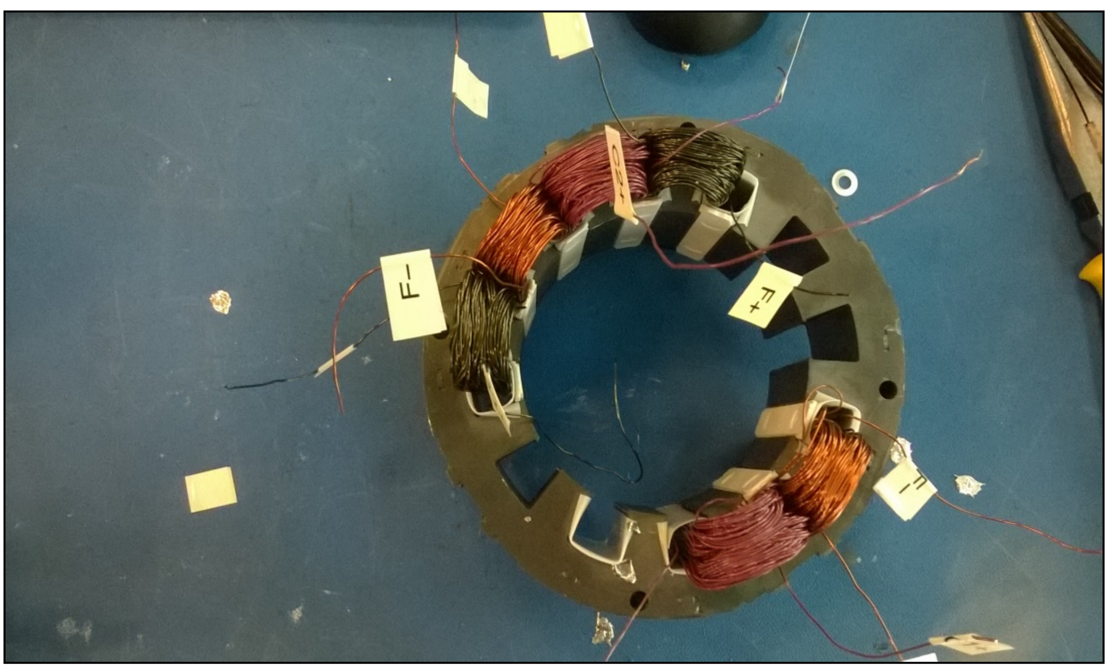

Figure 25: The stator and phase windings of benchmark SRM

3.6.1 Rated Performance Comparison

The performance of the concentrated winding topology was compared with the conventional benchmark SRM at base speed of 1000RPM. The base speed is defined as the minimum speed for rated power and maximum average torque with rated current. To compare the maximum torque density and power density of the two topologies, the performance is compared at base speed. Finite Element models of both the benchmark SRM and proposed topology were developed using Flux2D software and the performance was compared.

Fig (26) shows the electro-magnetic torque produced by the benchmark SRM when excited with continuous phase currents. Under the same excitation level, Fig (27) presents the response of the proposed Concentrated Winding DC-assisted MCSRM

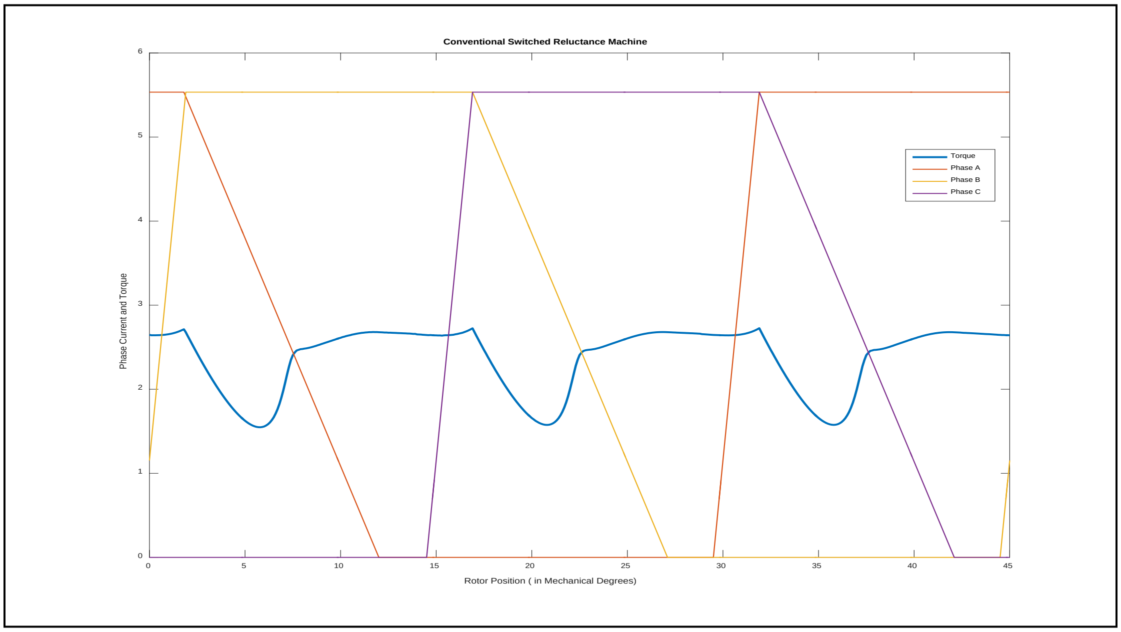

Figure 26: EM Torque production of conventional SRM

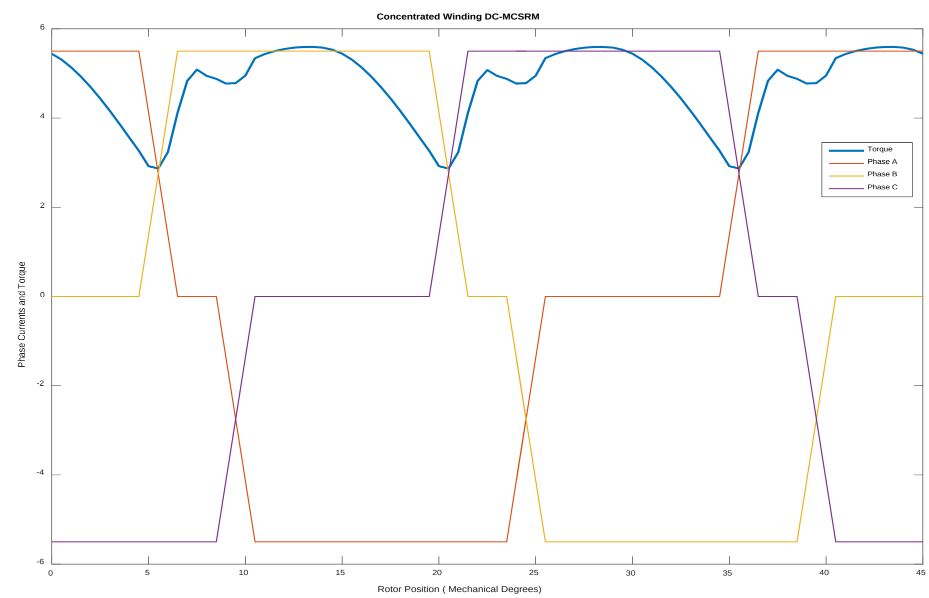

Figure 27: EM Torque production of concentrated winding DC-MCSRM

Table 1: Performance Comparison of the two machines at base speed, 1000 RPM

Parameters	**Conventional SRM**	**CWDC-MCSRM**
Average Torque	2.375 Nm	4.738 Nm
Torque ripple	57.63%	49.6%
RMS Phase current	3.611 A	4.43 A
Torque Density	-	185%
Power Density	-	120%

Results obtained show an improvement in the torque and torque ripple performance for the proposed Concentrated Winding DC-assisted MCSRM. The proposed topology also has a higher torque and power density than the benchmark SRM.

3.6.2 $T - i - \theta$ *Characteristics*

The performance of the proposed topology has been analyzed primarily using the $T - i - \theta$ characteristics obtained through FEA simulations. To derive the $T - i - \theta$ characteristics, one phase of the machine is excited with fixed amount of positive current, while another phase of the machine is excited with a same amount of negative current. The third phase is kept unexcited. The generated shaft is logged for a complete electrical rotor position sweep and the process is repeated for the entire operating current range with a fixed step change from the lowest to the highest step. The $T - i - \theta$ characteristics of the proposed topology are presented in Fig (28). For motoring mode, positive torque is used and for generating mode, negative torque is used.

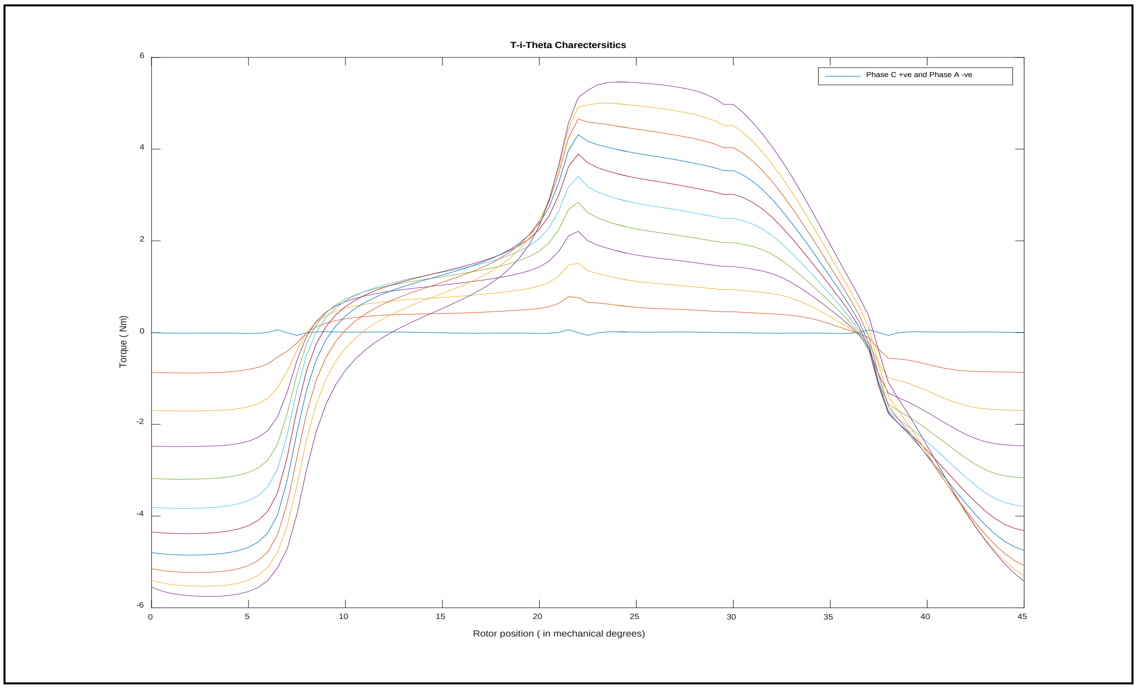

Figure 28: T-i-θ Characteristics of the machine with Phase C carrying positive current and Phase A carrying negative current

Fig (29) shows the static $T - i - \theta$ characteristics for different phase excitation combination. From this profile, the phase excitation sequence is determined so as to produce continuous positive torque over the entire electrical cycle.

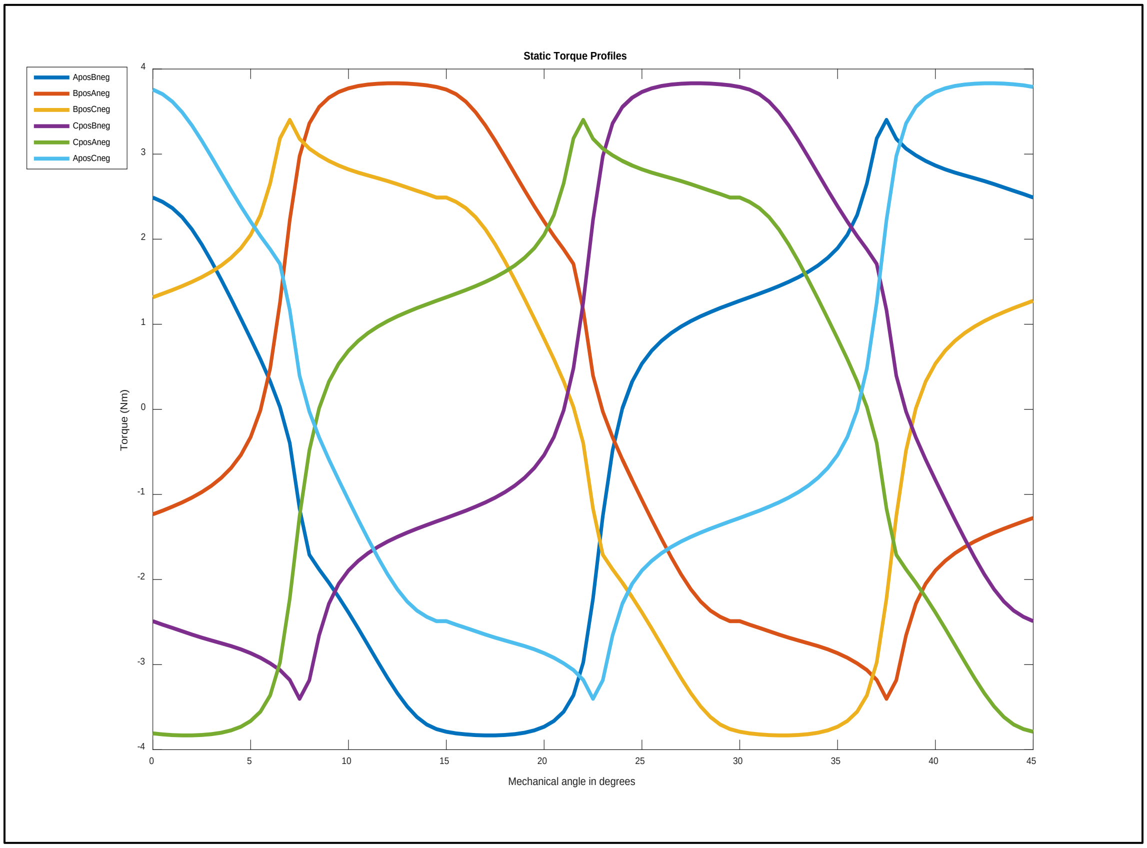

Figure 29: T-i-θ Characteristics for different phase excitation combination

Table 2: Dimensions, configuration parameters and rating of the 12/8 benchmark SRM [17]

Parameters	Symbol	Value	Units
Shaft Radius	R_{sh}	0.6	Inches
Radius to Rotor Yoke	R_{ry}	1.2025	Inches
Radius to Air Gap	R_{ag}	1.6325	Inches
Radius to Stator Yoke	R_{sy}	2.233	Inches
Outer Radius	R_{out}	2.7435	Inches
Air-Gap	A_g	0.015	Inches
Number of Phases	N_{ph}	3	-
Number of Stator Poles	N_s	12	-
Number of Rotor Poles	N_r	8	-
Number of Repetitions	N_{rep}	2	-
Periodicity	P	90	Degrees
Rotor pole width	P_w	15	Degrees
Stator pole separation	SEP	30	Degrees
Magnetic saturation	B_{sat}	1.8	Tesla
Magnetic permeability	μ_0	$4\pi\times10^{-7}$	Henry/meter
Relative permeability	μ_r	3300	-
Fill Factor	$Fill$	0.453	-
Stacking factor	STF	0.9	-
Length of Stack	L_{sstk}	1.846	Inches
Phase resistance	R_{ph}	2.1	Ohms
# of turns/pole	N_p	153	-
# of coils in series	N_{ser}	2	-
# of coils in parallel	N_{par}	2	-
Max. current in coil	I_{max}	5.5	Amperes
Power delivered	P	660	Watts
Operating Speed	ω	1000	Revolutions per minute

CHAPTER 4

CURRENT PROFILING FOR TORQUE RIPPLE MINIMIZATION

4.1 Introduction

To further improve the torque ripple performance of the DC-assisted Mutually Coupled Switched Reluctance Machine, an optimum current profile can be determined and follow it through a high bandwidth current regulator. This chapter presents a current profiling algorithm to minimize the ripple by taking advantage of finite element analysis design. The approach used in the proposed method creates a base profile for the operating torque-speed region, and then fine tuning it using real time feedback. The maximum machine speed or the base operating speed is considered while deriving the current profiles so that the profiles can perform well over the entire speed range.

To reduce torque ripple in a conventional Switched Reluctance Machine, various current profiling and phase torque distribution methods appear in the literature. The method used in this research has similarities with the direct instantaneous torque control method and has been successfully implemented to obtain a improved current profile for a Switched Reluctance Machine in [6][7]. Similar to [6][7], the proposed method uses an approach of creating an initial base profile for the operating torque-speed region, and then fine tuning it using a real-time torque feedback. The rising and the falling slopes of the base profile are determined offline and the maximum operating speed is considered while deriving the current profiles so that the profile can perform well over the entire operating speed range. This method for obtaining an optimum current profile heavily depends on the $T-i-\theta$

characteristics of the machine. The conventional $T - i - \theta$ characteristics of the DC-assisted MCSRM are not using flat, and this chapter shows that to obtain an optimum current profile for a wide range of torque commands, geometric optimization of the machine is needed to achieve a more flat $T - i - \theta$ characteristics. The current profiling method proposed in this chapter is not suitable for $T - i - \theta$ characteristics with peaks in this profile. In that case, the profiling algorithm results in a current profile with two prominent peaks in them, which are difficult to follow at high speeds. The $T - i - \theta$ characteristics of the test machine have a peaky profile for higher torque values, and the limitations that this result in the profiling algorithm is also presented in this chapter. The proposed method brings the machine and controller designs together in a single process.

There are some key issues that need to be considered in torque ripple sensitive applications which are not addressed in this chapter such as the unavoidable manufacturing variations which make the $T - i - \theta$ characteristics of the built machine different from that obtained from the finite element design.

4.2 Operating Torque-Speed Range of the Machine

The machine speed range is directly found from the torque speed characteristics. For the DC-assisted MCSRM, the base speed range is considered as the same the bench-mark Neptune conventional SRM, which was 1000 RPM. The machine is required to generate the average maximum torque and a predetermined level of torque ripple over this entire operating speed range. The proposed current profiling method takes into consideration the operating speed range, so that the phase current is able to follow the command current for the given DC Bus voltage. As it was mentioned in chapter 3, the rate of change in flux linkage is highest at the highest speed with maximum change in reference current.

$$\frac{d\lambda}{dt} \cong \frac{\lambda(i_{k+1},\theta_{k+1}) - \lambda(i_k,\theta_k)}{\Delta T} \quad \text{.........} \ (4.1)$$

Since the rate of change of flux linkage with time is equal to the voltage required to make the change is current, the torque ripple performance can be achieved at a higher speed, if the total required voltage corresponding to the rate of change of flux linkage with respect to time and the resistive voltage drop is less than the available bus voltage.

4.3 Initial Current Profile

The second aspect of the torque ripple minimization method involves high performance controller. In a DC-assisted MCSRM, the phases are continuously commutated in and out in synchronization with the rotor position to maintain a positive torque production and an unidirectional motion of rotation. Initially, an offline method is used to generate the initial base profiles based on the $T-i-\theta$ characteristics as shown in Fig (30)

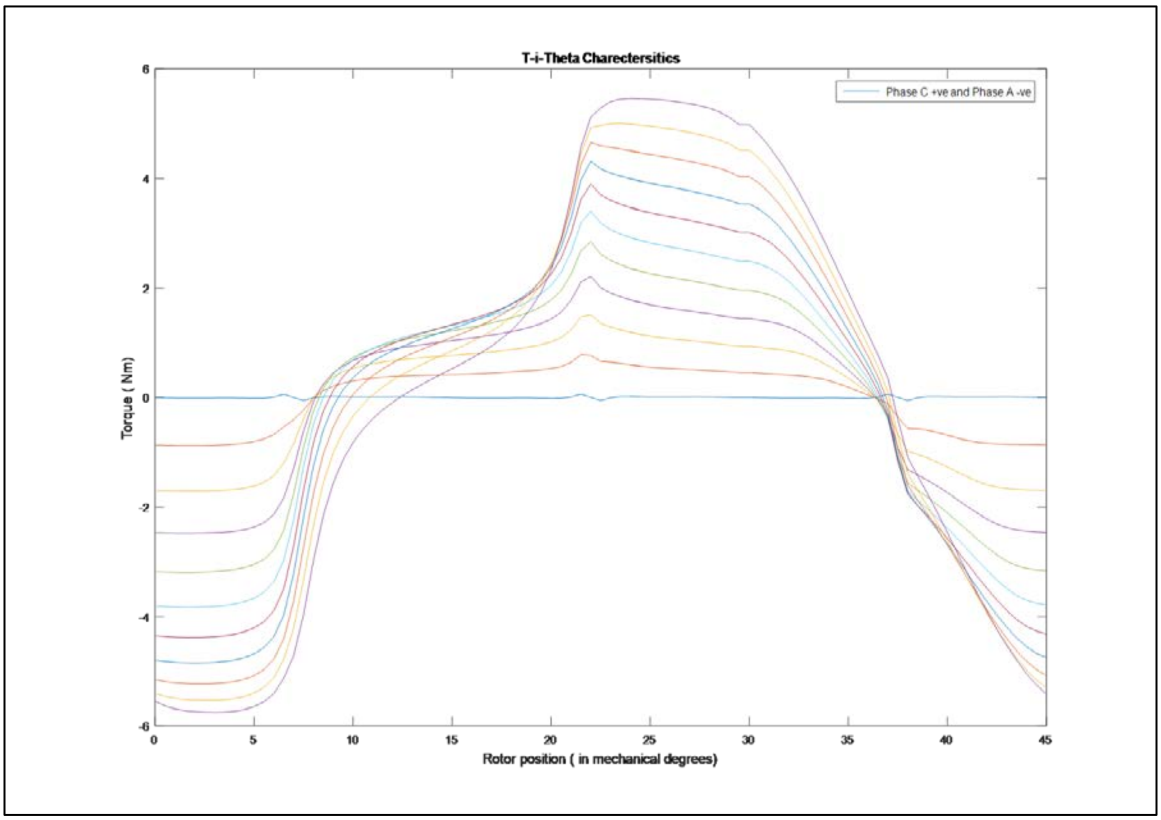

Figure 30: T-i-θ Characteristics of the machine with Phase C carrying positive current and Phase A carrying negative current

The machine controller is designed based on a fixed torque command. The initial $T-i-\theta$ characteristics are obtained from the static torque characteristics of the machine, which makes the initial current profile inadequate to minimize the torque ripple to the desired level. The current profile required to meet the given torque command is updated through a fine-tuning process.

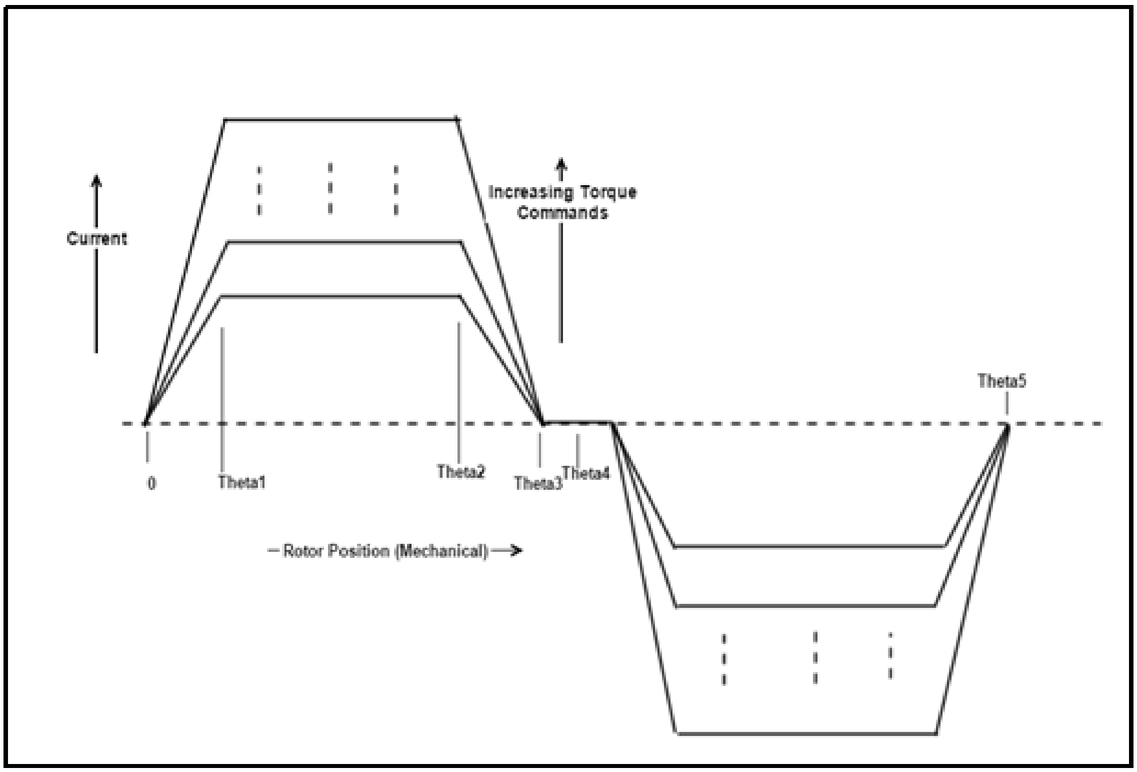

Figure 31: Initial Base Current Profiles

The Fig (31) shows the proposed initial base current profiles for different torque commands. For any phase combination, the angle zero is the point where the static torque profile for the given phase combination changes sign from negative to positive. The positive half of each current profile has 4 distinct regions based on the angular intervals shown in Fig (31). The angle θ_1 is the angle required to rise to the peak current level for the command torque. The slopes in the intervals of $0 to \theta_1$ and $\theta_1 to \theta_2$ depends on the torque-speed characteristics of the machine at rated operating speed, 1000 RPM in the case of this test machine. This is because the local slope of the current profile should not cross the achievable rate of change of current at any point in the profile; the objective is to follow a given current profile. The interval 0 to θ_1 is at the unaligned position for that phase combination. To find the angle θ_1, the worst case is selected. Therefore, at first it is required to find the maximum current required to produce the maximum command torque. This point corresponds to the maximum torque value from the $T-i-\theta$ characteristics and is denoted as $I(T_m,\theta_p)$, where T_m is the maximum torque from the $T-i-\theta$ characteristics and θ_p is the angular position where T_m is produced for the given phase excitation. The level of the current $I(T_m,\theta_p)$ is an important value which is required to be reached at the maximum speed for that command torque. For the machine under test, T_m is 5.6Nm, $I(T_m,\theta_p)$ is 10A and θ_p is 26.5 mechanical degrees at the maximum operating speed of 1000rpm, when phase A is excited with negative current, Phase C is excited with positive current and no current flowing through Phase B.

The value of θ_1 can be obtained in one of the following 2 ways:

1.) The first is an analytic approach to determine θ_1

$$V_{dc} = M(\theta)\frac{di}{dt} = \frac{M(\theta) di \omega_m}{d\theta}$$
$$\Rightarrow \theta_1 = \frac{M(\theta_1).I(T_m, \theta_p).\omega_m}{V_{dc}} \quad \text{......... (4.2)}$$

Where $M(\theta_1)$ is the mutual inductance at angle θ_1 from the inductance profile at low current, and V_{dc} is the magnitude of the supply voltage. The back-EMF term is neglected in the above equation since at the unaligned position and the stator core is not saturated. The resistive voltage drop is also being ignored in the derivation for initial profiles.

2.) The other method is to use finite element analysis to determine the angle θ_1. A coupled simulation platform is developed where the machine is a Flux2D based finite element model and the controller is developed on MATLAB-Simulink. The machine is operated at maximum operating speed and the T_m is the command torque, implying a command current of $I(T_m, \theta_p)$ for any one of the phases. For the given DC Bus voltage, the angle θ_1 is the mechanical degree equivalent of the time taken for the phase current to reach the command current value at the maximum operating speed.

A MATLAB script was developed to iteratively solve the equation (4.2)

In the angular interval of θ_1 to θ_2, the active phases have the maximum torque contribution to the total average torque. For the DC-assisted MCSRM, the during this interval one of the phases is carrying positive currents, the other phase is carrying an equal but opposite negative current and the third phase is carrying zero current. This implies, the interval θ_1 to θ_2 be the region where one of the phases has been completely commutated out of conduction. The active phases need to support the torque generation up until the angle θ_2, which is the summation of the average active phase angle and the rising angle θ_1. The active phase angle is given by $2\pi/(N_R N_{ph})$ and thereby, the angular position θ_2 is given as:

$$\theta_2 = \theta_1 + \frac{2\pi}{N_R N_{ph}} \quad \text{............ (4.3)}$$

Where N_R the number of rotor is poles and N_{ph} is the number of phases.

In the region between θ_2 to θ_3, the rotor pole is aligned with the stator pole and the back-EMF cannot be neglected. To determine the falling slop region, similar coupled simulation approach is taken to determine the minimum slope the current profile can have at the maximum operating speed with the given DC-Bus voltage.

The current is zero in the interval θ_3 to θ_4. The angle θ_4 is chosen to half of the angle θ_5 so that we obtain symmetrical conduction period for the positive half and negative half of the phase currents. The angle θ_5 is mechanical degrees equivalent of one complete electrical cycle. Since the DC-assisted MCSRM is an 8-pole machine, the angle θ_5 is obtained as 45 mechanical degrees and the angle θ_4 is thereby equivalent to 22.5 mechanical degrees.

These four angular positions are to be used to create the initial base profile for any machine. The values of θ_2 and θ_4 are $15+\theta_1$ and 22.5 mechanical degrees, respectively for the DC-assisted MCSRM tested in the research. These angular calculations are completed offline before the fine-tuning process. The fine-tuning process with the torque feedback will eventually take care of the corrections required for not accurately considered the back-EMF while generating the base profile. The rising and the falling slope of the current profile are given by

$$S_r(T) = \frac{I(T,\theta_p)}{\theta_1}$$

$$S_f(T) = \frac{I(T,\theta_p)}{\theta_3 - \theta_1} \qquad \text{………… (4.4)}$$

Where $I(T,\theta_p)$ is the current from the $T-i-\theta$ characteristics at the point (T,θ_p). The controller is required to follow the profile at the specified speed range for a torque command for maintaining the specified torque ripple. At higher load currents, the inductance profile changes due to saturation in the magnetic circuit. The inductance is not the same at a certain rotor position for various loading conditions. The current profile should be generated such that it can be followed over the entire speed range for a particular torque command. Therefore, for any given torque command there is always a maximum speed up to which the machine can be controlled to generate that torque. This allows maximum torque to be available within a certain minimum speed range, and the minimum torque to be available at the maximum speed range. The angular positions of $\theta_1, \theta_2, \theta_3, \theta_4$ and the peak torque values are the parameters required to generate the initial current profile. The angular positions of θ_1 and θ_3 are selected for the maximum operating speed, and the current profiles are assumed linear. To extract more torque from the phase currents at lower speeds, the initial base profiles can be done with a variable θ_1 and θ_3, since at low speeds the controller can follow a steeper slope. A changing slope compensation technique to adjust θ_1 and θ_3 as a function of the instantaneous speed can be accommodated to improve the efficiency. The performance will be better at the expense of increased burden on the controller processor.

A series of initial current profiles for a series of torque commands are created from the initial base profiles using the static $T - i - \theta$ characteristics. Finite Element Analysis was used to simulate the machine model with the initial base current profiles and based on the torque response of the machine; real time feedback is implemented to optimize the current profile to improve the torque ripple performance of the machine.

Fig (32) shows the FEA results for the initial base profiles. The peak current value is 5.5A and the average torque is 4.8Nm with a torque ripple of 53.4%.

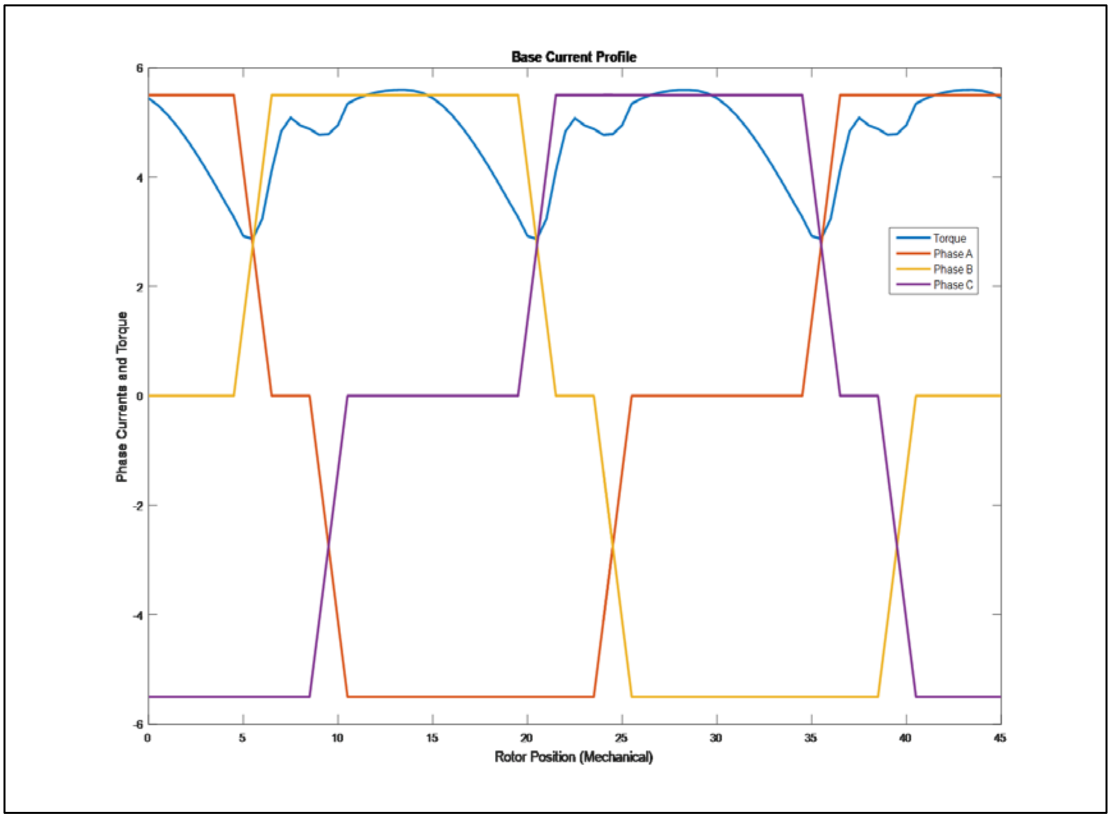

Figure 32: FEA simulation with the initial base current profiles

The $T-i-\theta$ characteristics give the magnitude of the current required to have a constant torque output. For a certain rotor position, it is directly available when there is no torque overlap. When the two phases overlap, the algorithm determines the shared magnitudes of currents in the two phases in such a way that the total torque can be maintained to be a constant. The algorithm modifies the same current profile at the interval where it overlaps with the linear segment of the incoming and outgoing phase current profiles. The algorithm initially works only on the positive half of the current profile and mirrors the optimization to the negative half. An example of the algorithm working on the positive half of the initial current profile is shown in Fig (34). The slopes in the $0-\theta_1$ and $\theta_2-\theta_3$ intervals are kept fixed while generating the initial profile. The static $T-i-\theta$ characteristics are generated with positive current in one phase and an equal but opposite current in other phase, with the third phase not carrying any current.

The required current in the profile for the position range from $0-\theta_1$ and $\theta_2-\theta_3$ is linear and obtained from Equations (4.2) to (4.4). The current in the profile for $\theta_1-\theta_2$ is generated in two steps as described in Fig (33). The figure explains the steps for an arbitrary position θ_i. At first, the portion of the profile I_1 is obtained from the adjacent conducting phase current falling or rising section, which is again available from the Equation (4.2) to (4.4). The portion I_2 is obtained from the following equation:

$$I_2 = i[\{T_{com} - T(I_1,\theta_i)\},\theta_i] \text{ .... } (4.5)$$

Where $T(I_1,\theta_i)$ is the torque generated due to the current I_1 at the position θ_i contributed from the adjacent conducting phase. The remaining torque and the same position are used to find the remaining portion of the profile. This two-step method is repeated for the range from θ_1 to θ_2.

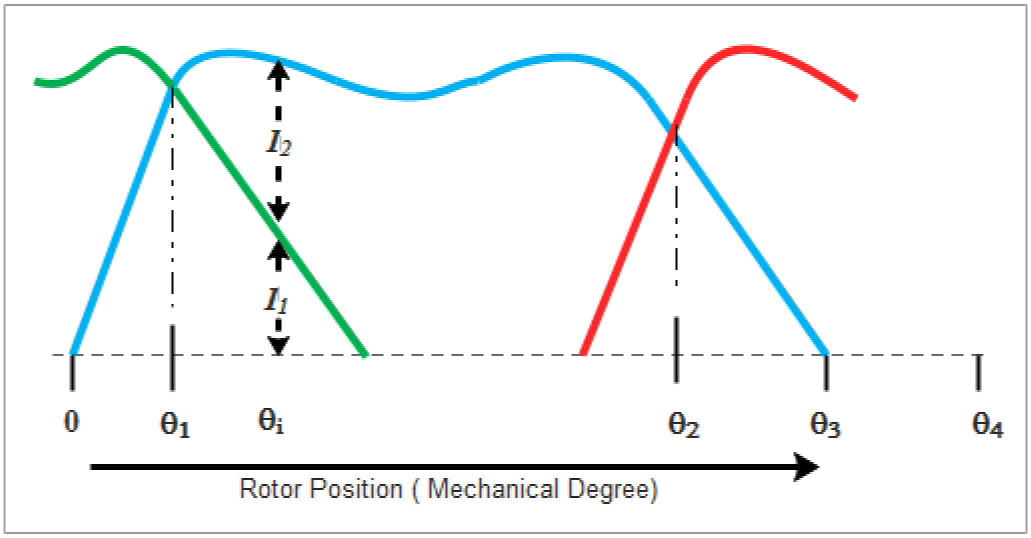

Figure 33: Generating the profile for active region

Fig (34) shows the current profile for a command torque of 2.0Nm, when the algorithm was applied on the positive half of the current profile. The change in the current profile in the

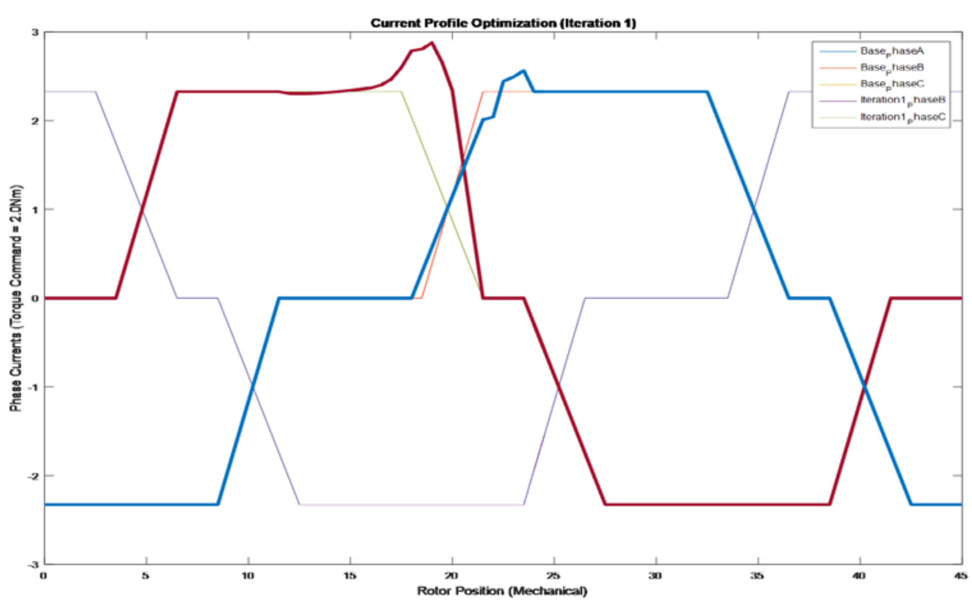

Figure 34: Torque Command = 2.0 Nm. Algorithm applied to positive half only

commutation region with respect to the initial base current profile is apparent. The same algorithm was then applied over the entire electrical cycle, which is equivalent to 45 degrees mechanical; the result of the 1st iteration of the optimized current profile is shown in Fig (35)

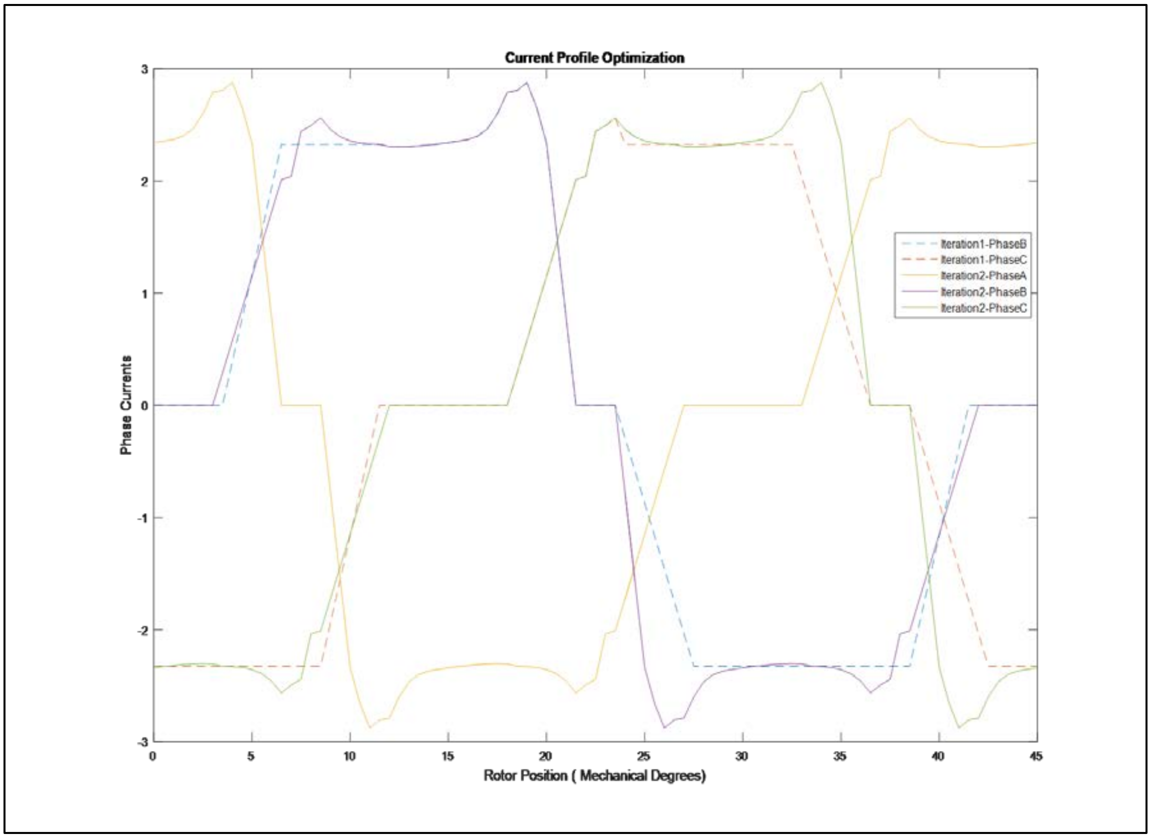

Figure 35: Current Profile after 1st iteration. Command Torque = 2.0 Nm

Unlike the conventional SRM, where the phase currents are independent of each other, normal operation of the DC-assisted MCSRM required that the summation of the three phase currents be equal to zero. Since the phase winding are Y-connected, which enabled us to use a standard six-switch VSI, we cannot have unbalanced current flowing through the phase winding. If the phase winding was Δ-connected, unbalanced currents would result in generation of negative torque and the hamper the torque performance of the machine.

4.4 Fine Tuning with Torque Feedback

The optimum current profile can only be found utilizing torque feedback either through a high-fidelity simulation model or from a dynamo-meter experiment. In the simulation approach, the current profile is generated through an offline coupled simulation model. A finite element machine model is coupled with a dynamic controller model with rotor position and torque feedback as shown in Fig (37) to derive the optimum current profile. The procedure is followed for all the current profiles in the desired torque speed range.

The current profile after fine tuning with position and torque feedback is shown in Fig (38). All the three phases are updated simultaneously while the fine-tuned profile is generated. A tuning of the rising and the falling slopes is allowed during the procedure to avoid any discontinuity at the junction of the fine-tuned segment and the fixed slope segment. The current profile can be shifted with several iterations for fine tuning. For the same machine, the same constant torque output can be achieved with different profiles. The final torque profiles for a constant torque command can be different for different values of θ_1 and θ_3. The final profile also depends on the algorithm which finds the initial profile. A current profile with lower dynamics is desired so that it can be easily followed in real time over the entire operating range. For a constant torque command, the commutation period is the critical region. The current controller must be capable of following the current profile for the maximum operating speed. If this can be ensured, then the controller can easily make the machine follow the current profile over the entire speed range of operation.

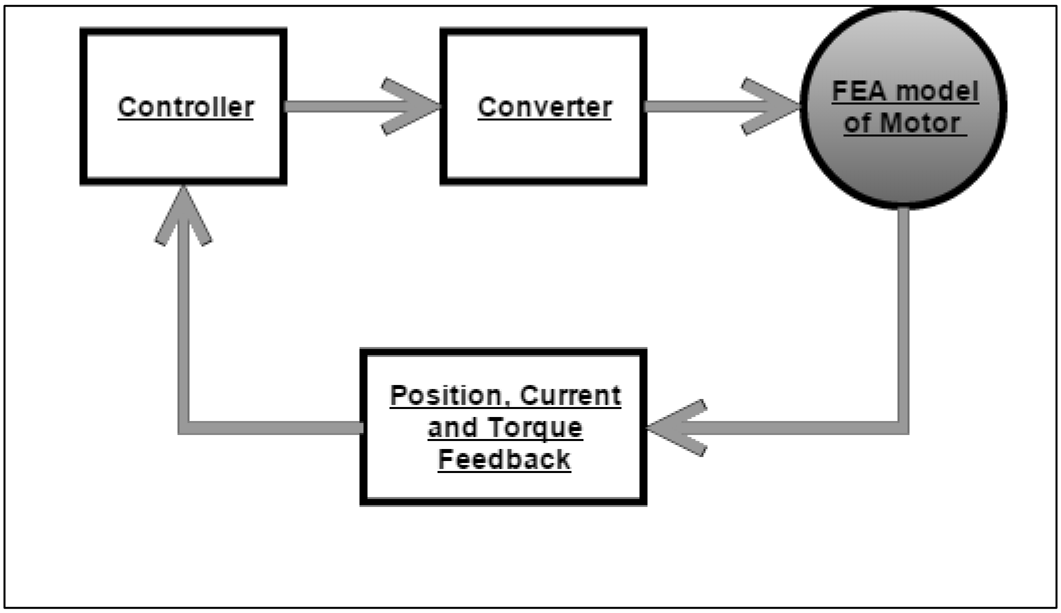

Figure 36: Fine tuning of torque profile

The proposed values of θ_1 and θ_3 are suitable for all the profiles at all speeds. The fine-tuning method allows slight variation in the values of these angles and comes up with a different profile with a different value of θ_1 and θ_3. The final profile depends heavily on the initial base profile which the fine-tuning algorithm starts with. The torque performance does not change if the controller can follow the current profile at the maximum operating speed.

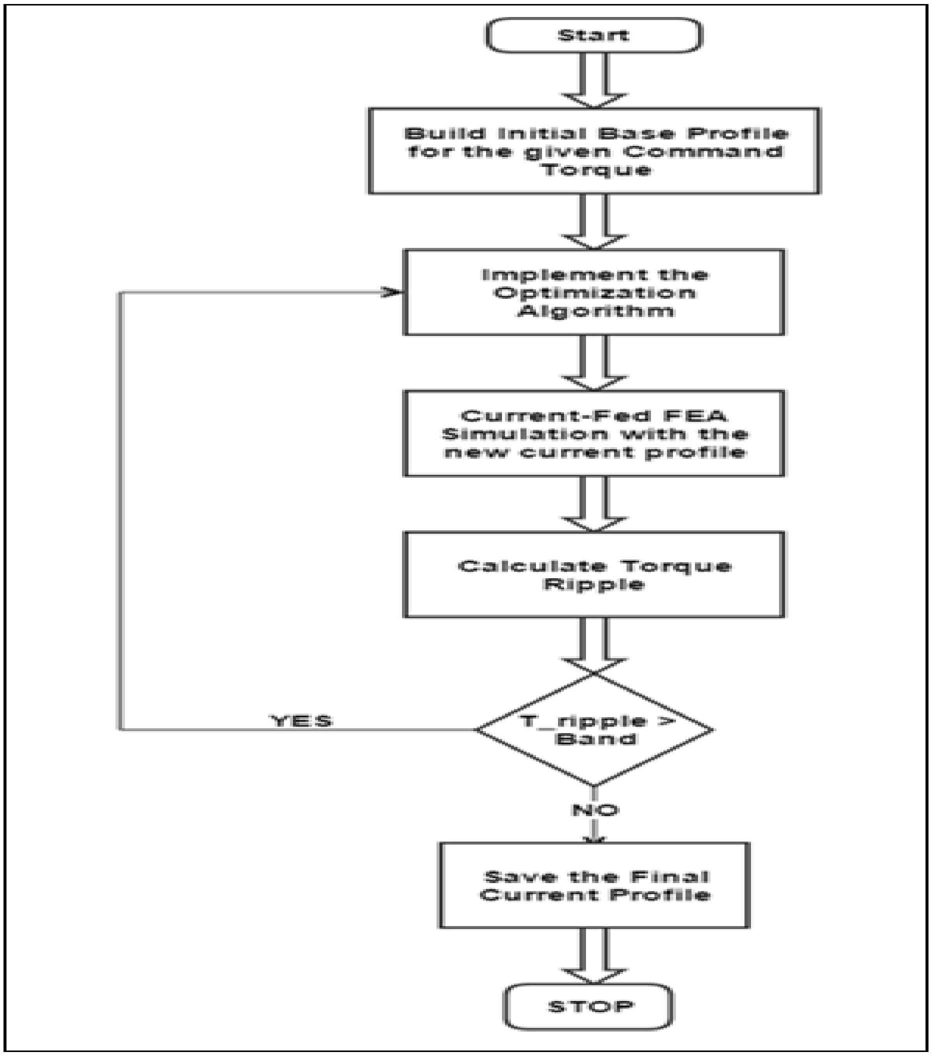

Figure 37: Flow chart of dynamic modulation

The desired current profiles are modified dynamically through the coupled simulation based on the torque output of the finite element model. The fine-tuning process start with the initial profile shown in Fig (35) and the coupled simulation follows the flow chart of Fig (37).

During the fine-tuning process, it saves the error between the command torque and the reference torque and based on the error, updates the current profile for the next iteration. The rising and falling slopes are adjusted accordingly and after multiple iterations, the torque ripple reaches an acceptable minimum level and the co-simulation stops.

Fig (38) shows the various current profiles generated during the fine-tuning process for a command torque of 2.0Nm. The corresponding torque profiles are shown in Fig (39).

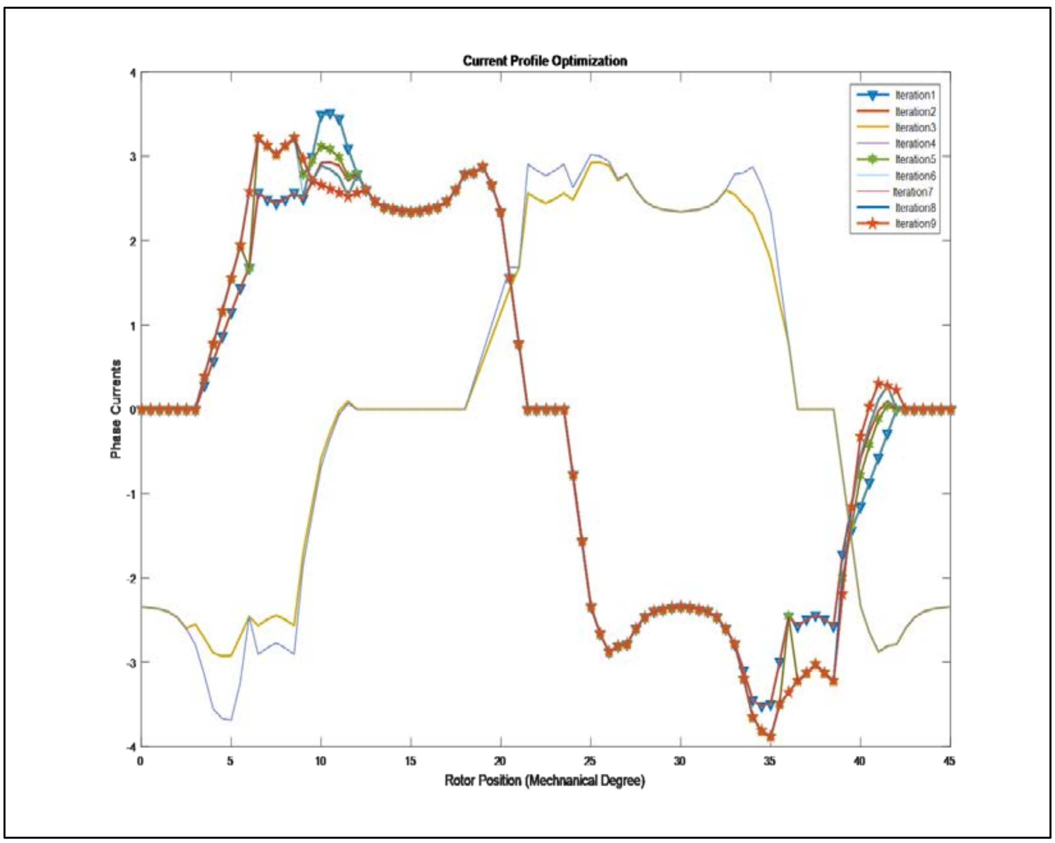

Figure 38: Optimization of current profiles

The initial high ripple in the torque profile is due to the sub-optimal current profile generated from the static $T-i-\theta$ characteristics. The current profiles are being effectively optimized during the fine-tuning process to bring down the ripple within a predefined band.

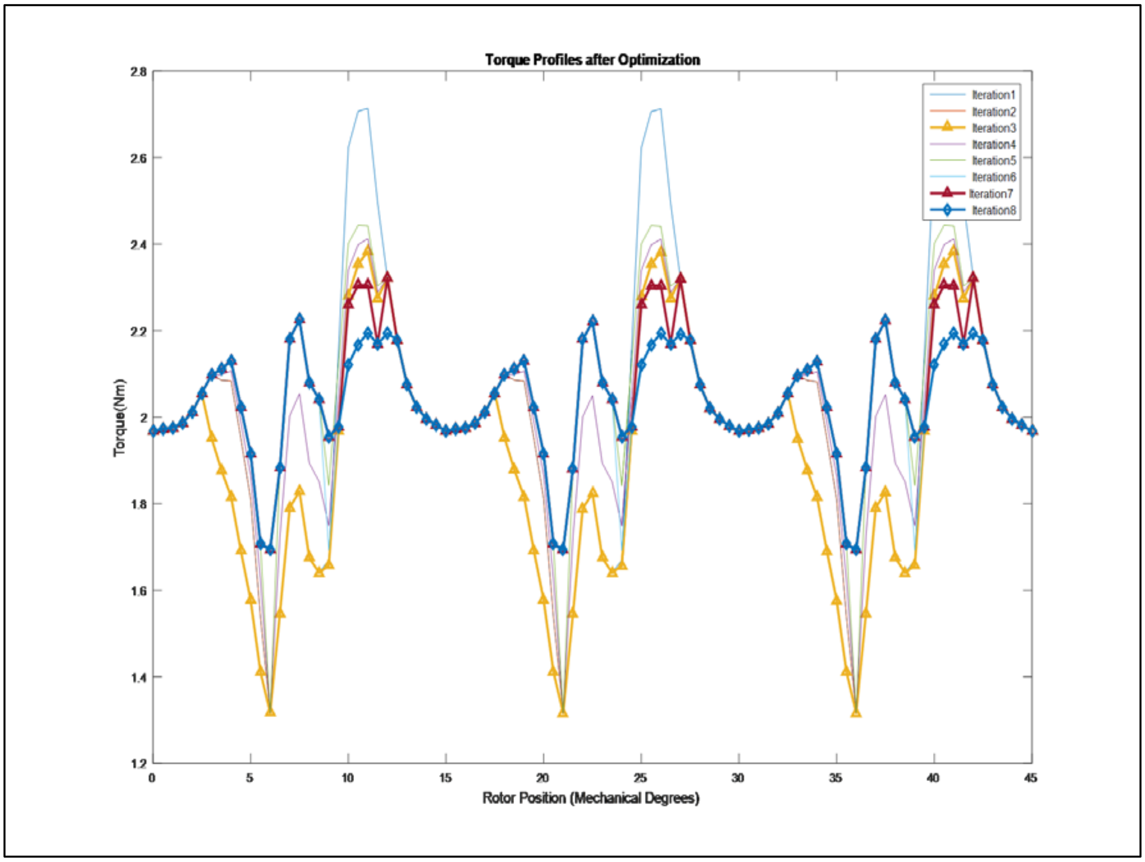

Figure 39: Corresponding torque profiles during the fine-tuning process.

Fig (40) shows a final comparison of the initial base current profile and the final optimized current profile obtained after fine tuning for a command torque of 2.0Nm. The output torque response obtained from the FEA model of the machine is also shown in the figure.

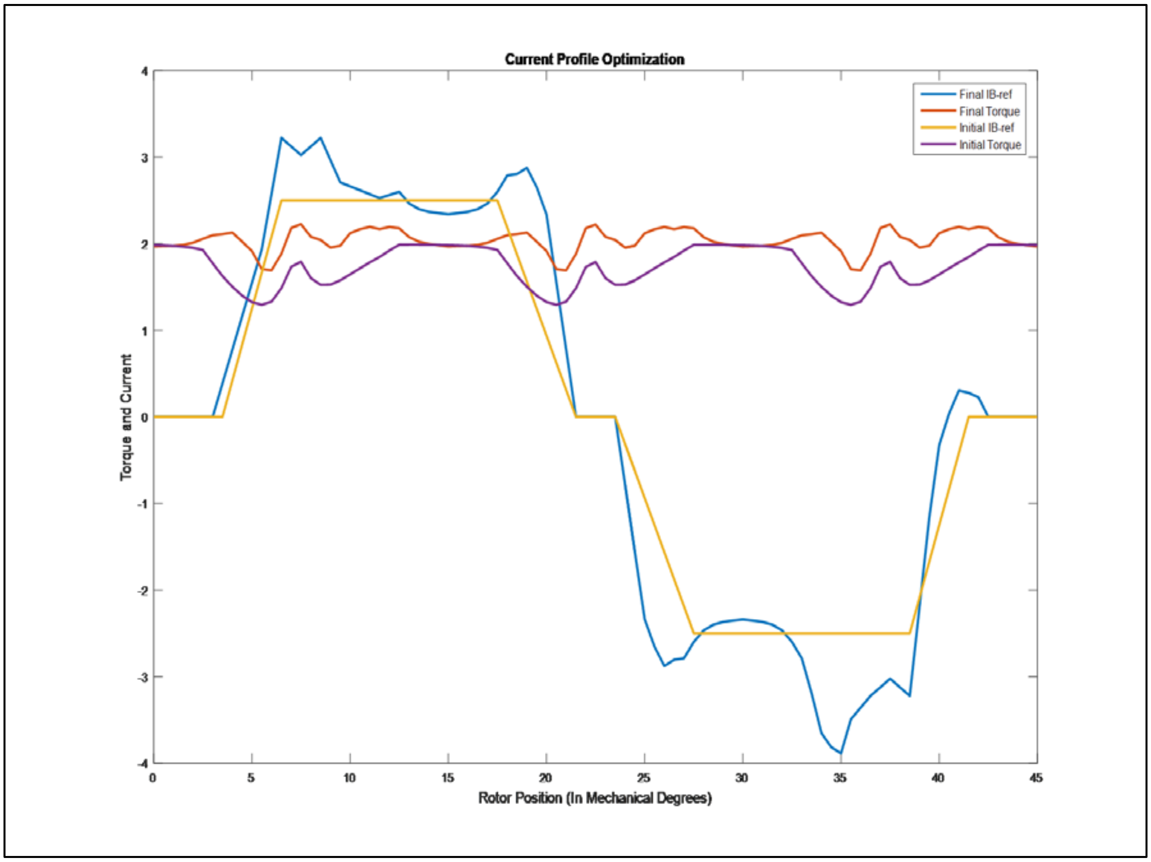

Figure 40: Comparison of the EM Torque with optimized current profile

The current optimization technique presented in this chapter helped reduce the torque ripple from 48.2% for the initial base current profile to 25.8% for the final optimized current profile for a torque command of 2.0Nm.

As it was mentioned in the chapter earlier, the current profiling algorithm depends heavily on the static $T-i-\theta$ characteristics of the machine and for the optimization algorithm to provide a smoother current profile; it is preferred to have a more flat static $T-i-\theta$ characteristics. As we can see in Fig (30), as the command torque increases, the static $T-i-\theta$ characteristics no longer have the flat profile and this results in the optimized command current to have a peaky profile. This can be seen in Fig (41) where for a command torque of 3.5Nm, the current profiles have sharp peaks.

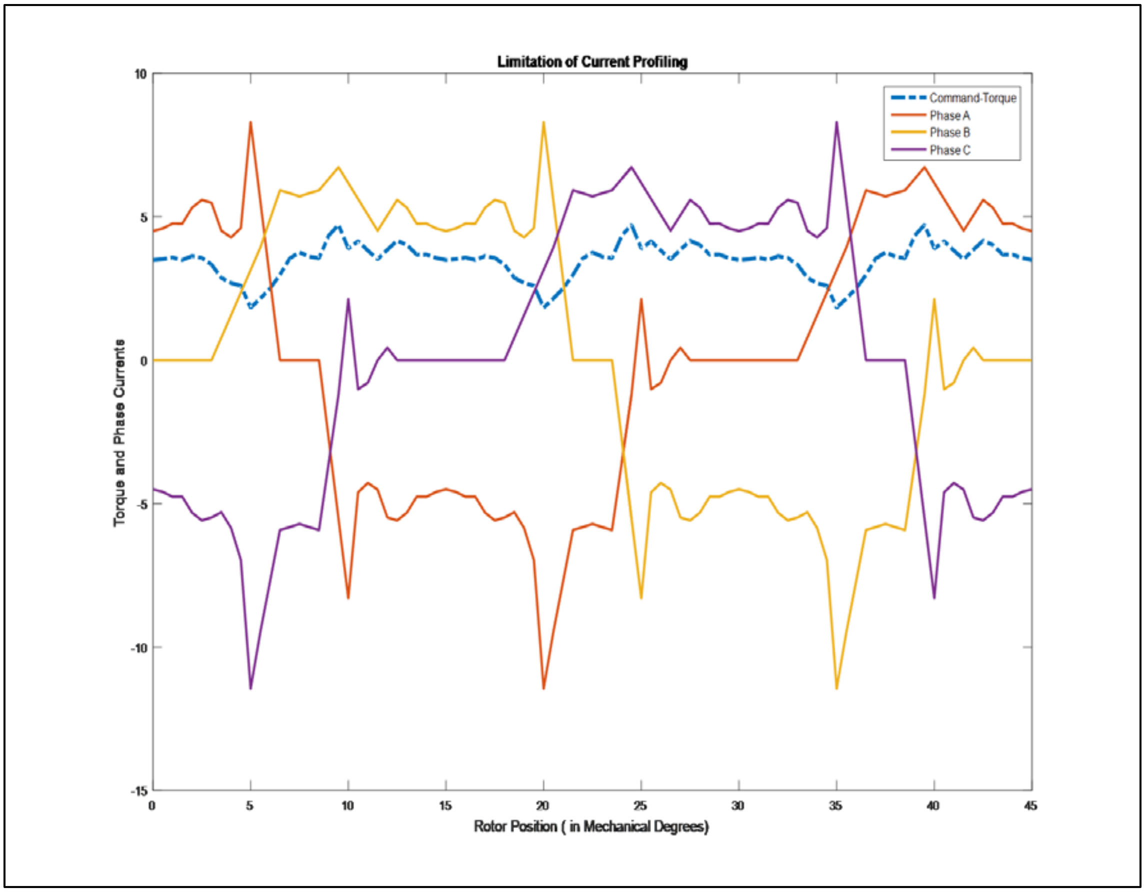

Figure 41: Limitation of the profiling algorithm for non-flat torque profiles

For the given supply voltage, it is very improbable for a high-bandwidth current regulator to be able to follow such a peak current profile. A failure to follow the command current profile will result in a higher torque ripple performance of the machine. Thereby, for the DC-assisted MCSRM under test, the maximum command torque was limited to 3.0Nm.

Fig (42) shows the series of optimum current profiles obtained for a series of torque commands.

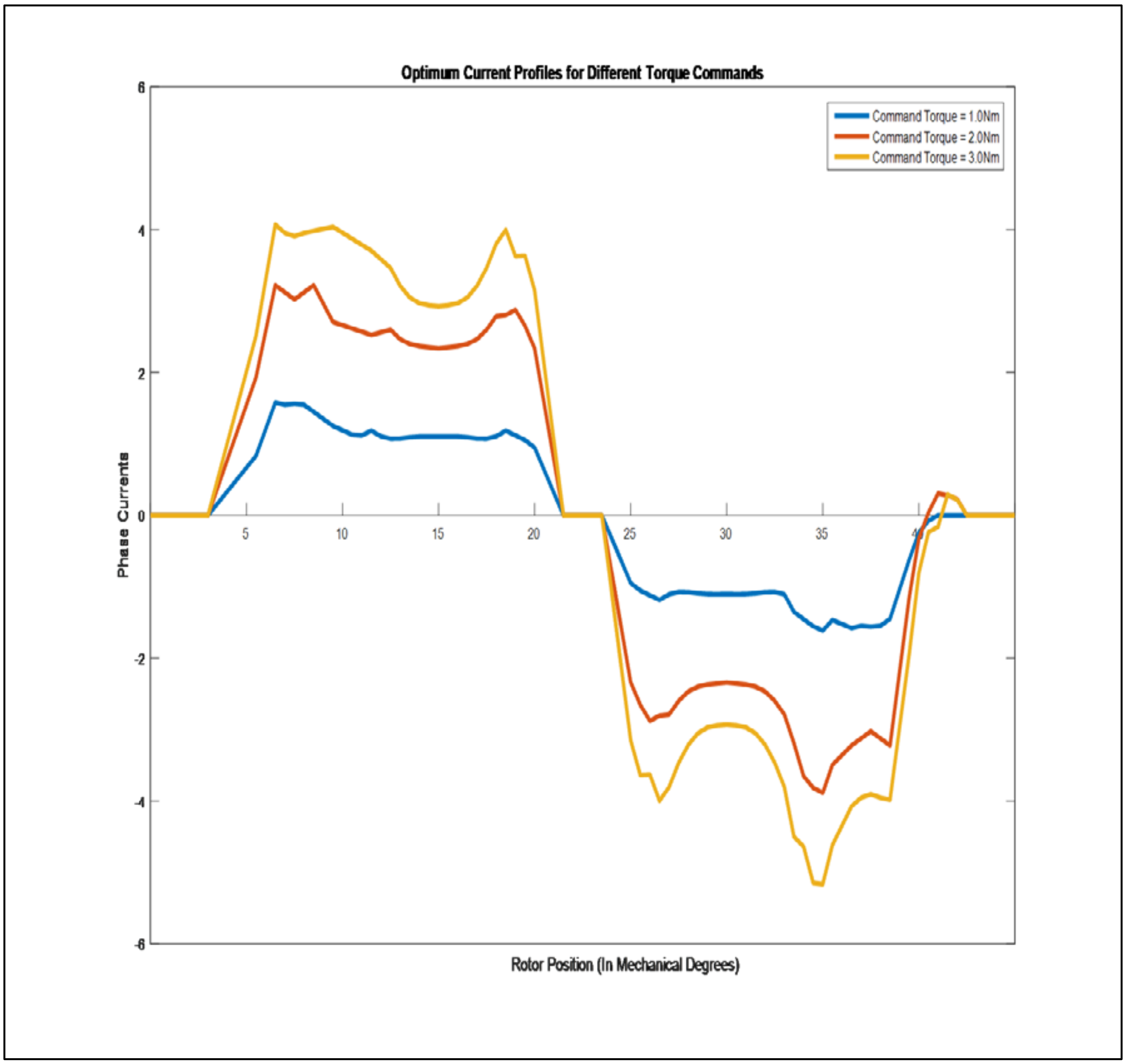

Figure 42: Optimized Current Profiles for different Torque Commands

4.5 Simulation of the DC-assisted MCSRM using MATLAB-Simulink and Flux2D

Most of the control algorithms depend on shaping the phase currents to produce a smooth torque profile. Online methods calculate the reference or command current instantaneously, while offline methods fetch the command current from a pre-calculated look-up table. Both the methods compensate for torque fluctuations throughout the conduction interval. The hysteresis type current control, although has the drawback of a varying frequency, has a better dynamic response. Also, the ease of implementing a hysteresis current control makes it a preferred control algorithm for proof of concept experimental tests. While PI regulators have the advantage of fixed switching frequency, the highly non-linear nature of DC-assisted MCSRM requires speed and position dependent PI constants, which increase the complexity of the control.

For the DC-assisted MCSRM, for a given torque command, each phase have a command current depending on the position. It is critical to follow the command current in torque ripple sensitive applications. In digital implementation of the controller, the inverter voltage command is updated in every ISR subroutine. Because of the nature of hysteresis current control, it is possible that the phase current will deviate from the reference current for a complete digital time period, which will increase the torque ripple. This error cannot be avoided but the extent by which the phase currents deviates can be reduced by lowering the hysteresis band value.

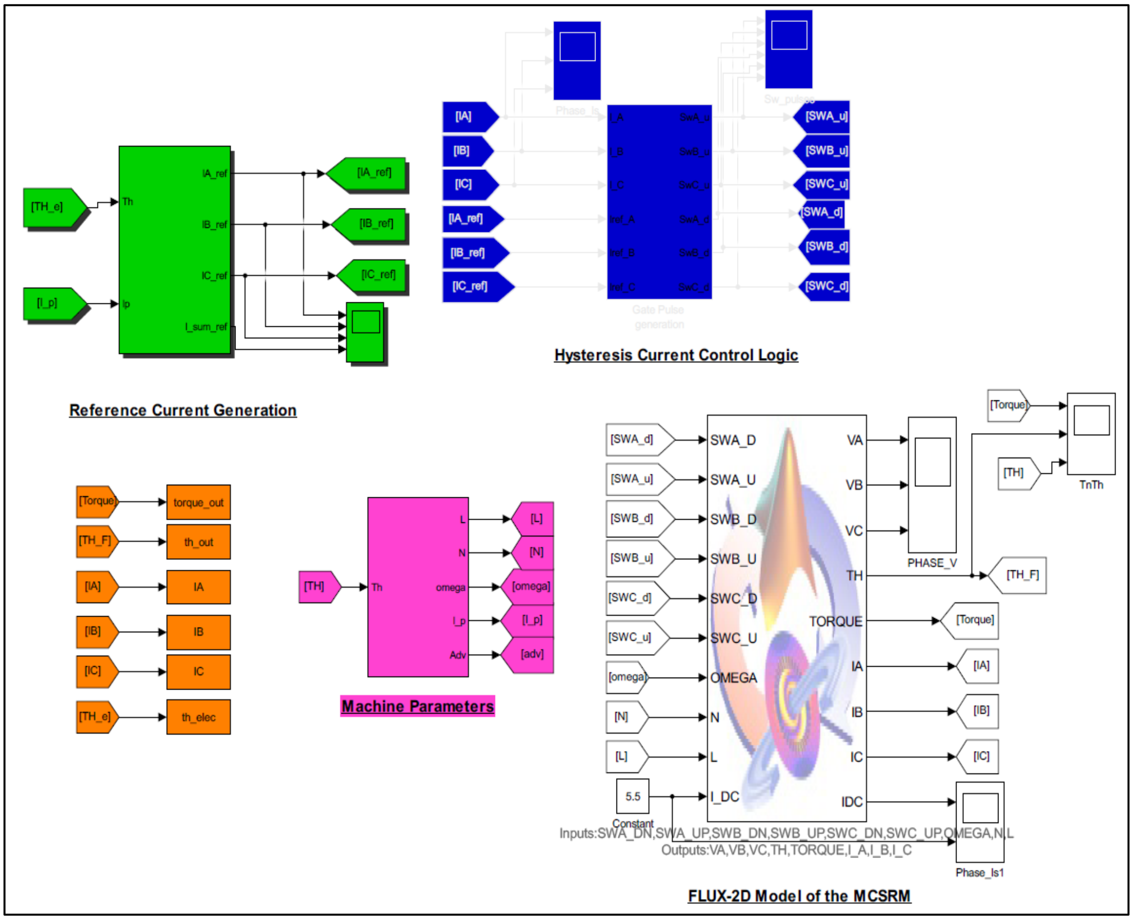

Figure 43: Hysteresis Current Control for CWDC-MCSRM

The hysteresis current control was implemented for two sets of command current with a 50µs digital time step and the results are presented in the following figures. A finite element and MATLAB/Simulink based dynamic coupled simulation has been done to verify the hysteresis current control performance. The simulation also verified the effectiveness of the optimum current profile in reducing torque ripple of the machine. The Fig (43) shows the MATLAB/Simulink environment of the hysteresis current control.

Two sets of simulation results are shown in the following plots. The first set is with the initial base profile set as the reference command and the second set is with the optimized current profiles as the reference command.

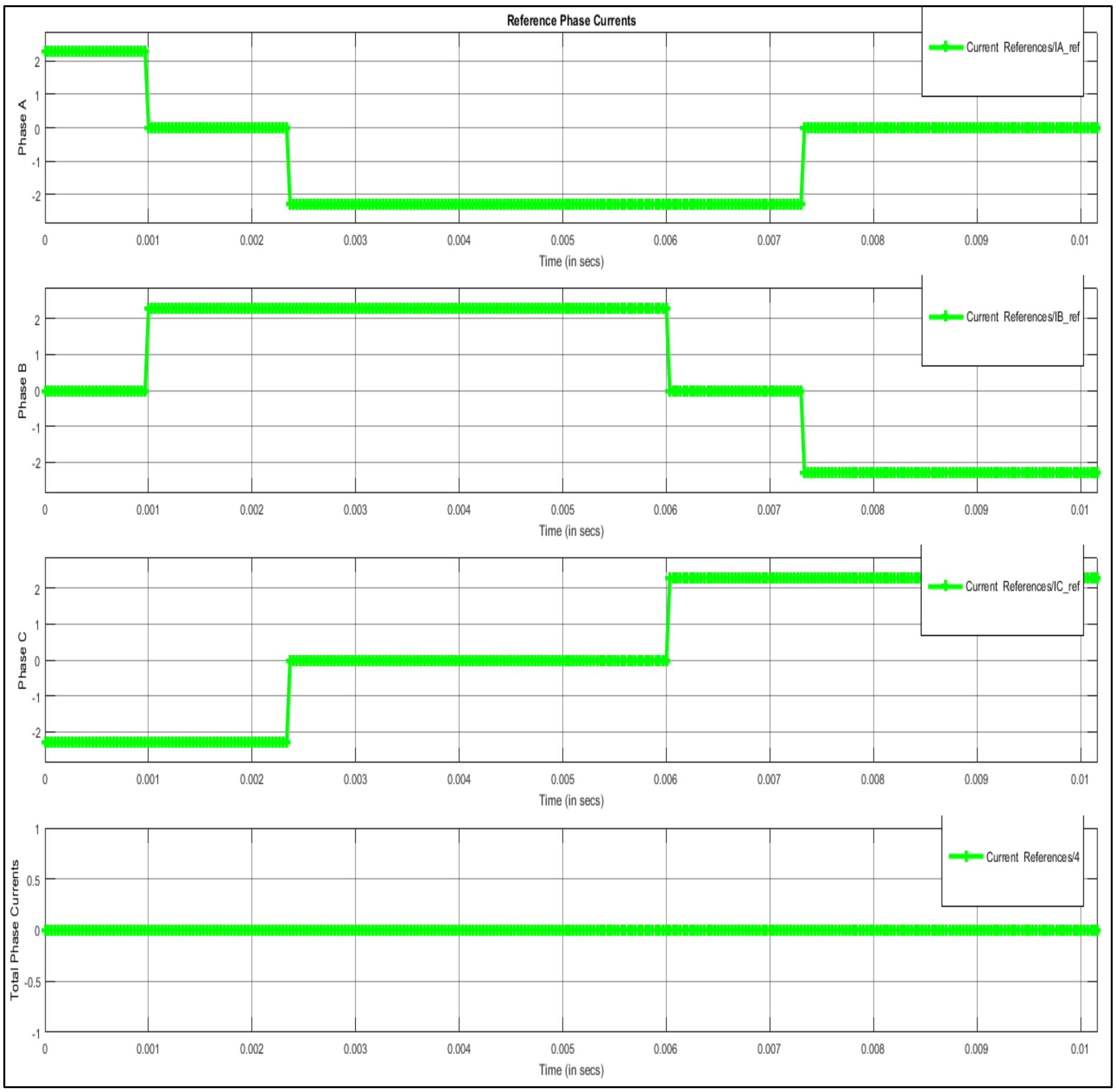

Figure 44: Reference Currents (Phase A, B, C and (Ia+Ib+Ic) - Initial Base Profile

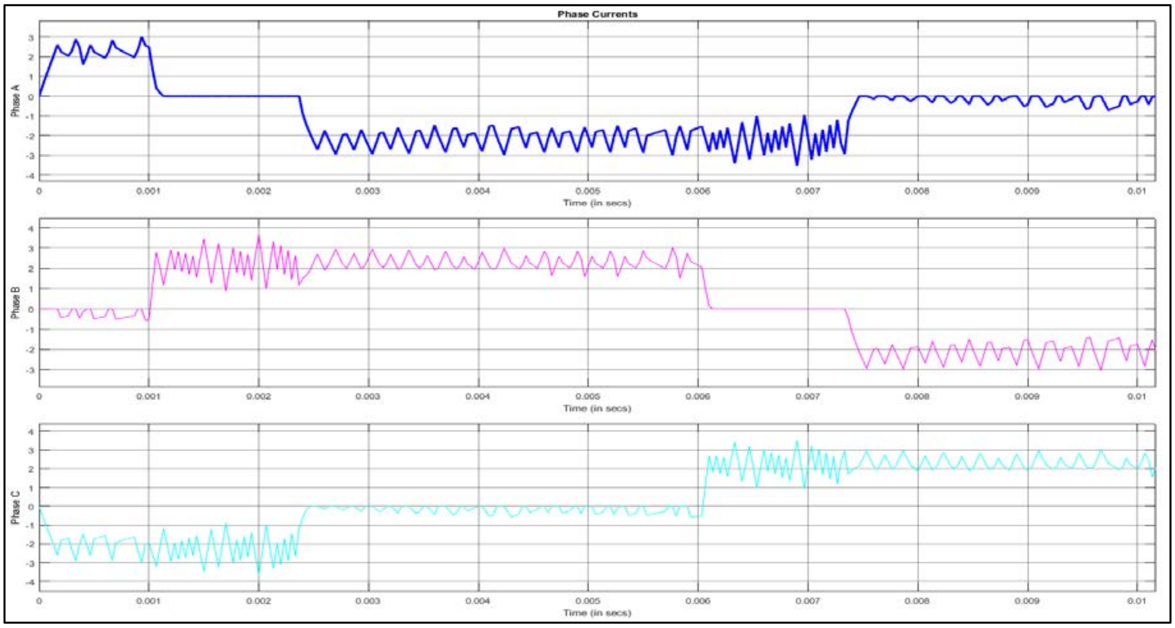

Figure 45: Phase A, B and C Currents - Initial Base Profile

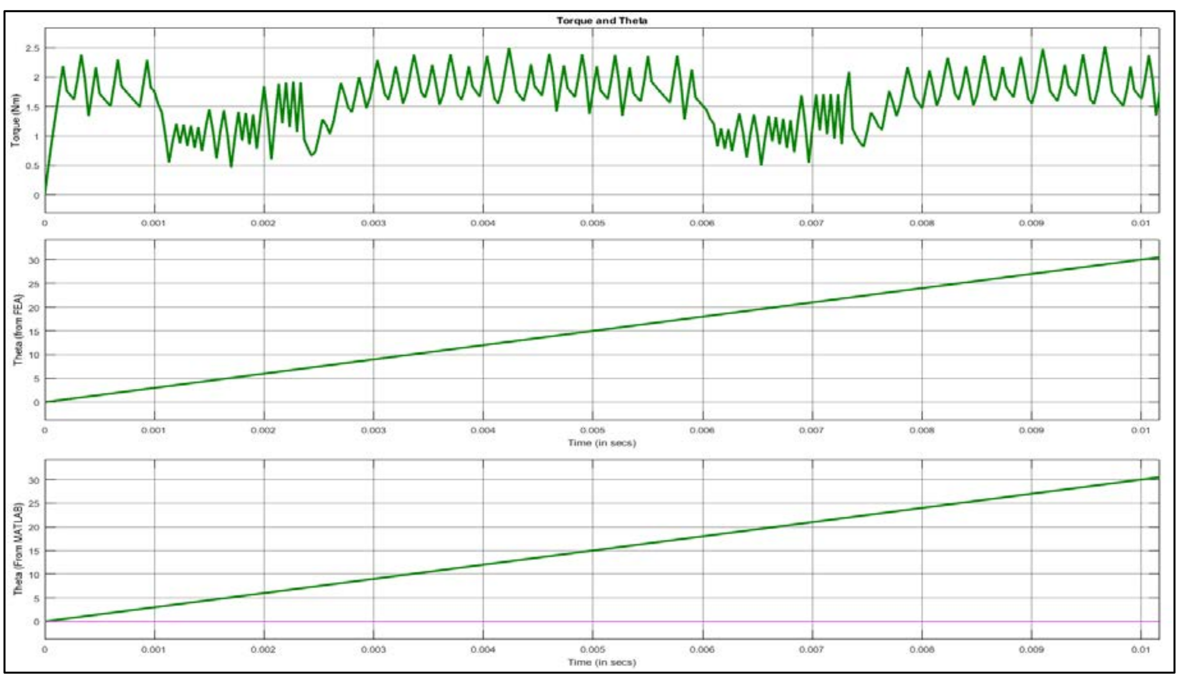

Figure 46: Electromagnetic Torque generated and Rotor Position in Mechanical degrees: Initial Base Profile

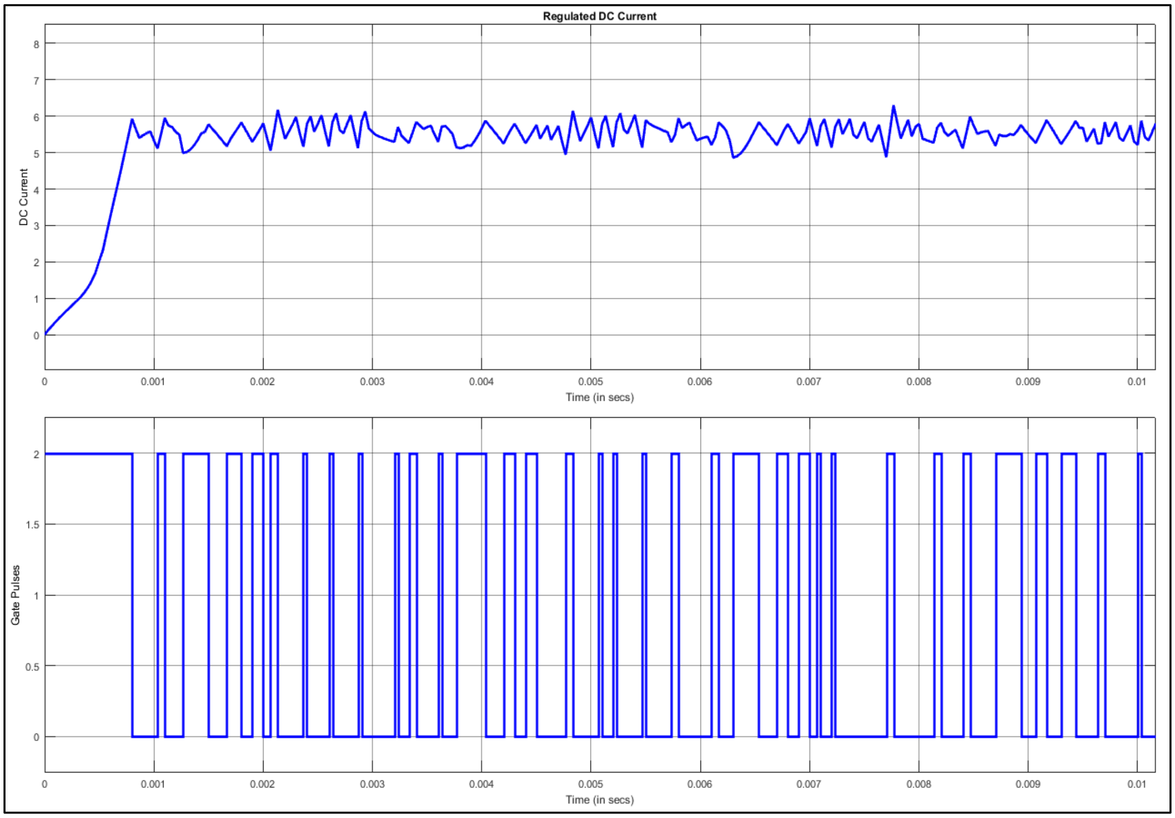

Figure 47: Regulated DC Current Profile

From the above simulation results, we can see that the phase currents are able to follow the reference current profile. Depending on the hysteresis band value, the phase currents and the DC field winding current deviate from the command value. This deviation of the phase currents from the command value is also reflected in the electromagnetic torque that is produced. Thereby, in comparison to torque response for ideal current excitation, the torque produced by hysteresis current control has a higher torque ripple. By using a finer hysteresis band and further reducing the digital time-step, the torque ripple can be reduced. The average torque in the above plot is 2.0 Nm and the torque ripple is around 75.3%.

The effectiveness of the current profiling algorithm was determined by running a similar simulation using the optimized current profiles as the command current. The simulation results are shown below and the torque ripple performance is compared.

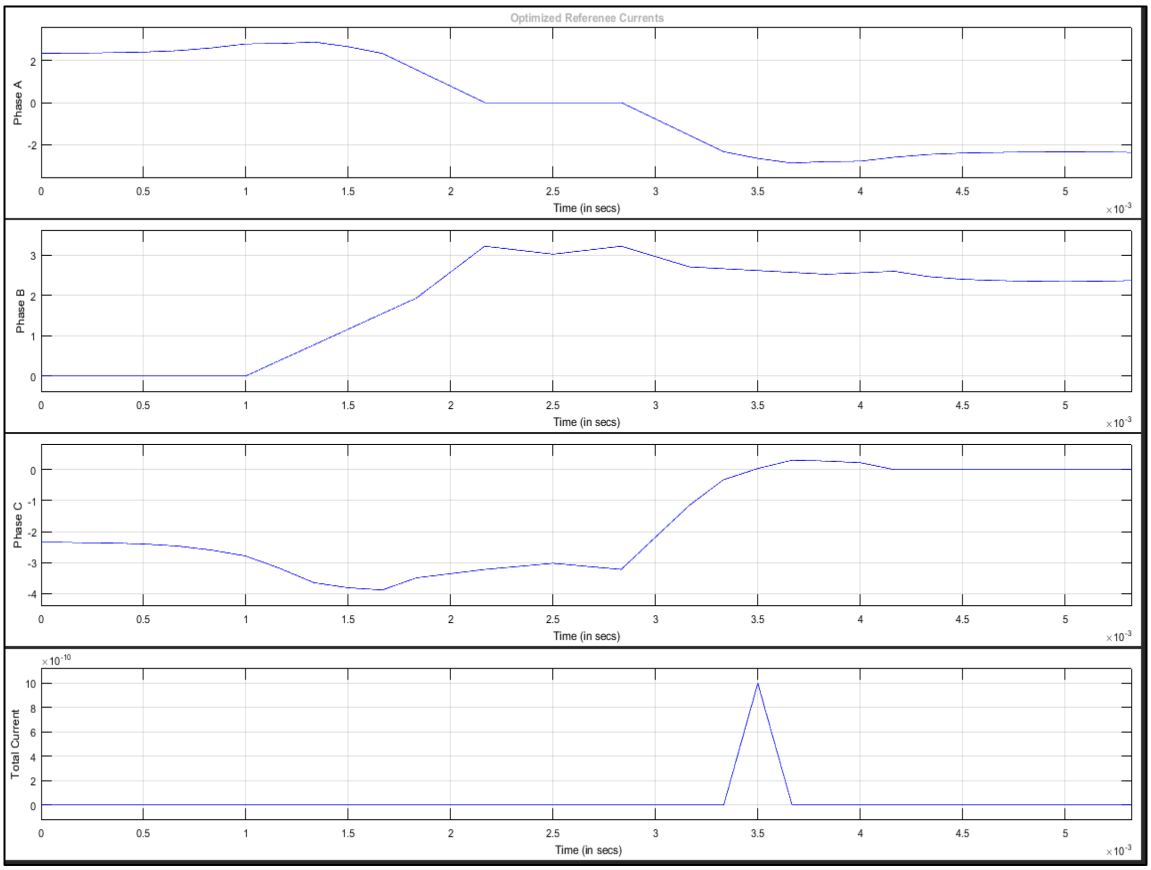

Figure 48: Reference Currents (Phase A, B, C and (Ia+Ib+Ic) - Optimized Current Profile

With the optimized current profiles, the average value of the electromagnetic torque produced remained at 2.0 Nm; however, the torque ripple was reduced to 47.6 %. Thus, the effectiveness of the current profiling method was validated and the controller was implemented in hardware.

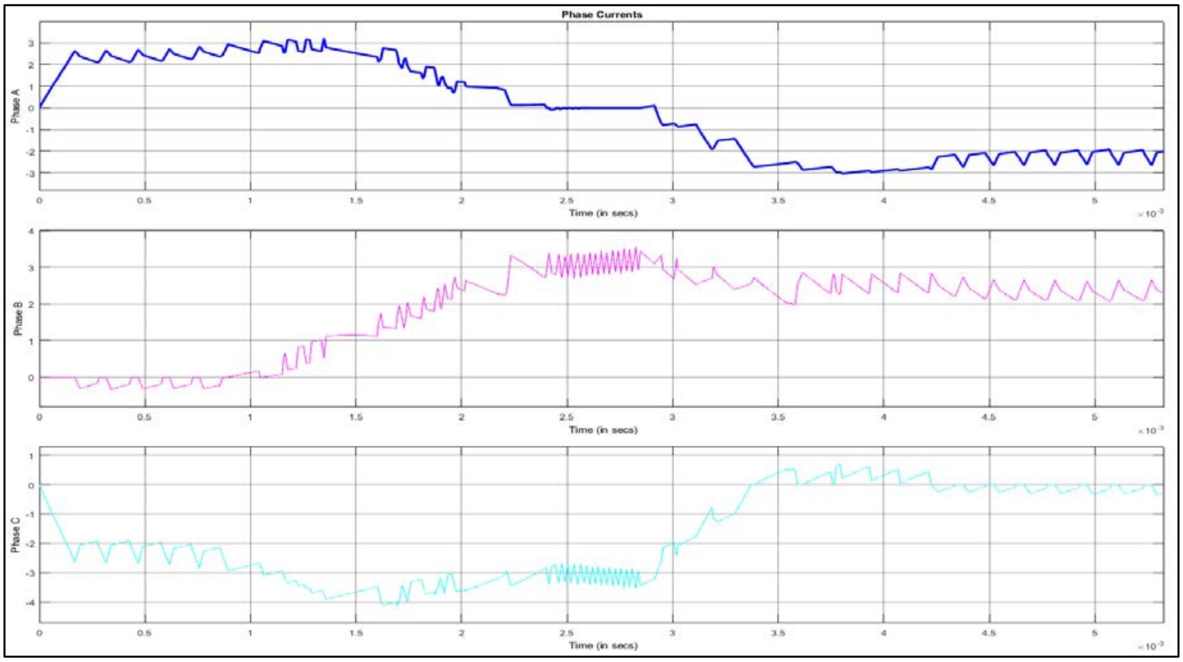

Figure 49: Phase A, B and C Currents - Optimized Current Profile

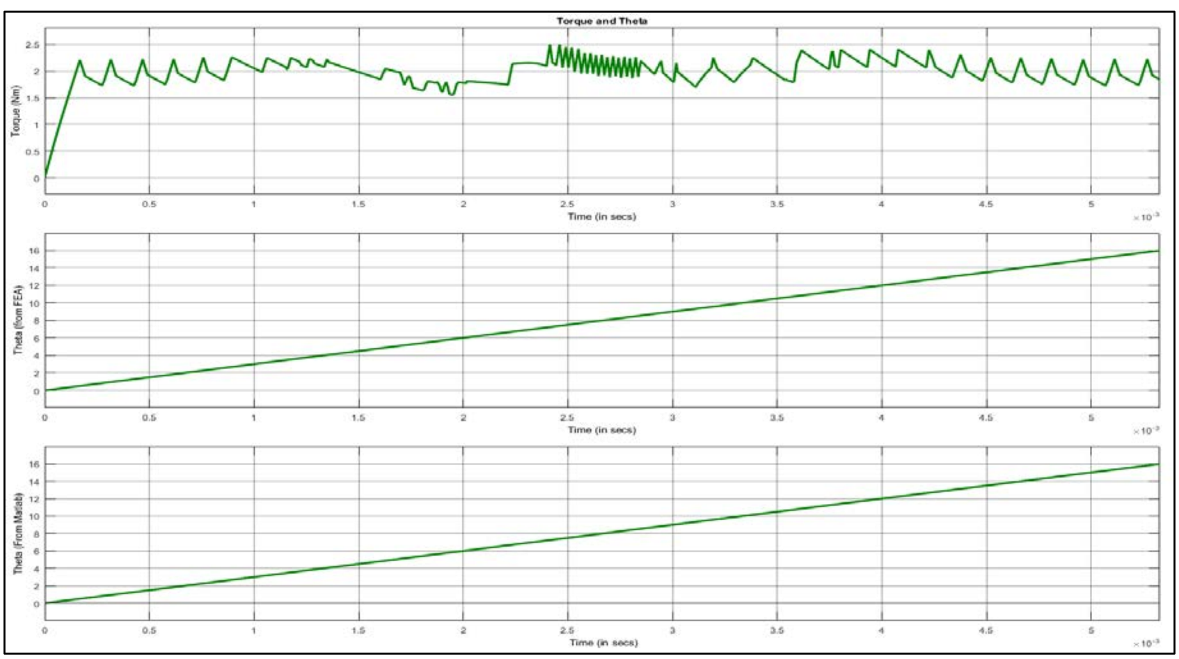

Figure 50: Figure 11: Electromagnetic Torque generated and Rotor Position in Mechanical degrees: Optimized Current Profile

CHAPTER 5

DC-ASSISTED MCSRM DRIVE HARDWARE IMPLEMENTATION

5.1 Introduction

The objective of this experiment is to implement a hysteresis current control of the DC-assisted MCSRM on a hardware setup. The various hardware devices used in the experiment are TI Digital Signal Processor (DSP) controller, power converter board, current sensors, encoder and prime mover as shown in Fig (52). The MCSRM is operated in motoring mode where electrical energy is input to the SRM for the desired mechanical output.

The DSP (TMS320F28377D & TMS320F28035) from Texas Instrument is a motor control and power electronics applications based controller. A number of peripherals has been integrated on the DSP chip such as ADC (analog to digital converter), QEP (quadrature encoder peripheral), I2C (inter integrated circuit) etc.

The DSP controller algorithm has been developed using the companion development tool called the code composer studio (CCStudio). The CCStudio is the microcontroller programming software which has the compiler and programmer to flash the code to DSP. The software code written in this package can be in either embedded C language or assembly level language. The program written can be flashed into DSP using parallel port or emulator. The CCStudio package can be configured and interfaced to various microcontrollers in the TI’ 28XX family. This software has the advantage of sending the real-time commands to control the machine. Fig (51) shows the phase windings of the Concentrated Winding DC-MCSRM, after the conventional SRM was rewound and reconnected.

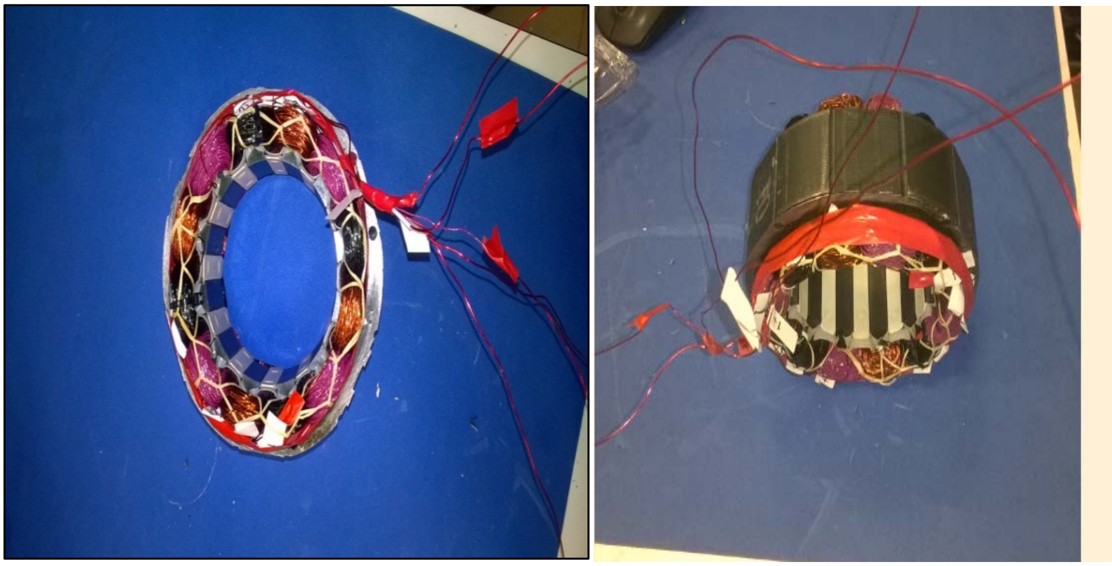

Figure 51: CWDC-MCSRM Stator

5.2 Experimental Setup

The DC-assisted MCSRM drive is implemented using two boards. The first board is TI's C2000 Design Drive Development kit for Industrial Motor Control with the TMS320F28377D DSP controller embedded on the board. The DesignDrive kit is a single platform to develop a control for 3-phase motor rated for up to 400W and a current capability of 10 amperes. The DesignDrive kit also includes four high performance 16-bit ADCs and eight windowed comparators, to support both shunt and LEM based fluxgate/Hall current sensing simultaneously. For position feedback, the kit leverages integrated MCU support for interfacing to resolvers and incremental encoders. The kit also includes the Inverter Power Stage and a fault protection circuitry. This board is used to regulate the 3-phase currents in the DC-assisted MCSRM. To regulate the constant DC-excitation in the field winding, a second board is used. This is the TI's High Voltage Motor Control and PFC Developer's kit with the TMS320F28035 DSP controller embedded on the board. Similar to the DesignDrive board, this board also includes the 3-phase power inverter stage and is rated to drive a 1.5kW rated motor. Since this board was used to control the DC field excitation, only 2 legs of the 3-phase inverter were used and operated as a half-bridge inverter. Another option to control the constant DC-field excitation has been explored by using a single leg of an asymmetric half bridge inverter. The asymmetric half bridge inverter board consists of an International Rectifier IR2101 Gate Driver IC and IRF644 N-channel Power Mosfets rated for 200V, 10A. In addition, the Model-260 quadrature incremental encoder by Madison Electric Product is placed on the rotor shaft to get rotor position feedback [17].

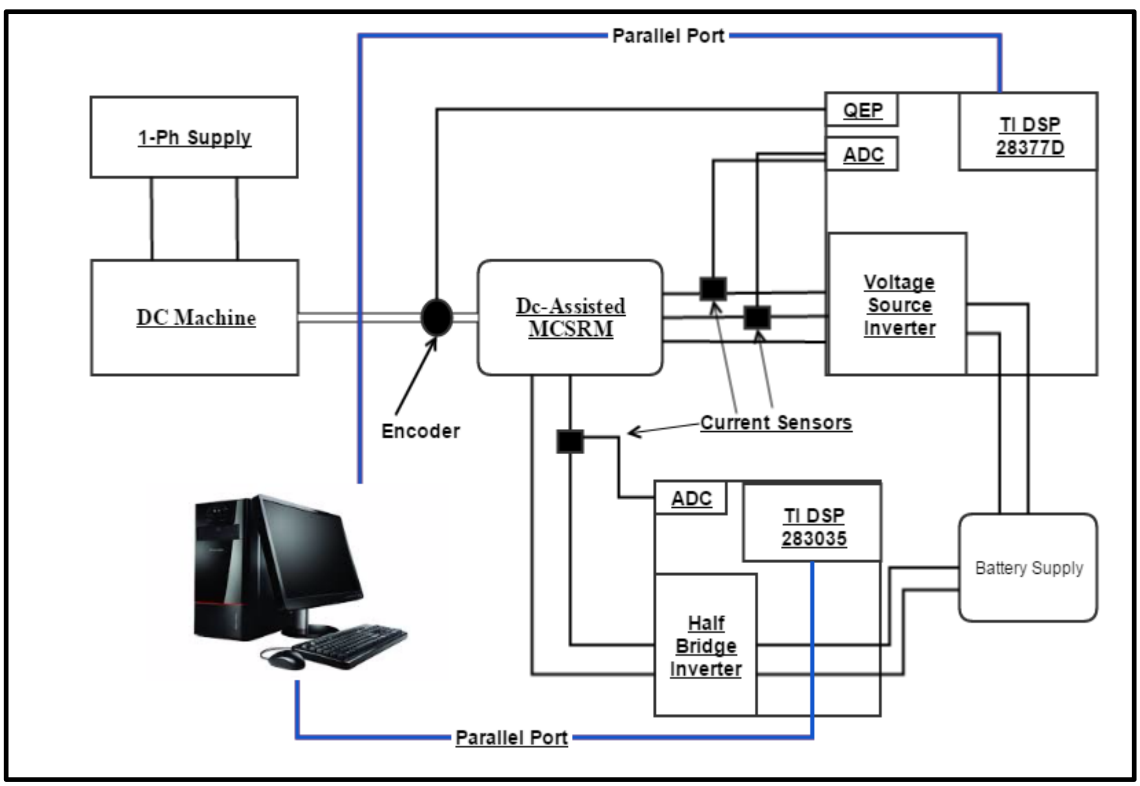

Figure 52: Overall view of the experimental setup

5.3 Hardware Implementation

The configuration for the incremental encoder and current sensors that are interfaced to DSP and the initial alignment routine are explained as follows:

5.3.1 Position Feedback and Encoder Initialization

In the experimental implementation of the MCSRM drive, the rotor position information is obtained from an incremental encoder. The phase excitation sequence is determined from the position information processed by the QEP module of the TI DSP. The output signals from the encoder channels QepA, QepB and index pulse are interfaced with the QEP peripheral. Depending on the direction of rotation, the QEP_count value will increase or decrease. Since both the edges of QepA and QepB are sensed by the QEP module, the QEP_count timer counts four times for every cycle of channels QepA and QepB signals. The QEP_count value is reset every time at the occurrence of an index pulse. Since the encoder output is an open collector output, 2.2KΩ pull-up resistors are used to connect the QEP side input to 5.0V source.

The excitation sequence of the phase currents in the DC-assisted MCSRM drive must be synchronized with the rotor position to obtain maximum positive torque output with minimum ripple. Therefore, the reference rotor position must be known, before starting the motor for continuous operation. Initially when the encoder is mounted on the rotor shaft for the first time, the offset between the index pulse location and the stator phase-A aligned position is measured to be used for phase current controller operation. Once the encoder physical mounting is fixed, the position offset should remain the same. Even after adding the encoder mounting offset to the position measurement, the encoder cannot provide the initial rotor position when we first power the drive unit. In addition, unlike, a PMSM, since there are no permanent magnets on the rotor, we cannot align the rotor with a d-axis reference. So, a starting technique needs to be implemented before actually starting the motoring operation. The starting technique is based on aligning the rotor poles to a known stator pole location, by excitation a certain phase for a set number of PWM cycles. The encoder initialization code operates such that, initially Phase A is excited with a positive current of 1.0 amperes and Phase B and Phase C are excited with a negative current of (-0.5) amperes each for a duration of 20,000 PWM cycles (i.e. 2 secs for 10kHz PWM signal). This ensures the rotor pole is aligned to the nearest stator phase-A pole. When this alignment is achieved, the position offset is loaded as a preset condition and the appropriate reference phase currents are generated to ensure unidirectional torque production for continuous motion. Care should be taken that the initial excitation period is long enough to guarantee the alignment of the rotor and stator poles. If the excitation period is too short, the rotor would not reach the aligned position due to load and friction.

5.3.2 Current Feedback

The stator phase current and dc-field current need to be measured and fed back for the hysteresis current control. For the phase current sensing, Hall Effect based LEM current sensing was used, and for the DC-field excitation, the series resistance was used for current sensing. The current sensing unit for both the phase currents and field current was a part of the TI’s motor control board. The TMS320F28377D has a dual 16-bit Analog to Digital converter with an input voltage range of 0-3V, while the TMS320F28035 has a dual 12-bit Analog to Digital converter. The maximum winding current for both the board was 10A, such that a current of 10A would develop a voltage of 3V at the ADC peripheral of the DSP controller. The digital equivalent value for a 3.0V was 4096 and the reference current values for the hysteresis current control were initialized accordingly.

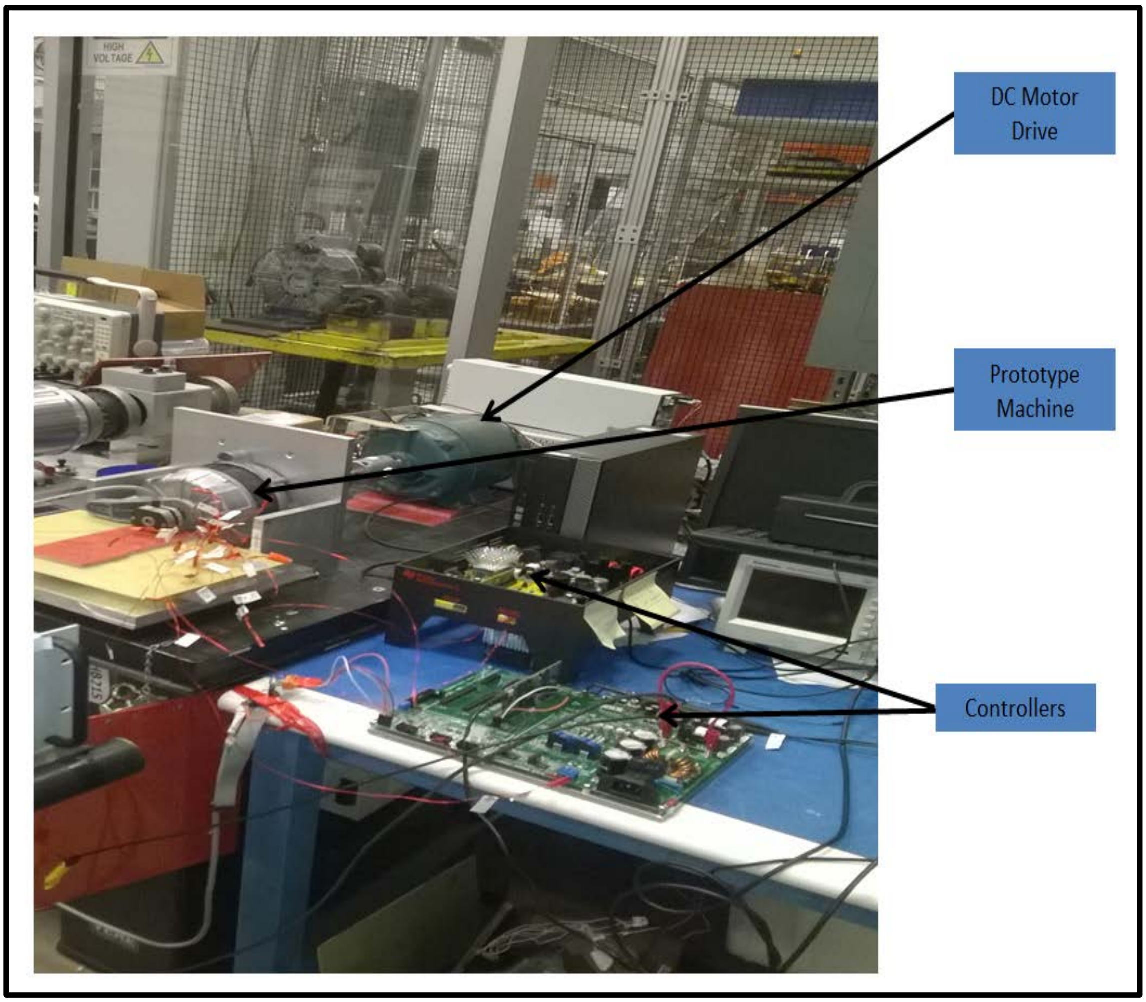

Figure 53: The experimental setup for CWDC-MCSRM

5.4 Approach to implement Hysteresis Current Control

To validate the experimental setup and hysteresis current control code developed using CCStudio, an initial set of tests were performed on a 400W Permanent Magnet Synchronous Machine (PMSM). The PMSM used for the initial tests is a Texas Instrument Synchronous Motor is rated for 200V, 2.7A with an operating speed of 3000rpm and is shown in figure 5.2. The motor has a built-in incremental encoder which is interfaced with the QEP module of the controller board.

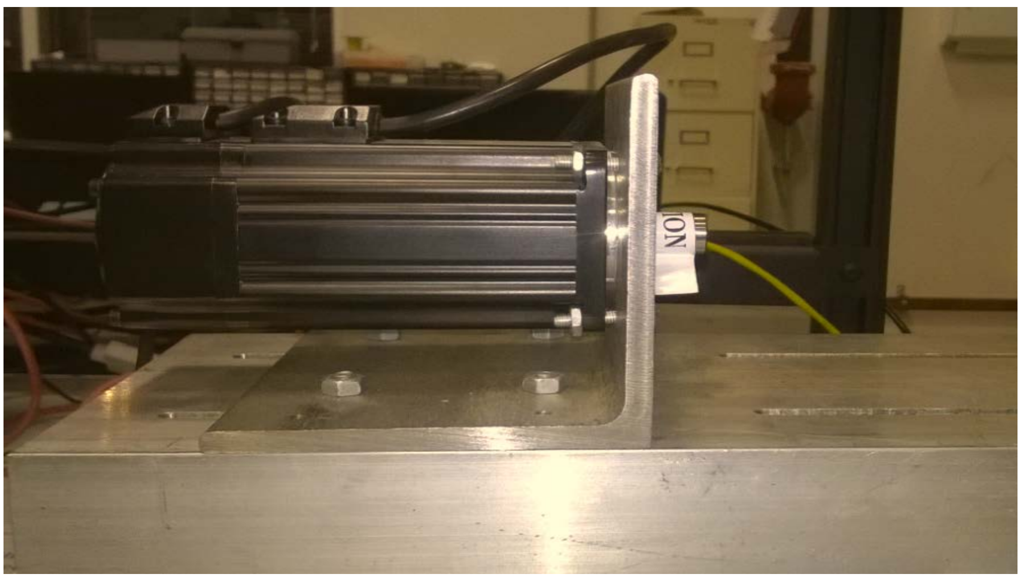

Figure 54: The 400W PMSM

The experiment on the PMSM is conducted the following steps:

a.) Using TMS320F38277D controller, speed controller was implemented in hardware using Space-Vector PWM technique.

b.) A Speed Controller using a hysteresis current control scheme was implemented in hardware and compared with the results of the space-vector PWM technique.

c.) Once current regulation was achieved using hysteresis current control on the PMSM, experiments were performed on the DC-assisted MCSRM.

5.4.2 Field Oriented Control (FOC) using Space Vector PWM technique:

The block diagram representing the control flow for the speed control of a 3-phase PMSM is shown in Fig (55).

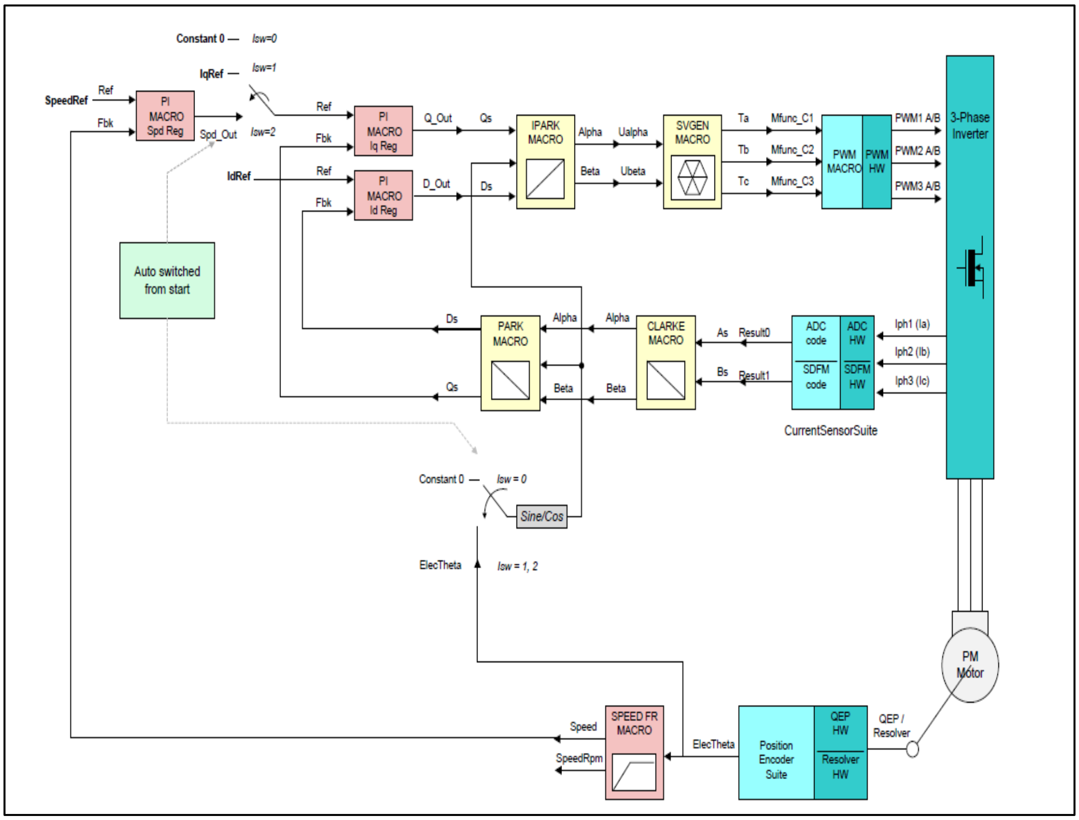

Figure 55: Block Diagram of the FOC of the PMSM using SVPWM

TI's DesignDrive kit and TMS320F28377D DSP control card is used to implement the controller. Phase A and Phase B currents are sensed using a Hall Sensor/LEM based current sensor unit and sensed voltage is fed to the Analog to Digital converter channels of the microcontroller. The PMSM came with a built-in incremental encoder which is interfaced with the QEP module of the microcontroller. Based on the position feedback, the speed is calculated and a PI regulator in the outer speed loop generator the q-axis reference current based on the error between the reference speed and the actual speed signal. The d-axis reference current is fixed at 0, since the motor is operated at low speed and field weakening is not required. Sensed Phase currents undergo Park and Clarke transforms to convert the 3-phase time and position varying parameters to fixed DC quantities. The two PI regulators in the inner current loop generate the D-axis and Q-axis reference voltages depending on the error between reference currents and actual phase currents. The D-axis and Q-axis reference voltages are then passed through a Space Vector PWM module which generate the desired duty cycle for the speed controller to operate. Based on these duty cycles, appropriate gate pulses for the three legs of the six-switch inverter are generated at the GPIO pins of the TI DSP.

The input signals coming into or the output signals going out of the DSP are processed inside the DSP in a timely manner based on the Interrupt Service Routine. The code can be divided into two sections; 1) Software initialization 2) Controller algorithm

The initialization section is responsible for declaration of all the variables and the initial configuration of ADC and General Purpose Input/output Pins. The encoder QEP module, the enhanced PWM (ePWM) modules and the TripZone registers are also initialized in this subroutine of the main code. Once the initialization is complete, the code enters an infinite while loop, where it waits for Interrupt Flag to go high. This Interrupt Service Routine (ISR) sets the Interrupt Flag high in a timely manner, where the frequency of the ISR sets the PWM switching frequency and is decided by the user. Once the interrupt flag goes high, the code enters the Interrupt Service Routine where the Field Oriented Control of the PMSM is performed. The interrupt service routine executes the conversion of the ADC channels, clears the interrupt flag, performs Clarke and Park Transform, executes the PID modules, executes the inverse park transform and executes the Space Vector PWM module to drive the PWM gate drivers, and returns to the infinite while loop once all the computations are done. The code also incorporates a speed-loop prescalar, which ensures that the ISR executes the Speed PI macro only once every ten times it executes the Current PI macro. This ensures that the outer speed loop is 10 times slower than the inner current loop and helps reduce processing overhead.

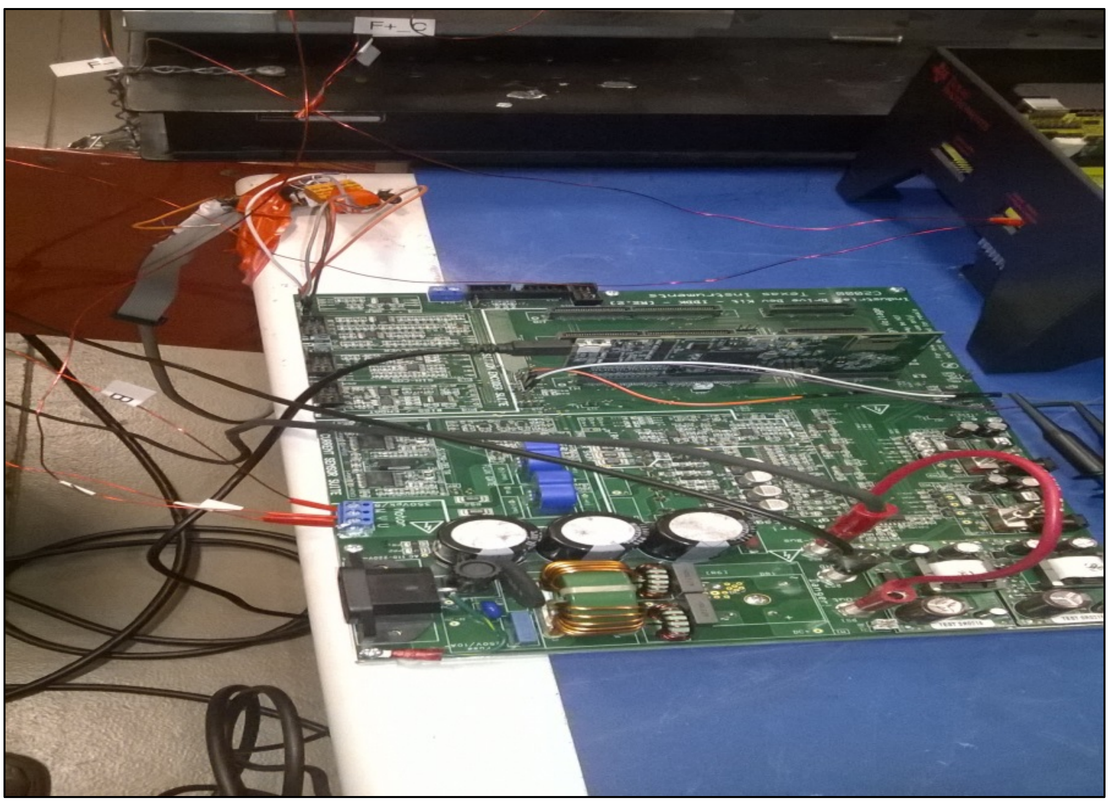

Figure 56: TI’s DesignDrive kit and TMS320F28377D DSP control card

The experimental results are shown in the following plots.

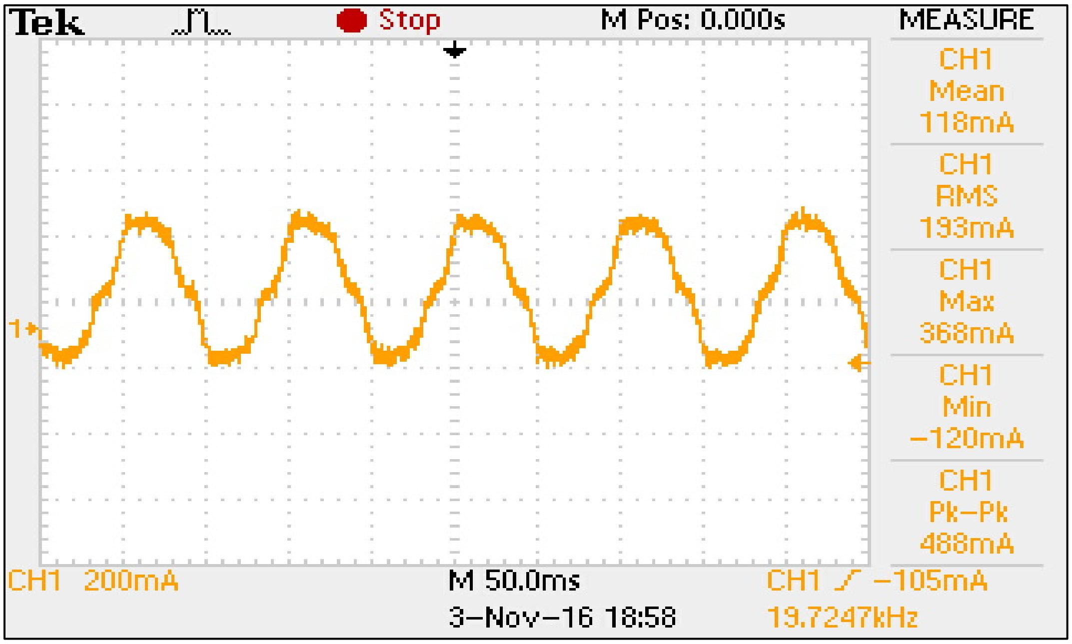

Figure 57: FOC of PMSM using SVPWM - Phase A current

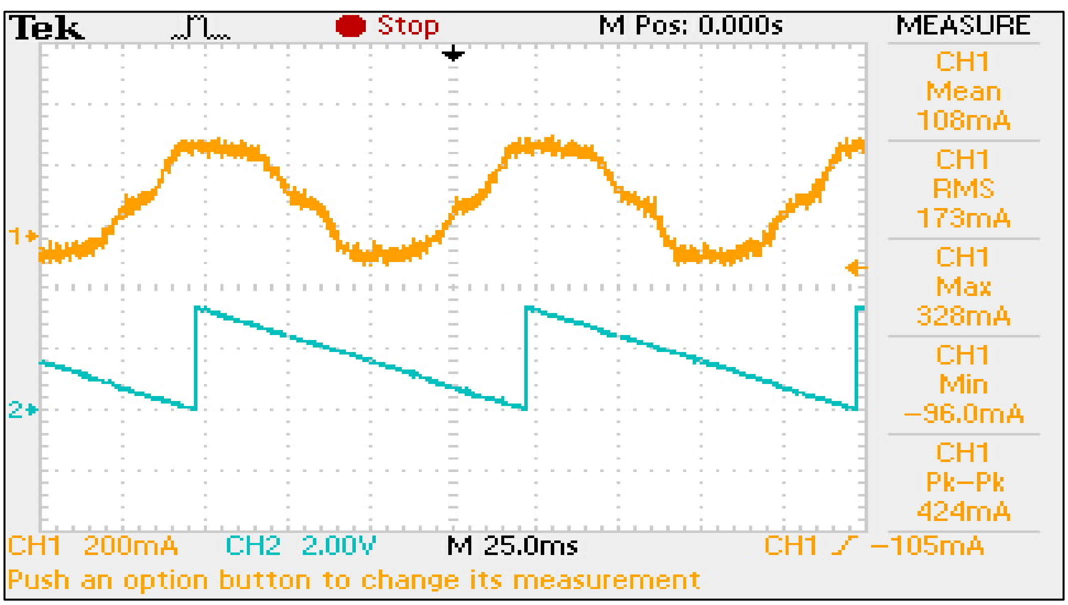

Figure 58: FOC of PMSM using SVPWM - Phase A current and Position Encoder feedback

5.4.2 Speed Controller using Hysteresis Current Control technique:

After the Field Oriented control of the PMSM was implemented using the space vector PWM technique, the PMSM was tested for field oriented control, using hysteresis current control. The block diagram of the FOC of PMSM using hysteresis current control is shown below.

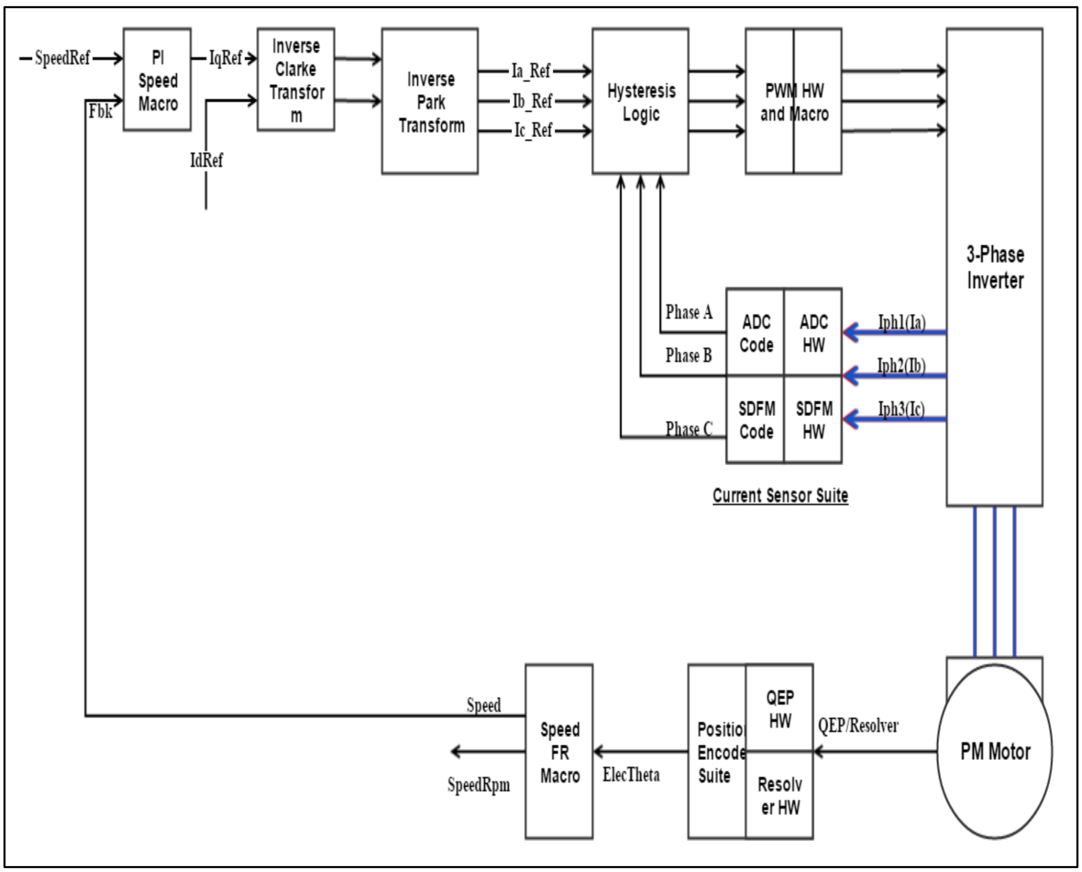

Figure 59: Block Diagram of the FOC of the PMSM using Hysteresis Current Control

The experimental setup remained the same and appropriate changes were made in the CCStudio code. In the ISR portion of the code, instead of performing Clarke transform on the phase currents, the phase currents were directly compared with reference currents. The hysteresis band value is set as variable, allowing real-time variation in the hysteresis band. The inner PI loop was no longer required and this provided a better computational overhead for the program. The hysteresis current control was test on the PMSM and the results are shown below.

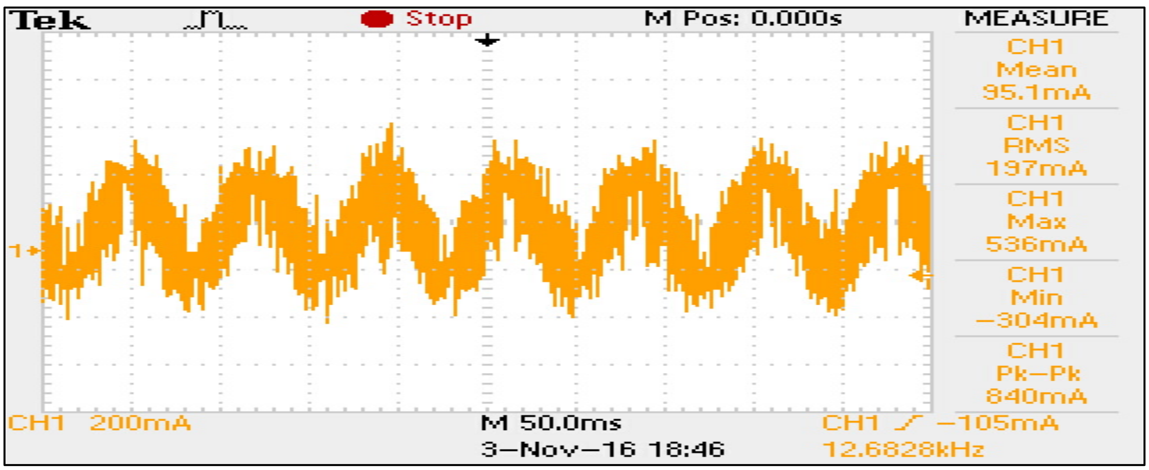

Figure 60: FOC of PMSM using Hysteresis Current Control - Phase A current

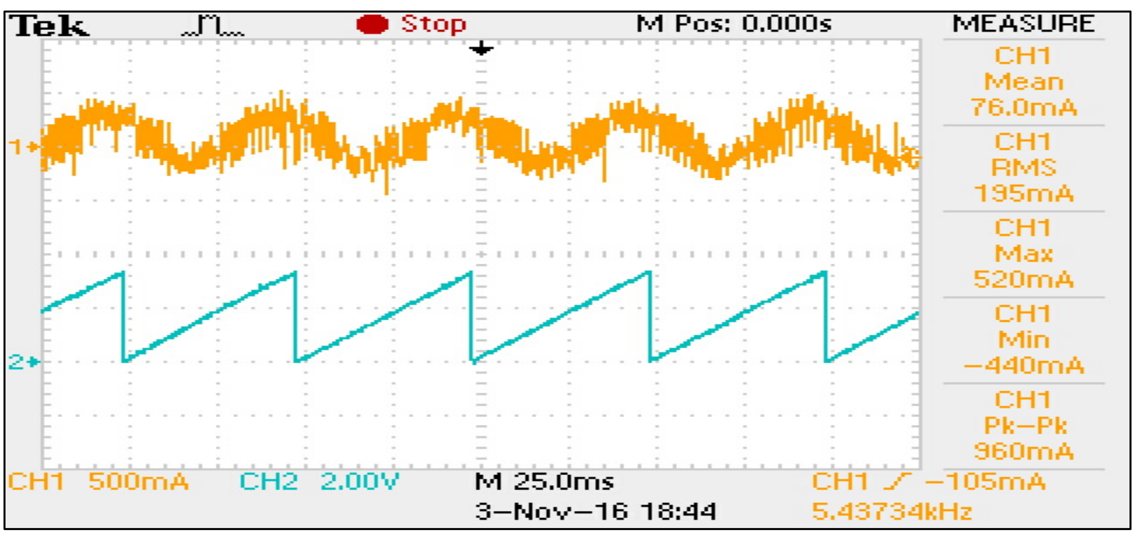

Figure 61: FOC of PMSM using Hysteresis Current Control- Phase A current and encoder position feedback

A comparison of Phase A current waveform under the two approaches is shown below. The RMS current value remains the same under both control scheme, but the peak-peak current is higher in the Hysteresis Current Control test. This can be further improved by choosing a finer Hysteresis Band.

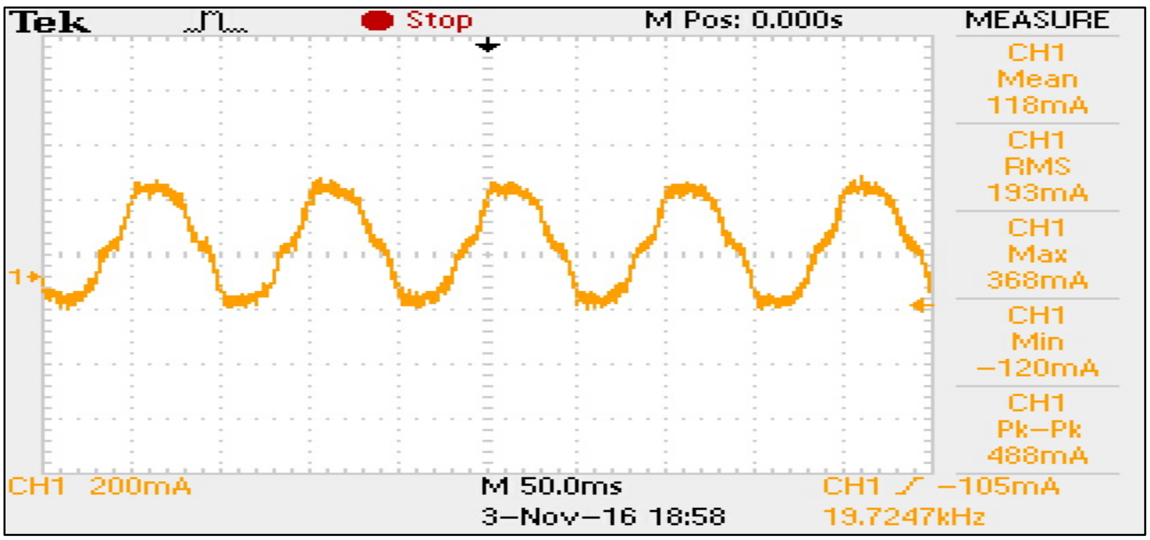

Figure 62: Phase A current: SVPWM

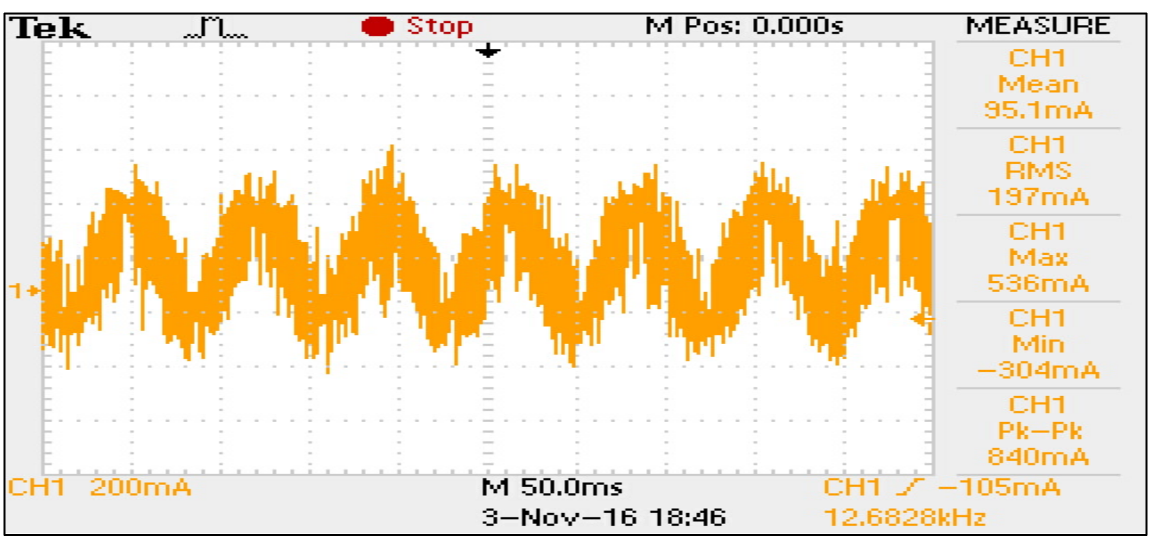

Figure 63: Phase A current: Hysteresis Current Control

5.4.3 Field Winding - DC Current Regulation

After the performance of the hysteresis current controller was validated on the PMSM, the field winding of the DC-assisted MCSRM was excited with regulated current.

TI's High Voltage Motor Control and PFC kit and TMS320F28012 DSP control card is used to implement the controller. Since the commutation overhead to regulate the DC current is not very high, the TMS320F28012 control card, which is a fixed point 32-bit MCU is used. Field winding currents is sensed using a shunt resistance based current sensor unit and sensed voltage is fed to the Analog to Digital converter channels of the microcontroller. Since the DC command current is fixed irrespective of position of the rotor, encoder feedback is not required.

Figure 64: TI's High Voltage Motor Control and PFC kit and TMS320F28012 DSP control card

The power inverter in the TI's Motor Control kit is an integrated standard six-switch VSI module. The circuit diagram and the peripheral of the inverter module are shown in Fig (65).

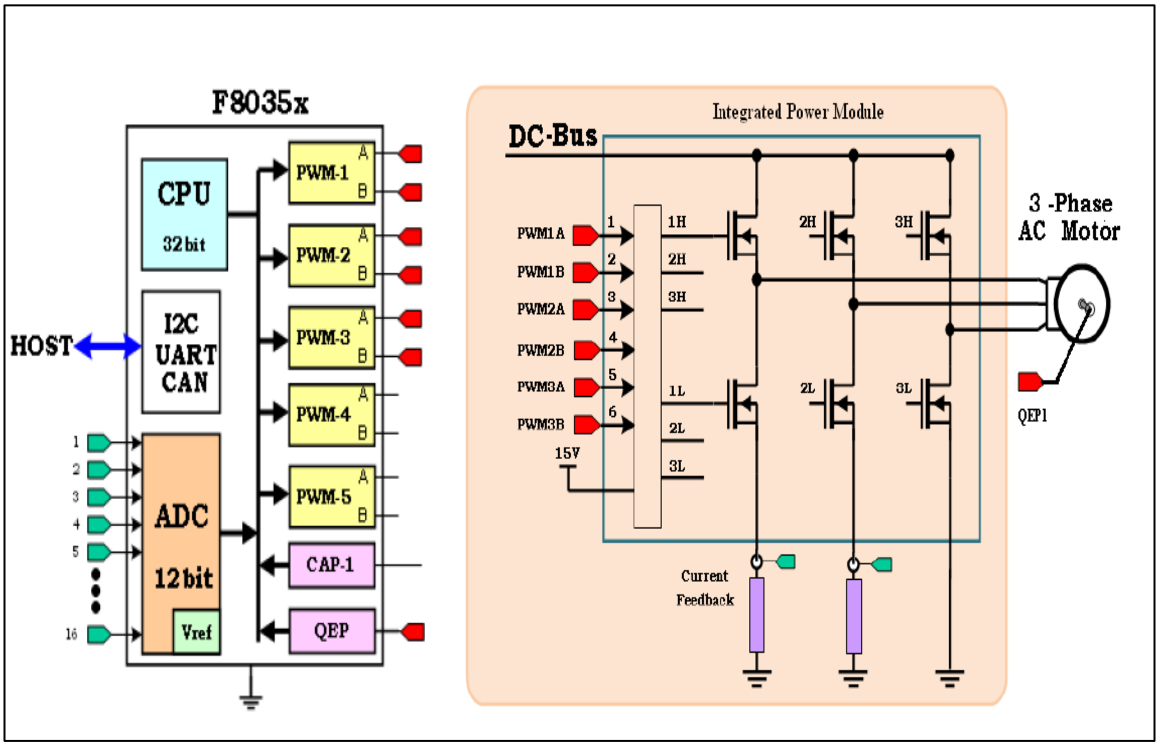

Figure 65: TI's integrated Standard VSI module

To control the DC-field winding current, the 3rd leg of the inverter is completely turned OFF and the switches in the other 2 legs are controlled. The regulated DC-current waveforms under command values are shown below. The ISR frequency for regulating the DC current was set as 20 kHz.

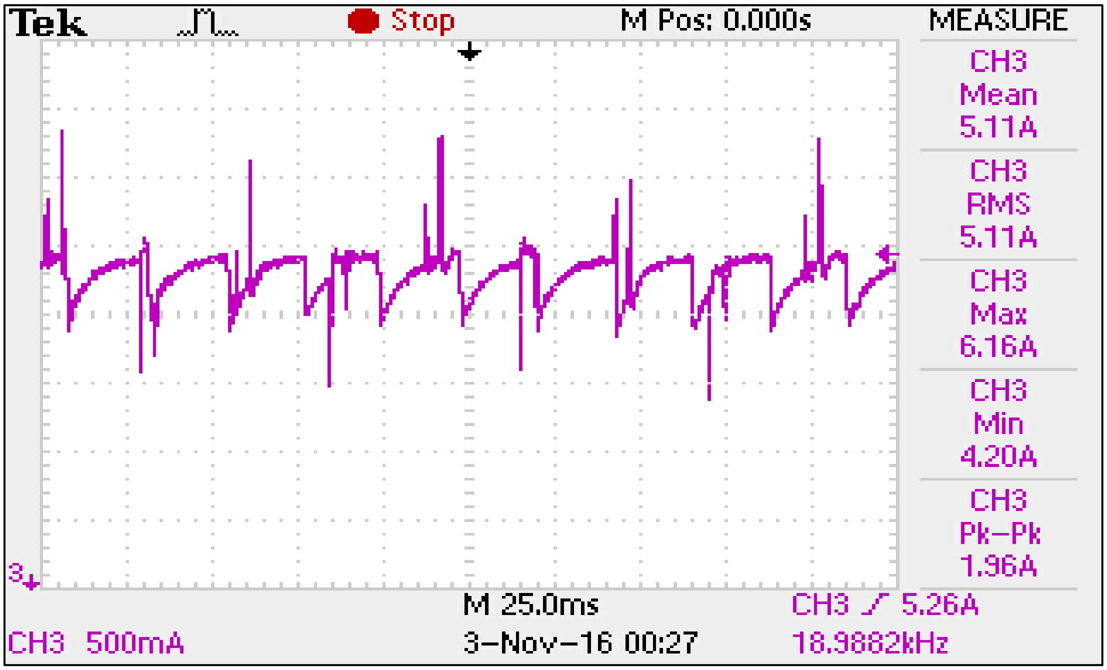

Figure 66: Field Winding DC current; Reference value = 5.0A

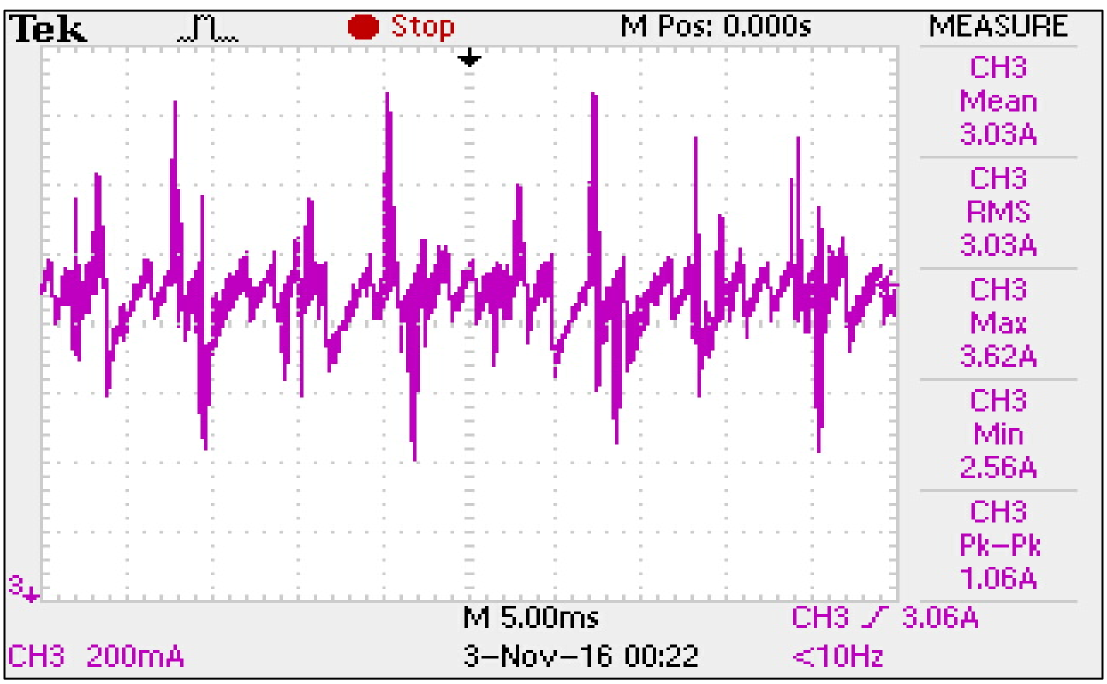

Figure 67: Field Winding DC current; Reference value = 3.0A

5.4.4 Phase winding current regulation

Similar to the PMSM control, a TI's DesignDrive kit and TMS320F28377D DSP control card is used to implement the controller for the phase windings. Phase A and Phase B currents are sensed using a Hall Sensor/LEM based current sensor unit and sensed voltage is fed to the Analog to Digital converter channels of the microcontroller. An incremental encoder is connected the shaft of the machine which is interfaced with the QEP module of the microcontroller. Based on the position feedback, the three phase reference currents are generated and a hysteresis current control is performed to regulate the phase currents.

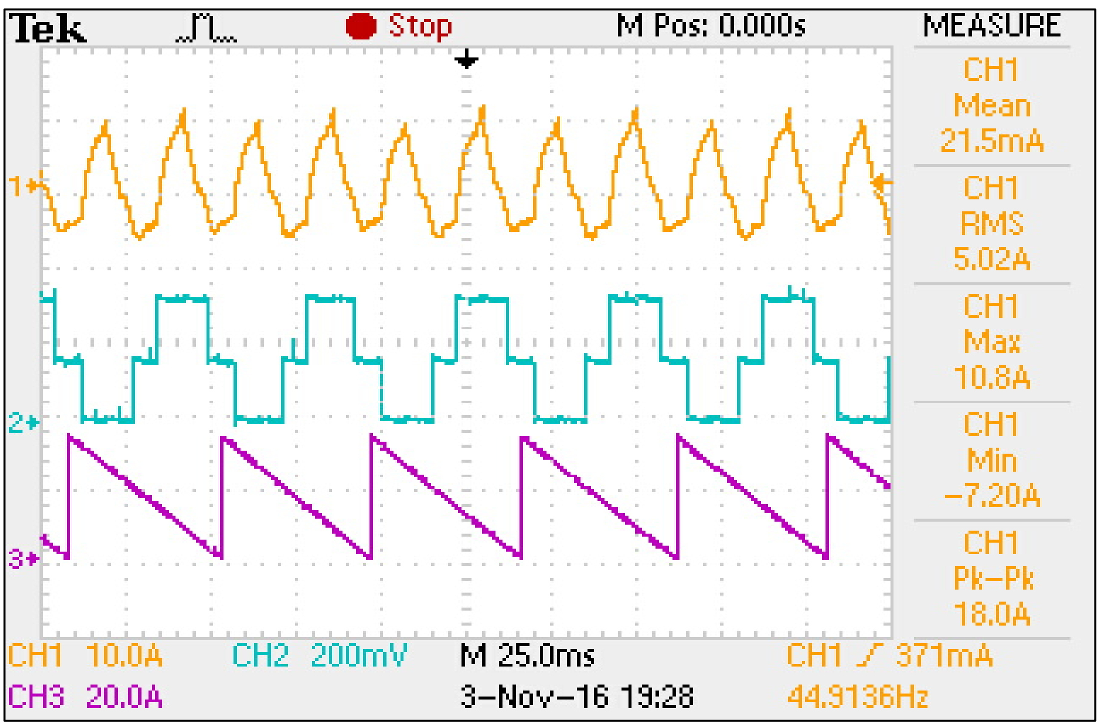

Figure 68: Phase Current regulation of DC-MCSRM

As we can see, the controller is not able to force the phase currents to follow the commanded current profile. More debugging is required to determine the cause of this failure and to regulate the phase currents.

CHAPTER 6

CONCLUSION AND FUTURE WORK

6.1 Summary and Conclusions

A brief summary on the chapters including the finite element analysis, MATLAB simulation and hardware implementation of the drive are presented in this chapter.

6.1.1 Operating Principle of the DC-Assisted Mutually Coupled Switched Reluctance Machine

The research started with operating principle of the switched reluctance machine and the primary drawbacks of the SRM drive were considered. To enable the use of standard six-switch inverter to drive a reluctance machine, the Mutually Coupled Switched Reluctance Machine (MCSRM) with bipolar phase excitation was introduced. The torque producing capability of this machine was limited for wide-speed operation as only half the bus voltage was available across the windings. With the motivation of designing a switched reluctance motor with bipolar excitation capability and wide speed operating range, two hybrid excitation topologies have been proposed, namely: Fully-Pitched Winding DC-Assisted MCSRM and Concentrated Winding DC-Assisted MCSRM

6.1.2 Finite Elemental Analysis of the DC-MCSRM

Finite Elemental Analysis is used to evaluate the characteristics of the DC-MCSRM. An insight in the torque producing capability of the DC-MCSRM is achieved after evaluating the magnetic circuit utilization of the proposed topologies. The motivation behind adding the DC-Field excitation and the benefits of the same have been discussed. Thorough analysis of the operating principle of the proposed DC-MCSRM has been performed using FEA software and is compared with that of a conventional SRM. The proposed topologies have the capability of producing continuous positive torque with bipolar excitation, thus enabling the use of standard six-switch inverter. With the DC-assisted field windings, wide speed range capability is achieved and the efficiency is also improved, since the need for an advancing angle at higher speed is diminished. In the finite element software, the 660W, 12/8 benchmark SRM is constructed based on the mechanical specifications of the machine. The material and dynamic properties of the machine are also defined in the model. The machine is operated at constant base speed with a fixed current excitation in different time-steps completing the mechanical rotations. The Concentrated Winding DC-MCSRM topology is also constructed using the FEA software. The geometric parameters are held constant, but the phase winding configurations are changed. Similar tests under the same excitation levels are performed on the DC-MCSRM and the performance of the machine is compared with that of the conventional SRM. Based on the FEA results, the proposed topology has an improved torque producing capability and has a higher torque and power density.

6.1.3 Optimum Current Profile to Torque Ripple Minimization

An optimized current profile is obtained over the entire operating speed range. The primary region of ripple minimization is the commutation region, where current regulator should be capable to track the reference current profile. A torque feedback based fine tuning method has been introduced to reduce the torque ripple of the machine. The limitations of the profiling technique have also been discussed and geometric optimization of the motor for a flatter torque profile is suggested. A set of current profiles for different torque commands have been obtained. The performances of the optimized current profiles are tested using a hysteresis current control algorithm and a dynamically coupled simulation using MATLAB/Simulink is performed.

6.1.4 Hardware Implementation of the DC-MCSRM drive

An attempt has been made to implement the hysteresis current control on hardware. Before implementing the controller on the DC-MCSRM, a control algorithm was tested on a 400W PMSM. A speed controller for the PMSM was developed and Field Oriented Control was implemented. The performance of the machine with Space-Vector PWM technique and Hysteresis Current Control Technique was compared. Once the validation of the hysteresis current control was obtained, the DC-field winding current was regulated using TI DSP control cards. The hysteresis controller was then used to regulate the phase currents; however, satisfactory results were not obtained. To operate the machine in unidirectional motion, with regulated phase and field currents is the next focus of this research.

6.2 Research Contributions

The primary contributions of this thesis are:

1.) Defined the operating principle of the DC-assisted Mutually Coupled Switched Reluctance Machine.

2.) Achieve wide speed range operation and higher torque producing capability from a switched reluctance motor, which can be driven using a standard six-switch voltage source inverter.

3.) A current profiling technique has been proposed which helped reduce the torque ripple to almost half the initial value

4.) Hardware implementation of the DC-MCSRM drive using hysteresis current control.

6.3 Future Work

The following future works are suggested for further improvement of the system

1.) Develop a high fidelity mathematical model for the DC-MCSRM. This will help reduce the simulation time and assist with debugging.

2.) Explore sinusoidal excitation of the phase windings and compare performance with square-wave excitation.

3.) Develop a fixed-frequency dead-beat current controller for more precise tracking of the command currents.

REFERENCES

[1] Energy Efficiency of Electric Vehicles – Energy Saving and Optimal Control Technologies
By Guoqing Xu, Chunhua Zheng, Yanhui Zhang, Kun Xu and Jianing Liang: SRM picture reference

[2] M. A. Kabir and I. Husain, "Design of Mutually Coupled Switched Reluctance Motors (MCSRMs) for Extended Speed Applications Using 3-Phase Standard Inverters," in *IEEE Transactions on Energy Conversion*, vol. 31, no. 2, pp. 436-445, June 2016.l

[3] M. A. Kabir and I. Husain, "Hybrid excitation topologies for three-phase mutually coupled reluctance machine with standard inverters," *2015 IEEE Power & Energy Society General Meeting*, Denver, CO, 2015, pp. 1-5.

[4] M. A. Kabir and I. Husain, "Mutually coupled switched reluctance machine (MCSRM) for electric and hybrid vehicles," *2014 IEEE PES General Meeting | Conference & Exposition*, National Harbor, MD, 2014, pp. 1-5.

[5] B. C. Mecrow, "New winding configurations for doubly salient reluctance machines," in *IEEE Transactions on Industry Applications*, vol. 32, no. 6, pp. 1348-1356, Nov/Dec 1996.

[6] R. Mikail, I. Husain, M. S. Islam, Y. Sozer and T. Sebastian, "Four-Quadrant Torque Ripple Minimization of Switched Reluctance Machine Through Current Profiling With Mitigation of Rotor Eccentricity Problem and Sensor Errors," in *IEEE Transactions on Industry Applications*, vol. 51, no. 3, pp. 2097-2104, May-June 2015.

[7] R. Mikail, I. Husain, Y. Sozer, M. S. Islam and T. Sebastian, "Torque-Ripple Minimization of Switched Reluctance Machines Through Current Profiling," in *IEEE Transactions on Industry Applications*, vol. 49, no. 3, pp. 1258-1267, May-June 2013.

[8] S. Narla, Y. Sozer and I. Husain, "Switched Reluctance Generator Controls for Optimal Power Generation and Battery Charging," in *IEEE Transactions on Industry Applications*, vol. 48, no. 5, pp. 1452-1459, Sept.-Oct. 2012.

[9] B. C. Mecrow, C. Weiner and A. C. Clothier, "The modeling of switched reluctance machines with magnetically coupled windings," in *IEEE Transactions on Industry Applications*, vol. 37, no. 6,

[10] T.J.E. Miller, "*Switched Reluctance Motors and their Control*," Magna Physics Publishing and Clarendon Press, Oxford, 1993.

[11] R. Krishnan, “*Switched Reluctance Motor Drive: Modeling, simulation, Analysis, Design and application*,” Magna Physics Publishing, 2001.

[12] J. Sun, S. Wang, Z. Kuang and H. Wu, "Torque ripple comparison of short-pitched and fully-pitched winding switched reluctance machine," *Electrical Machines and Systems (ICEMS), 2012 15th International Conference on*, Sapporo, 2012, pp. 1-6.

[13] Yue Li, J. D. Lloyd and G. E. Horst, "Switched reluctance motor with DC assisted excitation," *Industry Applications Conference, 1996. Thirty-First IAS Annual Meeting, IAS '96., Conference Record of the 1996 IEEE*, San Diego, CA, 1996, pp. 801-807 vol.2.

[14] K. Tungpimolrut, S. Kachapornkul, P. Jitkreeyarn, P. Somsiri, N. Chayopitak and C. Akira, "Torque improvement of three-phases full bridge converter based switched reluctance motor with DC assisted winding," *Electrical Machines and Systems (ICEMS), 2012 15th International Conference on*, Sapporo, 2012, pp. 1-5.

[15] X. Liu *et al.*, "Performance comparison between unipolar and bipolar excitations in switched reluctance machine with sinusoidal and rectangular waveforms," *2011 IEEE Energy Conversion Congress and Exposition*, Phoenix, AZ, 2011, pp. 1590-1595.

[16] Z. Azar and Z. Q. Zhu, "Comparative study of electromagnetic performance of switched reluctance machines under different excitation techniques," *2013 IEEE Energy Conversion Congress and Exposition*, Denver, CO, 2013, pp. 4334-4341.

[17] Sandeep Narla’s Thesis: Modeling and Control of Switched Reluctance Machines for Four-Quadrant Operation http://rave.ohiolink.edu/etdc/view?acc_num=akron1291919332

APPENDICES

Appendix A

Final Optimized Phase B Current Profiles

Theta	Command Torque = 1.0nm	Command Torque = 2.0nm	Command Torque = 3.0nm
0	0	0	0
0.5	0	0	0
1	0	0	0
1.5	0	0	0
2	0	0	0
2.5	0	0	0
3	0	0	0
3.5	0.166799	0.386939	0.503457
4	0.333598	0.773878	1.006915
4.5	0.500397	1.160817	1.510372
5	0.667195	1.547756	2.01383
5.5	0.833994	1.934695	2.517287
6	1.207018	2.5785	3.295208
6.5	1.580041	3.22226	4.073129
7	1.547622	3.123149	3.953354
7.5	1.560399	3.023331	3.906994

8	1.547622	3.123149	3.953354
8.5	1.44929	3.22226	3.982268
9	1.350958	2.965	4.011182
9.5	1.252625	2.708114	4.040096
10	1.191394	2.662679	3.956552
10.5	1.130163	2.617243	3.873009
11	1.12036	2.571808	3.789465
11.5	1.185628	2.526372	3.705921
12	1.1064	2.562619	3.585102
12.5	1.07358	2.598865	3.464283
13	1.076115	2.466665	3.213752
13.5	1.093191	2.399987	3.051436
14	1.103413	2.368431	2.969961
14.5	1.10531	2.35342	2.940685
15	1.102914	2.340043	2.928762
15.5	1.10531	2.35342	2.940685
16	1.103413	2.368431	2.969961
16.5	1.093191	2.399987	3.051436
17	1.076115	2.466665	3.213752
17.5	1.07358	2.598865	3.464283
18	1.1064	2.788342	3.804104

18.5	1.185628	2.804617	3.997065
19	1.12036	2.877145	3.629203
19.5	1.053339	2.654071	3.636409
20	0.947631	2.337687	3.149764
20.5	0.631754	1.558458	2.099843
21	0.315877	0.779229	1.049921
21.5	0	0	0
22	0	0	0
22.5	0	0	0
23	0	0	0
23.5	0	0	0
24	-0.31588	-0.77923	-1.04992
24.5	-0.63175	-1.55846	-2.09984
25	-0.94763	-2.33769	-3.14976
25.5	-1.05334	-2.65407	-3.63641
26	-1.12036	-2.87715	-3.6292
26.5	-1.18563	-2.80462	-3.99707
27	-1.1064	-2.78834	-3.8041
27.5	-1.07358	-2.59886	-3.46428
28	-1.07612	-2.46666	-3.21375
28.5	-1.09319	-2.39999	-3.05144

29	-1.10341	-2.36843	-2.96996
29.5	-1.10531	-2.35342	-2.94069
30	-1.10291	-2.34004	-2.92876
30.5	-1.10531	-2.35342	-2.94069
31	-1.10341	-2.36843	-2.96996
31.5	-1.09319	-2.39999	-3.05144
32	-1.07612	-2.46666	-3.21375
32.5	-1.07358	-2.59886	-3.46428
33	-1.1064	-2.78834	-3.8041
33.5	-1.35243	-3.19156	-4.50052
34	-1.45396	-3.65102	-4.63612
34.5	-1.55374	-3.81489	-5.14678
35	-1.61483	-3.88544	-5.16359
35.5	-1.46575	-3.49315	-4.61713
36	-1.52289	-3.35773	-4.34513
36.5	-1.58004	-3.22226	-4.07313
37	-1.54762	-3.12315	-3.95335
37.5	-1.5604	-3.02333	-3.90699
38	-1.54762	-3.12315	-3.95335
38.5	-1.44929	-3.22226	-3.98227
39	-1.03508	-2.18577	-2.96126

39.5	-0.62087	-1.14966	-1.94025
40	-0.24376	-0.32499	-0.80679
40.5	-0.07682	0.036828	-0.2366
41	0	0.305338	-0.16026
41.5	0	0.278245	0.291144
42	0	0.225723	0.219002
42.5	0	0	0
43	0	0	0
43.5	0	0	0
44	0	0	0
44.5	0	0	0
45	0	0	0

Appendix B

$T - i - \theta$ characteristics

Theta	IA = 0, IB = 0	IA = 1, IB = -1	IA = 2, IB = -2	IA = 3, IB = -3	IA = 4, IB = -4	IA = 5, IB = -5	IA = 6, IB = -6	IA = 7, IB = -7	IA = 8, IB = -8	IA = 9, IB = -9
0	-4.21E-05	0.454054	0.935086	1.440873	1.961743	2.489739	3.015539	3.531809	4.032774	4.514132
0.5	-0.00367	0.441405	0.915987	1.413767	1.924718	2.438541	2.945155	3.435871	3.908253	4.362053
1	-0.00784	0.429963	0.896929	1.382679	1.87691	2.365403	2.841039	3.299027	3.740851	4.167312
1.5	-0.01115	0.419637	0.875566	1.342866	1.807917	2.258798	2.696083	3.120828	3.534062	3.937103
2	-0.01268	0.408812	0.848237	1.284986	1.707937	2.115315	2.512931	2.90649	3.293815	3.676221
2.5	-0.01268	0.395003	0.80887	1.201142	1.573883	1.939171	2.299145	2.661882	3.025095	3.387943
3	-0.01171	0.376595	0.75184	1.090988	1.415836	1.738846	2.065797	2.395992	2.734105	3.075204
3.5	-0.01062	0.348883	0.67331	0.961779	1.240014	1.522577	1.815748	2.116789	2.424395	2.740632
4	-0.00952	0.308342	0.577164	0.818647	1.0531	1.298112	1.554365	1.824856	2.103717	2.391444
4.5	-0.01049	0.252613	0.467289	0.664604	0.860878	1.065966	1.286942	1.520733	1.771447	2.034116
5	-0.0141	0.186339	0.348056	0.502293	0.661836	0.830611	1.013238	1.214471	1.431951	1.668106
5.5	-0.01732	0.115396	0.223666	0.333502	0.454765	0.589109	0.737193	0.90407	1.093449	1.300962
6	-0.0152	0.042884	0.092145	0.152785	0.231105	0.328988	0.447143	0.585824	0.746704	0.935594
6.5	0.006627	-0.02857	-0.05405	-0.05566	-0.02935	0.026203	0.11278	0.229421	0.375483	0.554786
7	0.061276	-0.11137	-0.25186	-0.34769	-0.39614	-0.39596	-0.34678	-0.24902	-0.10228	0.095502
7.5	6.16E-04	-0.36343	-0.67463	-0.91758	-1.08212	-1.16631	-1.1707	-1.09531	-0.93989	-0.70577
8	-0.0609	-0.56396	-0.98656	-1.32045	-1.5611	-1.70924	-1.76594	-1.73097	-1.60414	-1.38843
8.5	-0.00638	-0.57288	-1.04337	-1.41756	-1.69625	-1.88072	-1.97365	-1.97423	-1.88131	-1.69895
9	0.015293	-0.59761	-1.10414	-1.51063	-1.82107	-2.03746	-2.16127	-2.19291	-2.13357	-1.98947
9.5	0.017211	-0.6408	-1.18238	-1.61964	-1.96065	-2.20709	-2.3603	-2.42561	-2.40625	-2.29837
10	0.01389	-0.6916	-1.27029	-1.73946	-2.11034	-2.38669	-2.57398	-2.67725	-2.69356	-2.62596
10.5	0.010503	-0.74252	-1.362	-1.86503	-2.26631	-2.5756	-2.80086	-2.93917	-2.99433	-2.96175
11	0.010118	-0.78584	-1.45	-1.99001	-2.42459	-2.77123	-3.03146	-3.20838	-3.29575	-3.29484
11.5	0.010562	-0.81737	-1.52951	-2.11064	-2.58507	-2.96717	-3.26408	-3.47321	-3.59279	-3.62559
12	0.011864	-0.83647	-1.59287	-2.21978	-2.73752	-3.15831	-3.48873	-3.72832	-3.88123	-3.9435

12.5	**0.012761**	**-0.84732**	**-1.63667**	**-2.31244**	**-2.87513**	**-3.33656**	**-3.69973**	**-3.97295**	**-4.15338**	**-4.24114**
13	**0.013199**	**-0.85323**	**-1.66296**	**-2.3794**	**-2.98959**	**-3.49173**	**-3.8922**	**-4.1972**	**-4.40389**	**-4.51466**
13.5	**0.011617**	**-0.85712**	**-1.67821**	**-2.42196**	**-3.07205**	**-3.61636**	**-4.05636**	**-4.39347**	**-4.62801**	**-4.76269**
14	**0.008075**	**-0.85991**	**-1.68731**	**-2.44626**	**-3.12364**	**-3.70453**	**-4.18284**	**-4.55396**	**-4.81909**	**-4.98023**
14.5	**0.00396**	**-0.86237**	**-1.69301**	**-2.46086**	**-3.15284**	**-3.75837**	**-4.26779**	**-4.6725**	**-4.97016**	**-5.16159**
15	**4.43E-04**	**-0.86573**	**-1.6968**	**-2.47016**	**-3.17054**	**-3.78927**	**-4.31842**	**-4.7498**	**-5.07794**	**-5.30007**
15.5	**-0.00348**	**-0.87065**	**-1.69994**	**-2.47675**	**-3.1824**	**-3.80859**	**-4.34813**	**-4.79607**	**-5.14655**	**-5.39773**
16	**-0.00725**	**-0.87407**	**-1.70171**	**-2.48033**	**-3.18968**	**-3.82033**	**-4.36539**	**-4.82189**	**-5.18641**	**-5.45642**
16.5	**-0.01117**	**-0.8774**	**-1.70491**	**-2.48337**	**-3.19538**	**-3.82872**	**-4.37732**	**-4.83885**	**-5.21074**	**-5.49292**
17	**-0.01258**	**-0.87912**	**-1.70746**	**-2.48402**	**-3.19742**	**-3.83233**	**-4.38323**	**-4.84799**	**-5.2243**	**-5.51348**
17.5	**-0.01225**	**-0.8804**	**-1.70882**	**-2.48275**	**-3.19659**	**-3.83214**	**-4.38432**	**-4.85123**	**-5.23112**	**-5.52505**
18	**-0.01102**	**-0.8791**	**-1.70723**	**-2.47975**	**-3.19179**	**-3.82724**	**-4.38016**	**-4.84849**	**-5.2311**	**-5.52976**
18.5	**-0.01026**	**-0.87502**	**-1.70347**	**-2.47479**	**-3.18328**	**-3.8176**	**-4.37076**	**-4.84034**	**-5.22523**	**-5.5289**
19	**-0.00986**	**-0.86679**	**-1.69589**	**-2.46619**	**-3.16866**	**-3.80075**	**-4.35338**	**-4.824**	**-5.21156**	**-5.51969**
19.5	**-0.01042**	**-0.85371**	**-1.68218**	**-2.44844**	**-3.14461**	**-3.77314**	**-4.32427**	**-4.79588**	**-5.18619**	**-5.49828**
20	**-0.01361**	**-0.83445**	**-1.65847**	**-2.41853**	**-3.10769**	**-3.73057**	**-4.27937**	**-4.75083**	**-5.14539**	**-5.46004**
20.5	**-0.01691**	**-0.80486**	**-1.61803**	**-2.36841**	**-3.04879**	**-3.66285**	**-4.20827**	**-4.67972**	**-5.0779**	**-5.39607**
21	**-0.01551**	**-0.75859**	**-1.55039**	**-2.2854**	**-2.9533**	**-3.55417**	**-4.09422**	**-4.5669**	**-4.96872**	**-5.29363**
21.5	**0.005635**	**-0.67848**	**-1.42904**	**-2.13464**	**-2.77981**	**-3.36127**	**-3.89309**	**-4.36771**	**-4.77682**	**-5.11591**
22	**0.059874**	**-0.53275**	**-1.19623**	**-1.83348**	**-2.42856**	**-2.97551**	**-3.49193**	**-3.97291**	**-4.40322**	**-4.78113**
22.5	**-0.00178**	**-0.40627**	**-0.83993**	**-1.29317**	**-1.75808**	**-2.22507**	**-2.71012**	**-3.21303**	**-3.71364**	**-4.21337**
23	**-0.0606**	**-0.22736**	**-0.38265**	**-0.60619**	**-0.90117**	**-1.25648**	**-1.67989**	**-2.17371**	**-2.72073**	**-3.32086**
23.5	**-0.00633**	**-0.00693**	**0.002946**	**-0.07087**	**-0.23482**	**-0.48268**	**-0.8167**	**-1.24081**	**-1.74584**	**-2.32873**
24	**0.015163**	**0.125736**	**0.232205**	**0.249767**	**0.176018**	**0.011653**	**-0.24113**	**-0.58717**	**-1.0253**	**-1.55119**
24.5	**0.017213**	**0.208154**	**0.373902**	**0.448152**	**0.433426**	**0.325893**	**0.132049**	**-0.15285**	**-0.53362**	**-1.00544**
25	**0.013611**	**0.262777**	**0.467698**	**0.579833**	**0.605645**	**0.537237**	**0.385198**	**0.145085**	**-0.19217**	**-0.62142**
25.5	**0.010388**	**0.301449**	**0.533534**	**0.67365**	**0.728567**	**0.689126**	**0.567616**	**0.360978**	**0.056602**	**-0.33994**
26	**0.009828**	**0.330073**	**0.581978**	**0.744386**	**0.821138**	**0.804866**	**0.706839**	**0.525805**	**0.247373**	**-0.12332**
26.5	**0.010597**	**0.352073**	**0.618602**	**0.800117**	**0.893819**	**0.897246**	**0.818191**	**0.65684**	**0.40002**	**0.050606**
27	**0.011614**	**0.368607**	**0.647771**	**0.844731**	**0.952219**	**0.97283**	**0.909326**	**0.763467**	**0.524808**	**0.193224**
27.5	**0.012561**	**0.380806**	**0.672181**	**0.881856**	**1.001982**	**1.037406**	**0.987532**	**0.854057**	**0.631637**	**0.315724**

28	**0.012883**	**0.38926**	**0.693099**	**0.913198**	**1.045513**	**1.093716**	**1.055868**	**0.933102**	**0.724664**	**0.422824**
28.5	**0.010759**	**0.395493**	**0.710532**	**0.939568**	**1.084121**	**1.143559**	**1.116644**	**1.004107**	**0.807434**	**0.518997**
29	**0.007997**	**0.402429**	**0.726878**	**0.96546**	**1.121214**	**1.190847**	**1.174078**	**1.071225**	**0.884687**	**0.609098**
29.5	**0.003128**	**0.407304**	**0.739609**	**0.988447**	**1.154277**	**1.233489**	**1.226348**	**1.133164**	**0.955549**	**0.692409**
30	**-1.94E-04**	**0.412477**	**0.753127**	**1.01268**	**1.187798**	**1.276374**	**1.278705**	**1.19514**	**1.026311**	**0.774321**
30.5	**-0.00418**	**0.415787**	**0.766353**	**1.035624**	**1.219594**	**1.317295**	**1.329108**	**1.255323**	**1.096051**	**0.854385**
31	**-0.00828**	**0.420471**	**0.781344**	**1.059594**	**1.252624**	**1.359612**	**1.38115**	**1.317435**	**1.168272**	**0.936408**
31.5	**-0.01138**	**0.42676**	**0.797153**	**1.084061**	**1.286126**	**1.402634**	**1.434327**	**1.381337**	**1.24339**	**1.022066**
32	**-0.01328**	**0.434446**	**0.813733**	**1.110009**	**1.321799**	**1.448641**	**1.491352**	**1.450026**	**1.324241**	**1.114967**
32.5	**-0.01234**	**0.443969**	**0.83241**	**1.138352**	**1.360482**	**1.498539**	**1.553356**	**1.525002**	**1.412914**	**1.217843**
33	**-0.01209**	**0.453479**	**0.852065**	**1.16886**	**1.402735**	**1.553526**	**1.622051**	**1.608372**	**1.511853**	**1.333147**
33.5	**-0.01022**	**0.465468**	**0.875175**	**1.204192**	**1.451522**	**1.617079**	**1.701636**	**1.705255**	**1.627274**	**1.468109**
34	**-0.01023**	**0.477217**	**0.900115**	**1.243846**	**1.507404**	**1.690735**	**1.794569**	**1.81896**	**1.763201**	**1.627505**
34.5	**-0.01015**	**0.491319**	**0.930233**	**1.292013**	**1.57566**	**1.781121**	**1.909091**	**1.959547**	**1.931713**	**1.825685**
35	**-0.01392**	**0.505496**	**0.965079**	**1.3503**	**1.660041**	**1.894215**	**2.053379**	**2.137366**	**2.145363**	**2.077323**
35.5	**-0.01701**	**0.526649**	**1.01438**	**1.43171**	**1.777205**	**2.050531**	**2.252024**	**2.381363**	**2.437471**	**2.419802**
36	**-0.01511**	**0.563967**	**1.093108**	**1.557513**	**1.954728**	**2.28406**	**2.545251**	**2.737177**	**2.85813**	**2.906754**
36.5	**0.006671**	**0.641611**	**1.235756**	**1.772431**	**2.246726**	**2.656262**	**2.999214**	**3.272979**	**3.474869**	**3.602389**
37	**0.06232**	**0.780182**	**1.469254**	**2.106142**	**2.679317**	**3.184181**	**3.61642**	**3.972862**	**4.250308**	**4.447452**
37.5	**-5.10E-04**	**0.767823**	**1.51175**	**2.207531**	**2.839935**	**3.402718**	**3.894377**	**4.312516**	**4.655279**	**4.923097**
38	**-0.05883**	**0.65721**	**1.348594**	**2.002181**	**2.613901**	**3.179728**	**3.69927**	**4.170035**	**4.591804**	**4.962989**
38.5	**-0.00606**	**0.645032**	**1.287233**	**1.907522**	**2.500746**	**3.064261**	**3.597044**	**4.097577**	**4.565365**	**4.999701**
39	**0.016136**	**0.624032**	**1.237494**	**1.839199**	**2.422569**	**2.985438**	**3.525572**	**4.043154**	**4.536578**	**5.005408**
39.5	**0.017259**	**0.596015**	**1.190031**	**1.780121**	**2.357688**	**2.919617**	**3.465255**	**3.992693**	**4.501748**	**4.992239**
40	**0.014139**	**0.5715**	**1.149963**	**1.73103**	**2.304149**	**2.865857**	**3.414095**	**3.948309**	**4.468135**	**4.97206**
40.5	**0.010434**	**0.55151**	**1.117097**	**1.69058**	**2.259853**	**2.820468**	**3.370609**	**3.90936**	**4.435907**	**4.949992**
41	**0.009459**	**0.537327**	**1.091726**	**1.657767**	**2.223348**	**2.782441**	**3.333432**	**3.874652**	**4.406401**	**4.926566**
41.5	**0.010382**	**0.527041**	**1.071301**	**1.630179**	**2.191798**	**2.749191**	**3.299807**	**3.842972**	**4.376569**	**4.901122**
42	**0.01145**	**0.518262**	**1.053143**	**1.604739**	**2.161921**	**2.716656**	**3.266553**	**3.808657**	**4.34386**	**4.870893**

42.5	**0.012342**	**0.510198**	**1.03569**	**1.579707**	**2.131949**	**2.683247**	**3.230318**	**3.771722**	**4.307554**	**4.837201**
43	**0.012511**	**0.500993**	**1.017269**	**1.553462**	**2.099184**	**2.646798**	**3.191075**	**3.732236**	**4.268655**	**4.80043**
43.5	**0.011036**	**0.490404**	**0.997673**	**1.525737**	**2.064609**	**2.607676**	**3.150634**	**3.691205**	**4.22755**	**4.7576**
44	**0.007458**	**0.478018**	**0.976423**	**1.496073**	**2.028525**	**2.568584**	**3.109122**	**3.647196**	**4.179607**	**4.701856**
44.5	**0.003366**	**0.466101**	**0.955554**	**1.467674**	**1.994912**	**2.530781**	**3.067035**	**3.598323**	**4.11902**	**4.626406**
45	**-3.87E-04**	**0.453683**	**0.93469**	**1.440495**	**1.961354**	**2.489445**	**3.015523**	**3.531526**	**4.032327**	**4.513886**